Silicon-Based Epitaxy by Chemical Vapor Deposition Using Novel Precursor Neopentasilane

Keith H. Chung

a Dissertation

Presented to the Faculty

of Princeton University

in Candidacy for the Degree

of Doctor of Philosophy

Recommended For Acceptance

by the Deperatment of

Electrical Engineering

Advisor: James C. Sturm

June 2010

Abstract

Low temperature and high growth rates of epitaxial silicon deposition are desired for several practical reasons. The ability to grow epitaxial layers at low temperatures and for short times reduces the thermal budget and dopant diffusion. In has been previously shown that by increasing the silane order, (i.e. from silane to disilane to trisilane) the silicon growth rate increases for the same experimental conditions. The high-order silanes allow for the increase of growth rate but the cause has not been explained.

In this dissertation, we examine the use of neopentasilane (NPS) as the silicon source for silicon epitaxial growth by Chemical Vapor Deposition (CVD). The epitaxial layers grown with NPS are qualified using a variety of characterization techniques to determine the crystal quality, impurity levels in the films, and the electron and hole mobilities of the crystalline films. An atomistic mechanism for high-order silanes is proposed for the first time in this dissertation and tested rigorously against experimental results from our work and the data of other groups.

Both faster epitaxial growth rates and smoother silicon surfaces, implying a high surface diffusion coefficient, were achieved using the high-order silanes when compared with growth with silane. We hypothesize these effects are due more open sites on the surface during the growth. The increase is the result of surface-catalyzed reactions involving the consumption of surface hydrogen, thereby generating open sites. Indirect evidence of more open sites with high-order silanes was shown by measuring diborane and phosphorus adsorption.

The ability of high-order silanes to adsorb and deposit without the conventional hydrogen desorption to create open sites, and their ability to generate their own open surface sites are the main technological point of this dissertation. This unusual

characteristic of high-order silanes makes NPS an attractive candidate for growth of heavily doped n-type silicon and Si:C epitaxial layers.

Acknowledgements

The work presented in this dissertation would not have been possible without the contribution of many individuals. These people have my gratitude and will be mentioned in this section.

First and foremost, I would like to thank my thesis advisor, Professor James Sturm, for his consistent encouragement, enthusiasm, and patience throughout all my years in Princeton even the times when I was undeserving. His optimistic attitude throughout this work was essential for all the achievements of the present work.

I would like to thank all the members, past and present, of Prof. Sturm's group for their help and collaboration. Several members deserve additional mention. To Kun Yao, who was always there when an extra hand was needed for RTCVD reactor maintenance, regardless of the time and day. Rebecca Peterson, for spending her time to teach me how to use a variety of different equipment in the clean room and the RTCVD reactor when I first set foot in Prof. Sturm's lab. To John Davis and Troy Graves-Abe for their encouragement, friendship, and advice (personal and scientific). To Bahman Hekmatshoar, Yi Fei Huang and Hongzheng Jin for being excellent friends. To Prof. Chee-Wee Liu and Dr. Malcolm Carroll for their scientific advice

Outside of the lab, I would like to thank the following: James Donald, Sam Feng, Yue-Kai Huang, Neil McDaniel, Daniel Raburn, Sucharit Sarkar, Samuel Taylor, Wilson Tong, Alan Wan, and Chao Wang, for their excellent friendship and the wonderful times in Princeton.

The PRISM cleanroom staff, especially Joe Palmer, Carolyn Arnesen, and Sheila Gunning, who have been extremely helpful throughout the years. To the staff at Evans East, Dr Wei Ou and Dr. Jeffrey Mayer, for their help with SIMS analysis. I would also

like to thank Applied Energy Systems for the installation of the gas cabinet and Applied Materials for supplying the neopentasilane ampule and supporting the project.

A special mention goes to Prof. Jay Benziger, whose discussions on concerted reactions and hydrogenoylsis contributed to a significant portion of this thesis. I would also like to thank my readers Prof. Gmachl and Prof. Shayegan.

And finally to my parents who always believed in me, even when I didn't.

Two roads diverged in a wood, and I— I took the one less traveled by, And that has made all the difference.

-Robert Frost

There are two kinds of teachers: the kind that fill you with so much quail shot that you can't move, and the kind that just gives you a little prod behind and you jump to the skies.

-Robert Frost

Table of Contents

List of Figures

Appendixes

List of Tables

Chapter 1
Introduction

1.1 History of Low-Temperature Silicon-Based Chemical Vapor Deposition

There is a continuing trend of decreasing the temperature of the epitaxial growth of silicon. Historically, silicon epitaxy was only grown at high temperatures, over 1000 ^{o}C [1.1][1.2]. This was done typically at such temperatures in a hydrogen ambient, to keep the surface clean and free of oxygen. Oxygen desorbs from the silicon surface readily at high temperatures (as shown later by Lander and Morrison). The hydrogen can actually aid desorption, and can passivate the silicon surface against the adsorption of trace oxygen or water vapor contaminants. Lander and Morrison [1.3] later characterized the stability of background oxygen and water vapor at different partial pressures and temperatures in vacuum on the silicon surface. The presence of stable oxygen on the silicon surface in the temperature range of 1125K to 1070K led to hillocks and defects in epitaxy growth [1.4]. Lower partial pressures of water vapor and were required to maintain clean surfaces at lower temperatures. This led to the development of ultra-high vacuum deposition chambers [1.5]. By lowering the base pressure and working at low gas pressures (mtorr), gas contamination levels of oxygen, water vapor in the parts per billion levels were low enough to give partial pressures to enable high quality epitaxy at temperatures of 600 ^{o}C.

The use of a load-lock to minimize the transfer of gaseous impurities into the growth chamber upon entry and exit of the sample from the growth chamber and improvements in gas purification systems have reduced the water vapor and oxygen

concentrations to the 10 ppb range for reactor chamber pressures on the order of torr. Furthermore, it was founded that a hydrogen-passivated surface along with the slow diffusion of oxygen through the boundary layer reduces the oxygen sticking coefficient by a factor of 100 compared to that in UHV [1.6]. As a result, silicon epitaxial growth at low temperatures and higher pressures without the use of ultra-high vacuum technology is now possible [1.7]. There are currently three common types of CVD based on the pressure ranges; atmospheric, low pressure (several torr), and ultra-high vacuum (UHV CVD) ($< 10^{-8}$ torr). All of our work in this thesis will be done in the low-pressure range.

The reduction in the growth temperature of silicon compared to classical ~1000 ^{o}C temperatures provides many benefits. Less diffusion enables sharper doping profiles. In the temperature range of 500 ^{o}C –750 ^{o}C metastable layers of strained SiGe can be grown with larger thicknesses than the critical thickness model allows for, allowing for greater germanium fractions in raised source-drain applications [1.8][1.9]. Greater amounts of dopant, particularly n-type dopants such as phosphine and arsine, can be incorporated into the epilayers at lower temperatures than at higher temperatures due to the reduction of surface segregation effects [1.10]. $Si_{1-y}C_y$ (also referred to as Si:C) with dilute carbon concentrations of ~1% or less alloys can be grown with higher substitional carbon fractions at lower temperatures [1.11].

1.2 Motivation for Higher-Order Silanes

Traditionally, the reduction of the growth temperature also implies the reduction of growth rate. It has been observed that replacing the chlorine with hydrogen in the precursor (i.e. $SiCl_2H_2$ to silane, SiH_4) , and then increasing the silane order, i.e. going from silane (SiH_4) to disilane (Si_2H_6) to trisilane (Si_3H_8), increased the growth rate

significantly for the same growth temperature. Shown in Figure 1.1 below is an illustration of this phenomenon.

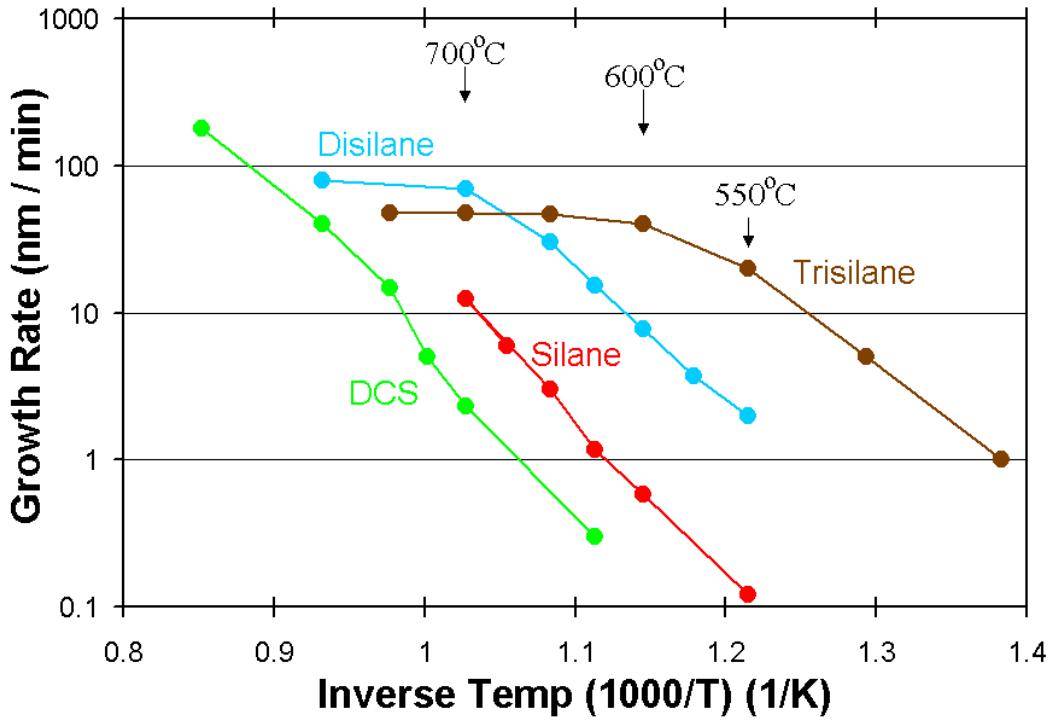

Figure 1.1. Comparison of low-pressure chemical vapor deposition (LPCVD) epitaxial growth rates of silicon vs. inverse temperature for sources of dichlorosilane (DCS), silane, dislane, and trisilane [data from Applied Materials, conditions not given] precursors on (100) silicon substrates. In all cases except for trisilane the carrier was hydrogen at pressure of 6 torr. The dichlorosilane, silane, and disilane and NPS partial pressures were 52 mtorr, 20 mtorr, and 10 mtorr respectively.

Increasing the silane order allows for the reduction of growth temperature without the reduction in growth rate. If this trend were to continue, further increasing the silane-order would further increase the growth rate for the same temperatures. With this motivation we investigated the application of neopentasilane (Si_5H_{12}), with the goal of being able to achieve higher growth rates than those of the existing precursor. This is done for high-throughput considerations for industrial applications as well as for Si:C alloy growth with high-carbon fractions.

1.3 Thesis Structure

Chapter 2 will describe our existing CVD system at Princeton and the modifications done to inject neopentasilane (NPS) into the chamber. Epitaxial growth rates with NPS and some initial characterization of epilayers grown with NPS are discussed.

In Chapter 3 characterization techniques (secondary ion mass spectrometry (SIMS), photoluminescence (PL), UV reflectance, cross-sectional TEM), are used to analyze epitaxial layers grown with NPS. Furthermore, we analyze field effect transistors (FETs) fabricated in epitaxial layers grown with NPS. We will compare the quality these layers with that of the crystalline silicon substrates based on carrier mobilities and current-voltage measurements.

The basic CVD growth theory is covered in chapter 4. A novel concerted reaction mechanism is proposed as the reason for the enhancement of growth rates with high-order silanes. This mechanism is supported by extensive experimental data.

The epitaxial growth of dilute random carbon alloys of silicon (Si:C) is described in chapter 5. A comparison of Si:C alloy epitaxial layers grown with disilane and NPS using our chamber is discussed.

In chapter 6, we describe experiments towards achieving selective epitaxy on patterned wafers. As part of this work, we conduct etching experiments with chlorine gas in nitrogen and hydrogen ambients. Chlorine can be used as an etchant for silicon to eliminate unwanted surface impurities as well as clean the silicon surface with a low thermal budget.

In chapter 7 we model the incorporation of phosphorus in silicon and silicon-germanium during CVD epitaxy using phosphine as a source. Segregation effects are described as well as the effect of different silicon precursors.

Chapter 2
Growth of Silicon using Neopentasilane

2.1 Experimental Setup

2.1.1 Princeton Rapid Thermal Chemical Vapor Deposition

All silicon growth experiments were conducted in the Princeton RTCVD (Rapid Thermal Chemical Vapor Deposition) reactor (Figure 2.1). The chamber is a quartz tube designed to hold wafers up to 6 inches in diameter. It is a cold-wall system and heated by infrared halogen lamps. The wafer is suspended on four tips of a quartz stand. A gold-polished reflector assembly in conjunction with a low thermal mass allows for rapid thermal applications. A baffle is used in an attempt to distribute the gas flow more uniformly. The gas flow in our system is parallel to the wafer. Usually <100>-oriented wafers are used and loaded with the gas flow parallel to the (011) direction. The chamber is pumped with a two-stage rotary vane pump (Alcatel 2033CP). A minimum pressure of 0.07 torr can be reached using the pump. The quartz tube is mounted to a steel chamber with a double O-ring which is vacuum-pumped between the two O-rings. This reduces the pressure drop on the inner O-ring to minimize the leak rate on this O-ring. A gate valve is used to separate the main chamber from the load-lock. The load-lock is used to minimize the undesirable introduction of unwanted moisture into the chamber when wafers are transferred into and out of the reactor.

Temperature control is done by measuring the infrared transmission through the wafer using two lasers, at 1.3 and 1.55 micron. The principles of temperature measurement by the use of lasers are well described in the work by other authors

[2.1][2.2][2.3]. The 1.3-micron laser is used to control the lower temperatures ranging from 450 ^{o}C – 625 ^{o}C. The 1.55-micron laser is used to control temperatures from 650 ^{o}C – 775 ^{o}C. At temperatures higher than 800 ^{o}C there is no detectable transmission with either wavelength, so for temperature above 800 ^{o}C, the temperature is estimated based on growth rate observed in past experiments. The typical growth pressure used in most experiments is 6 torr.

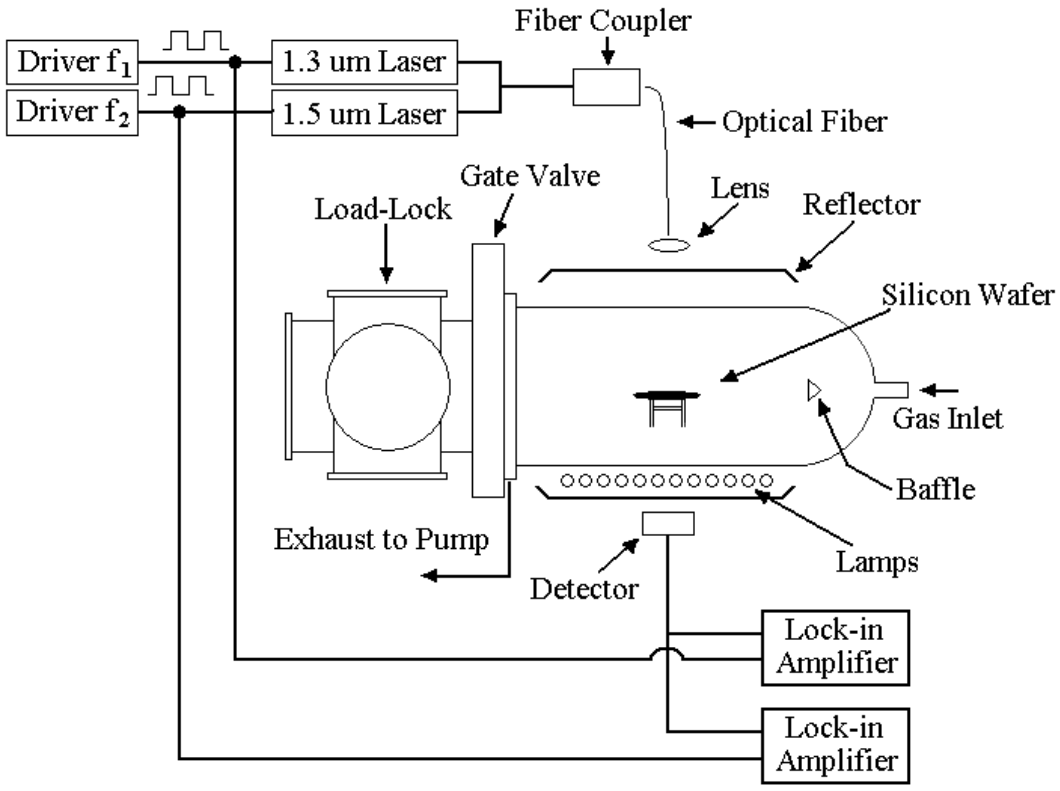

Figure 2.1. Schematic of the Princeton RTCVD. The reactor is an infrared-lamp-heated, cold-wall system. A load-lock is used to minimize the entry of moisture when transferring wafers into and out of the system. The wafer is suspended on four-tips of a quartz stand. A gold-polished reflector assembly in conjunction with a low thermal mass allows for rapid thermal applications. The gas flow direction is from left to right and is parallel to the wafer.

2.1.2 Neopentasilane Gas Delivery Panel

For growth with neopentasilane, a special gas delivery panel was installed into a ventilated cabinet in close proximity to the RTCVD reactor. Our existing hydrogen, main and vent lines are tied into the new cabinet. A detailed schematic of the changes made into our system is shown in the appendix. The gas delivery panel is shown in Figure 2.2 below:

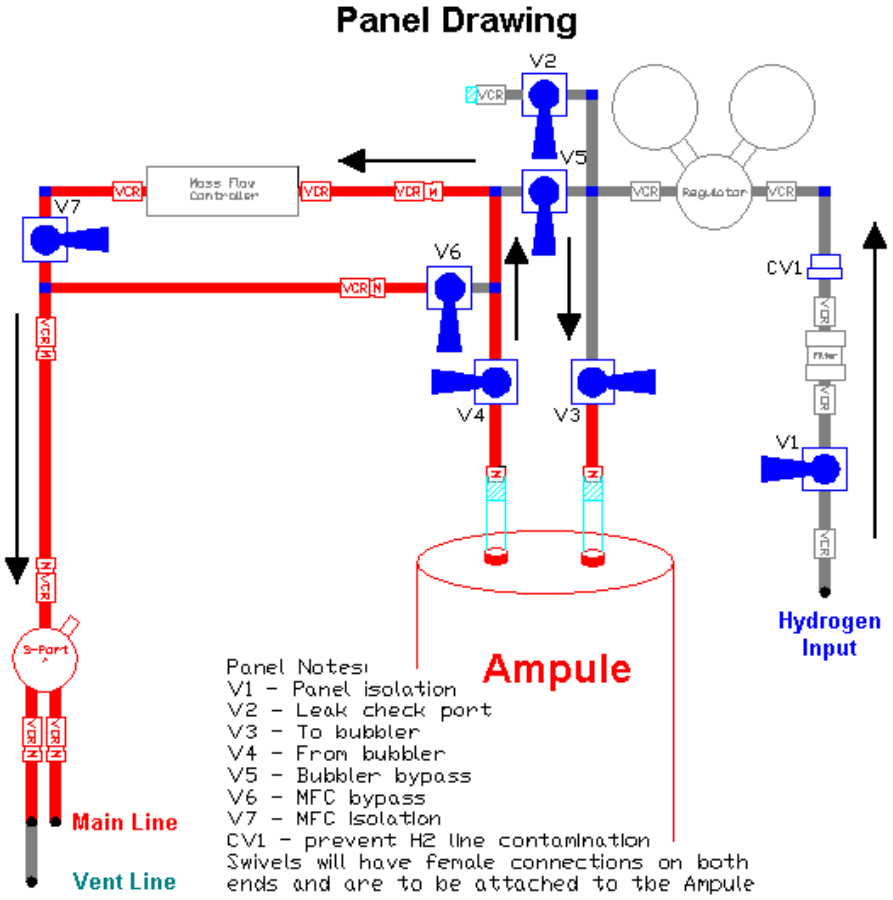

Figure 2.2. Schematic of gas delivery panel for neopentasilane (ampule). A bubbler system is contained in the ampule. Black arrows are used to show the direction of gas flow of hydrogen into the bubbler and NPS/Hydrogen bubbled out from the ampule. The gas then goes through the MFC and is injected into either the main line or the vent line. The plumbing shown in red is heated-traced at 55^{o}C. The plumbing was connected by "VCR" connections with a metal gasket. The swivel pieces to allow mechanical adjustment (coming out of the page) connecting to the ampule are shown in teal.

Hydrogen gas coming out from a Nanochem purifier is tied into the input side of the gas panel. The hydrogen passed through a filter (to remove unwanted particles) and the pressure is stepped down by the regulator to 0 psig (15 psia). A check valve (CV1) is there to prevent the backflow of NPS into the main hydrogen line. The hydrogen gas is then flowed into the input side of the ampule, in which the hydrogen is bubbled through the liquid NPS. From the output side of the ampule, the NPS/hydrogen mixture is controlled by the mass flow controller (MFC) and is injected into either the main chamber through the main line or into the vent line. The red plumbing lines shown in the figure above are heat traced to 55 ^{o}C. This is to prevent condensation in the gas lines, as NPS is a liquid source. The ampule is heated to 35 ^{o}C under normal conditions. V2 shown above is a leak check port. V5 is the ampule bypass valve that is used to flow hydrogen through the MFC instead of the NPS/hydrogen mixture. V6 is the MFC bypass valve (in case of MFC clogging). An air-operated automatic 3-port valve is used to select between the main line (to the chamber) and the vent line.

2.1.3 Difficulties with Liquid Source

The first growth experiments conducted with NPS resulted in relatively low growth rates, which were caused by the clogging of the mass flow controller (MFC). As a result the MFC was switched from a MFC designed for hydrogen to a MFC designed for dichlorosilane (DCS). A DCS MFC is believed to be less susceptible to clogging due to a larger orifice. All growth experiments are now done by flowing gas through the DCS MFC. The full range on the DCS MFC is 300 sccm (of DCS). Since most of our gas coming out of the bubbler is hydrogen, we use the calibration factor of 0.434 from DCS to hydrogen. For instance setting the MFC to flow 0.1 results in a flow rate of ~70 sccm and NOT 30 sccm (i.e. actual flow of hydrogen through a DCS MFC is 0.1 * 300 / 0.434

= 70 sccm). Despite the change to a DCS MFC, we still observed clogging of the MFC. An experiment was conducted at a growth temperature of 600 ^{o}C and 6 torr, using a MFC flow rate of 75 sccm (in addition to the 3 slpm hydrogen carrier flow through a different MFC). Growth was conducted on oxide substrates using two different growth times of 10 minutes and 20 minutes. The plot of silicon deposition vs. growth time is shown in Figure 2.3 below.

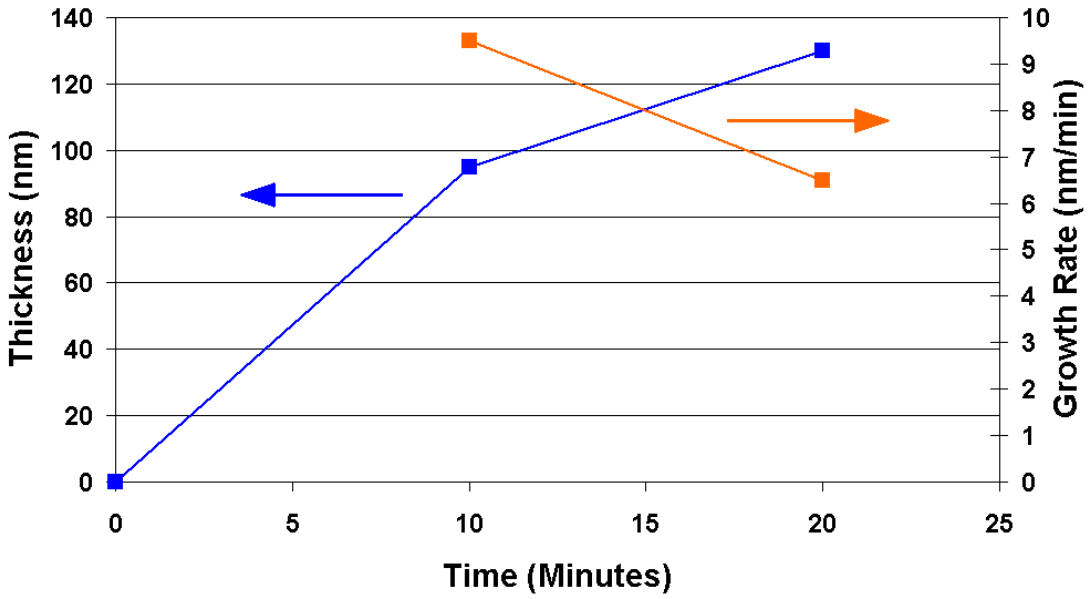

Figure 2.3. A plot of deposition thickness on oxide (blue) vs. growth time and the corresponding growth rate (orange) vs. growth time with the NPS bubbler flow of 75 sccm H_2. As shown in the plot above the thickness is NOT increasing linearly with growth time.

The deposition thickness on oxide was determined from Nanospec (which measures reflectance vs. wavelength) using the analysis program for polysilicon on oxide. (The film grown is actually amorphous, not polycrystalline, leading to an overestimate thickness error of around 10% due to the difference in the index of refraction of amorphous silicon vs. polysilicon). From Figure 2.3 above we observe that the rate of increase in the deposition thickness is decreasing with the growth time, corresponding

with a decrease in growth rate as shown on the secondary axis. This implies that the amount of gas coming from the MFC is decreasing with time, hence the reduction in growth rate over time. To test this theory we set up an experiment to measure if the quantity of gas coming out of the NPS MFC is constant with time. We fully open all valves in the chamber and closed all other sources. We used the equation Q = P * S, where Q is the gas flow, P is the pressure and S is the pumping speed of the pump. A separate experiment showed a pumping speed for hydrogen of 700 lpm. From the equation above we can determine the gas flow from our MFC based on the steady state chamber pressure. Three different MFC values (0.1, 0.3 and 0.4) were tested. The chamber pressure is plotted against the time. The result is shown in Figure 2.4 below:

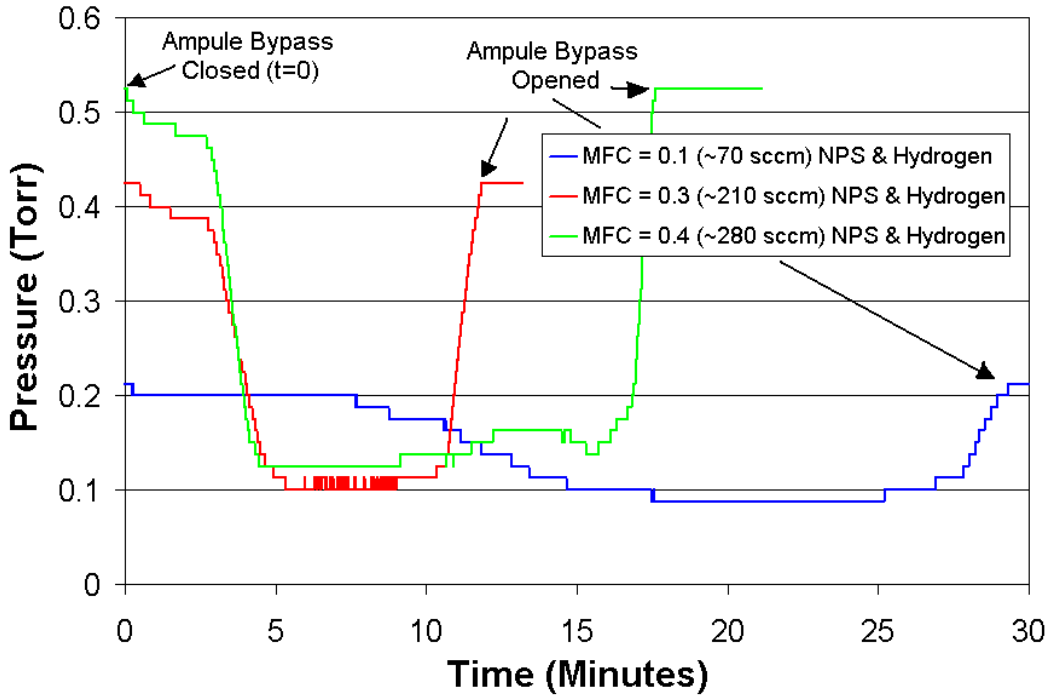

Figure 2.4. A plot of chamber pressure vs. the time of gas flow for three different settings of the MFC representing the hydrogen/NPS mixture. The gas (NPS/hydrogen mixture) from the ampule passing through the MFC was injected into the chamber at time 0. After several minutes the bypass valve was opened and hydrogen (only) was injected through the MFC.

Starting at time 0, the NPS/hydrogen mixture is coming directly from the ampule (see the schematic of Figure 2.2), with gas flowing through V3 into the ampule, out through V4, then into the MFC and then into the chamber. The pressure initially in all 3 experiments is proportional to the flow rate, after allowing for the chamber pressure to reach steady state (not shown in the plot). Then the pressure for all three cases begins to decrease with time indicating clogging. After several minutes, the ampule bypass valve V5 is then opened and V3 and V4 (the ampule valves) are closed. Now hydrogen is bypassing the ampule and flowing through the MFC. The chamber pressure begins to rise and saturates at its original value. The two higher flows of 0.3 and 0.4 clog the MFC in a shorter time (~ 5 minutes) than the lower MFC flow of 0.1 (~15 minutes). This clearly indicates that something coming from the NPS source gas is the culprit, which is clogging the MFC. We speculate that there may be microdroplets of liquid NPS coming out of the ampule and into the gas line. By flowing only hydrogen through the MFC (bypass configuration), the MFC can be unclogged (i.e. the NPS can evaporate). In Figure 2.5 below we plot the growth rate versus MFC flow rate for two different growth times of 10 minutes and 90 seconds.

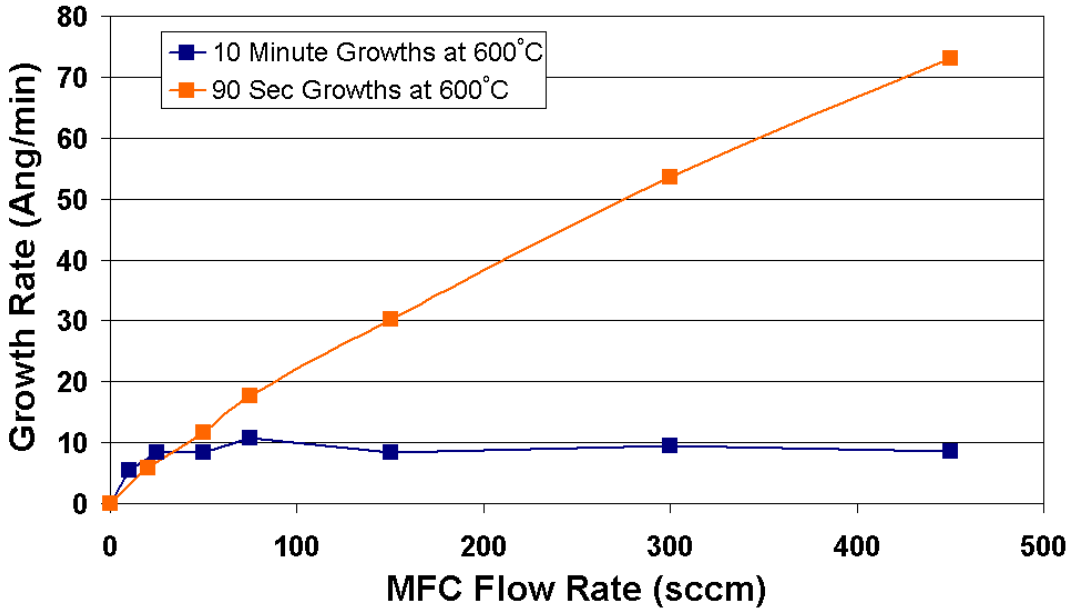

Figure 2.5. Plot of growth rate versus MFC flow rate at 600 ^{o}C using a growth time of 90 seconds and 10 minutes. The chamber pressure was held constant at 6 torr, and the hydrogen carrier flow of 3 slpm was used.

From Figure 2.5 above, we observe that the growth rate is increasing linearly with MFC flow rate for a short growth time (90 seconds) and saturates at an MFC flow rate of 50 sccm for a longer growth time (10 minutes). This implies that only short growth times (< 90 seconds) can be used for high MFC flow rates, to avoid clogging. This is consistent with Figure 2.4. For longer growth times only small MFC flow values can be used otherwise the MFC would clog over time. There was no clogging effect found using MFC flow rates of 50 sccm or less for flow times up to 30 minutes.

2.2 Properties of Neopentasilane

In this chapter we investigate silicon growth using the novel precursor neopentasilane. Neopentasilane, Si_5H_{12}, (Figure 2.6) was made from Dow Chemical and supplied to Princeton in an ampule (180 grams) through Applied Materials.

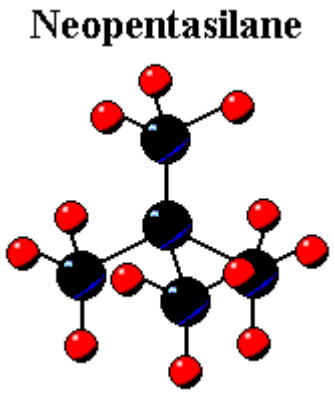

Figure 2.6. Chemical configuration of neopentasilane (NPS), Si_5H_{12} [2.4]. The large balls represent silicon atoms, and the small balls represent hydrogen atoms. The silicon atoms of neopentasilane are arranged in a tetrahedral fashion similar to a diamond lattice with the hydrogen atoms being the next nearest neighbors.

Neopentasilane is a branched silane with a silicon atom in the center, surrounded by four silicon atoms in tetrahedral positions, similar to crystalline silicon in a diamond lattice configuration. Neopentasilane is a liquid at room temperature with a vapor pressure of 15 torr. The vapor pressure follows the following equation [2.5]:

Equation 2.1 $\ln(P) = 49.8055 - 5610.77 / T - 4.0835 \ln(T) + 6.25243*10^{18} T^{6}$

where the units for P are in Pascal and T are in Kelvin. A plot of the vapor pressure vs. temperature of neopentasilane is shown in the Figure 2.7 below:

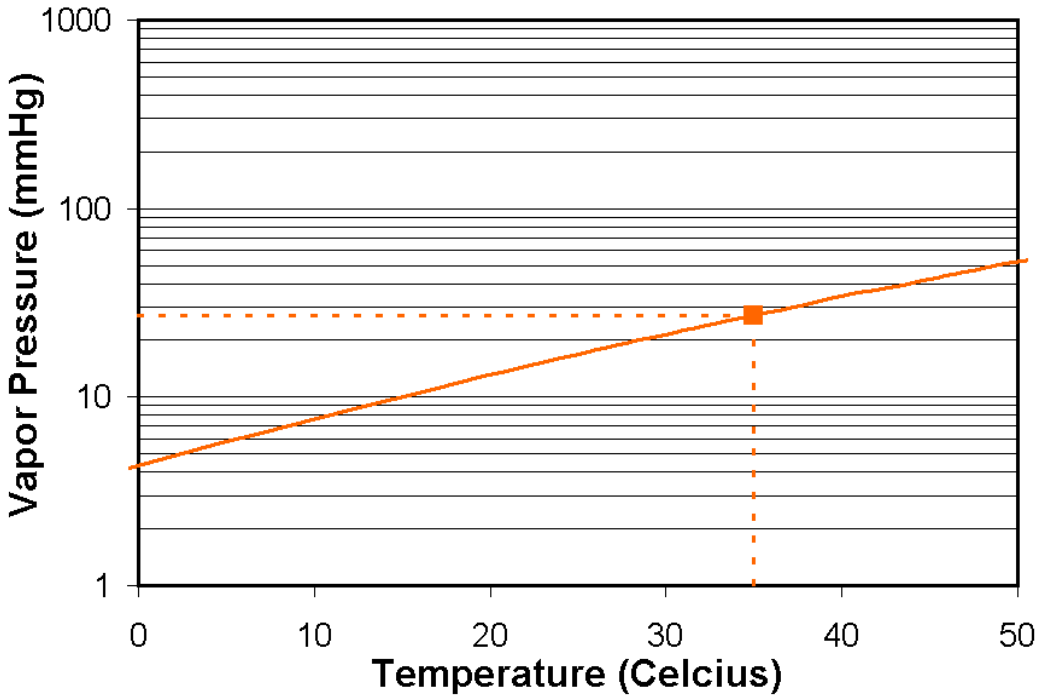

Figure 2.7. Plot of neopentasilane vapor pressure versus temperature (Celsius). Dotted lines indicate normal experimental conditions unless noted.

Our typical growth condition heats the ampule to 35 ^{o}C, corresponding to a vapor pressure of 30 torr. Hydrogen gas is bubbled through the ampule at an inlet pressure of 0 psig (15 psia). Assuming that the gas coming out is saturated (i.e. the hydrogen gas and the neopentasilane reach an equilibrium) the percentage of neopentasilane coming out of the ampule is 3.6% (NPS vapor pressure / hydrogen vapor pressure) of the hydrogen flowing through. Furthermore, if the bubbler is in saturation, the amount of NPS flow coming out of the bubbler should increase linearly with increasing vapor pressure. We will experimentally determine if the bubbler is in saturation by conducting growth rate experiments with different NPS ampule temperatures. Figure 2.8 below is a plot of growth rate vs. ampule temperature.

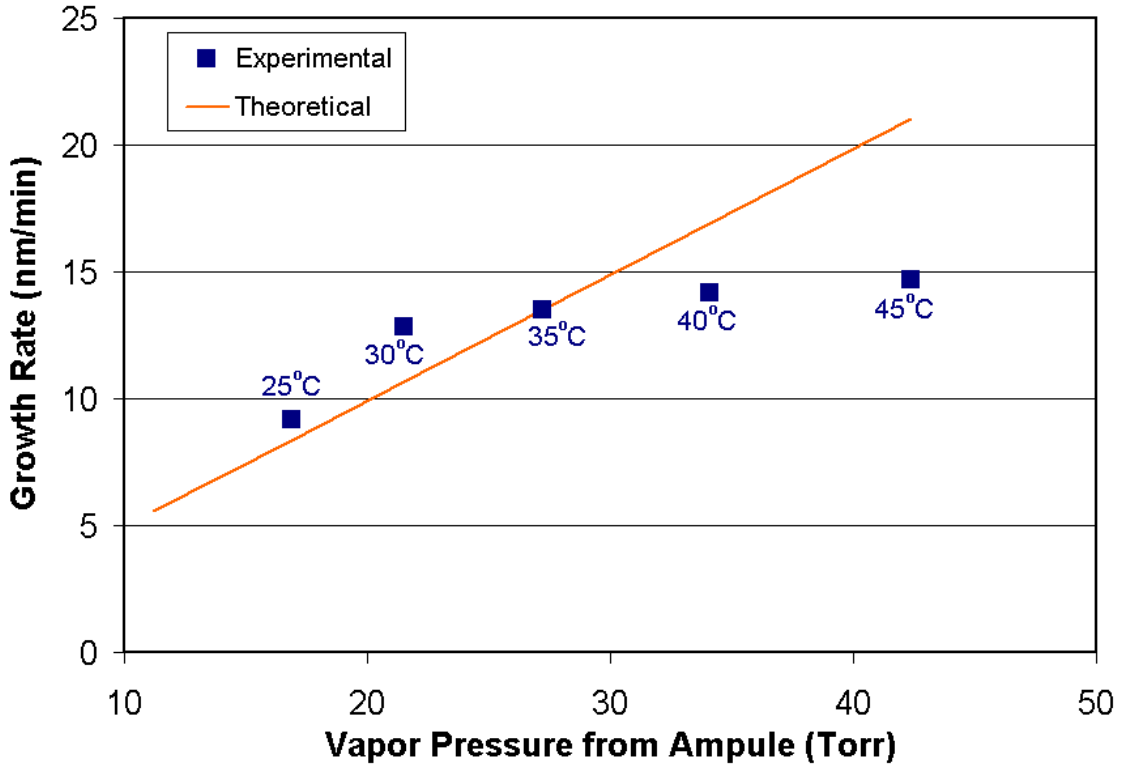

Figure 2.8. Growth rate vs. NPS ampule temperature. The theoretical data is calculated by assuming that the bubbler flow coming out of the ampule is in saturation, and extrapolating the growth rate assuming that the growth rate increases linearly with NPS flow based on the data point at 35 ^{o}C.

The theoretical values are calculated by assuming that the bubbler output is saturated with NPS. From this we can determine the NPS flow coming out of the bubbler. The theoretical growth rate is then linear extrapolated assuming that growth rate increases linearly with flow, and using the data point at 35 ^{o}C as the reference (i.e. NPS flow of each temperature corresponds to a growth rate based on the ratio of growth rate to flow rate at 35 ^{o}C). The experimental value is less than the theoretical value at temperatures higher than 35 ^{o}C and lower than the theoretical value at temperatures less than 35 ^{o}C. Therefore the NPS volume flow rate coming out of the bubbler is not increasing linearly with vapor pressure. The amount of NPS coming out of the bubbler is proportionally

smaller with the higher vapor pressures than the lower vapor pressures. This implies that the bubbler is not in saturation and that our earlier estimation of NPS flow rate based on saturation is an overestimation of the actual flow.

2.3 Epitaxial Growth with Neopentasilane

Growth rate experiments were done on prime grade <100> silicon wafers in our RTCVD system. It has been observed that an increased number of silicon atoms in hydride precursors (i.e. switching from silane, SiH_4 to disilane [2.6][2.7], Si_2H_6, to trisilane, Si_3H_8 [2.8][2.9]) leads to increased epitaxy growth rates at the same temperature under similar conditions and thus enables lower growth temperatures. Using our RTCVD system, we can compare the growth rates on <100> silicon wafers of four different precursors, dichlorosilane ($SiCl_2H_2$, chamber partial pressure = 52 mtorr), silane (SiH_4 , chamber partial pressure = 20 mtorr), disilane (Si_2H_6 , chamber partial pressure = 10 mtorr), and neopentasilane (upper limit (saturation approximation) to chamber partial pressure of 20 mtorr), with a 6 torr hydrogen carrier pressure, observed in our lab. Prior to loading into the reactor, the wafers were cleaned using a chemical mixture of sulfuric acid and hydrogen peroxide followed by a 2 min, dilute HF dip [2.10]. This is done to both remove surface contaminants and pre-passivate the surface with hydrogen. The growth rates were measured by step height measurements (See section 2.5) on patterned oxide wafers, one cm away from the center of the wafer, and are plotted in Figure 2.9 below:

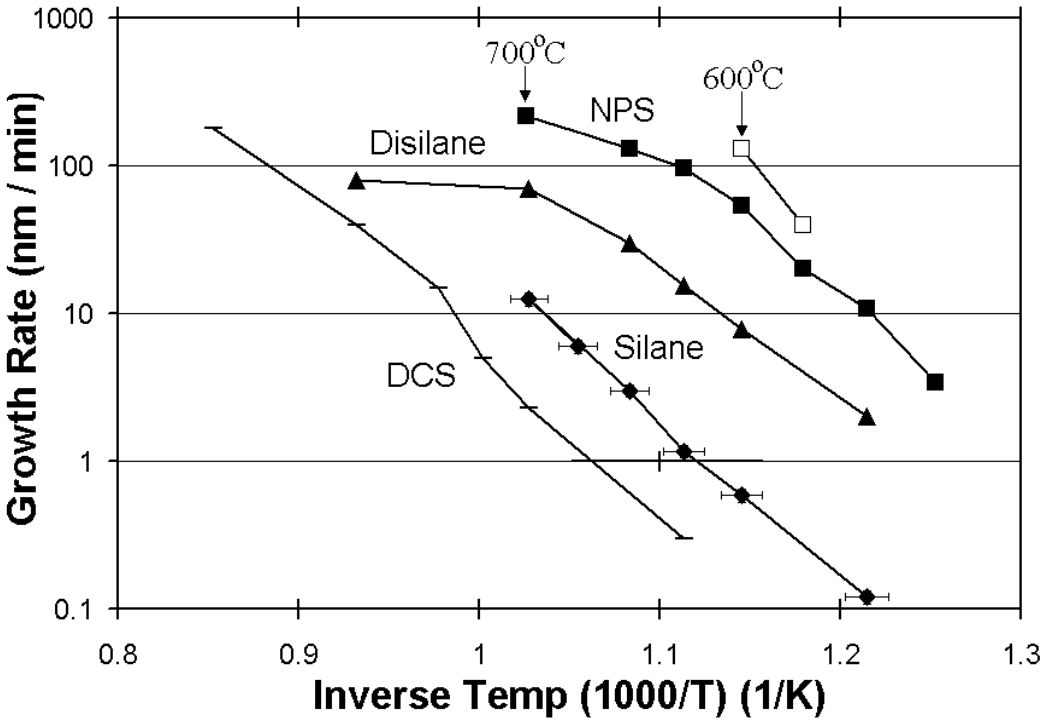

Figure 2.9. Comparison of low-pressure chemical vapor deposition (LPCVD) epitaxial growth rates vs. inverse temperature for sources of dichlorosilane (DCS), silane, disilane, and neopentasilane (NPS) precursor on (100) silicon substrates. In all cases the carrier was hydrogen at pressure of 6 torr. The dichlorosilane, silane, disilane and NPS partial pressures were 52 mtorr, 20 mtorr, 10 mtorr and 20 mtorr respectively. The open squares are NPS at a partial pressure of 65 mtorr. Estimated temperature error is +/- 1% and growth rate error is +/- 10%.

Comparing the growth rates at 600 ^{o}C, we observe that the growth rate of NPS is a factor of ten higher than the growth rate of disilane, and a factor of a hundred higher than the growth rate of silane. The growth rate of DCS at 600 ^{o}C is negligible. We will explain observed increase in the growth rate as the number of silicon atoms in the precursor is increased, in chapter 4 of this thesis. We believe a concerted reaction, not previously recognized, play an important role. The decrease of growth rate going from silane to DCS is to due a chlorinated vs. hydrogen-based chemistry [2.11]. The growth rate using neopentasilane increases linearly with partial pressure at 600^{o}C (Figure 2.10)

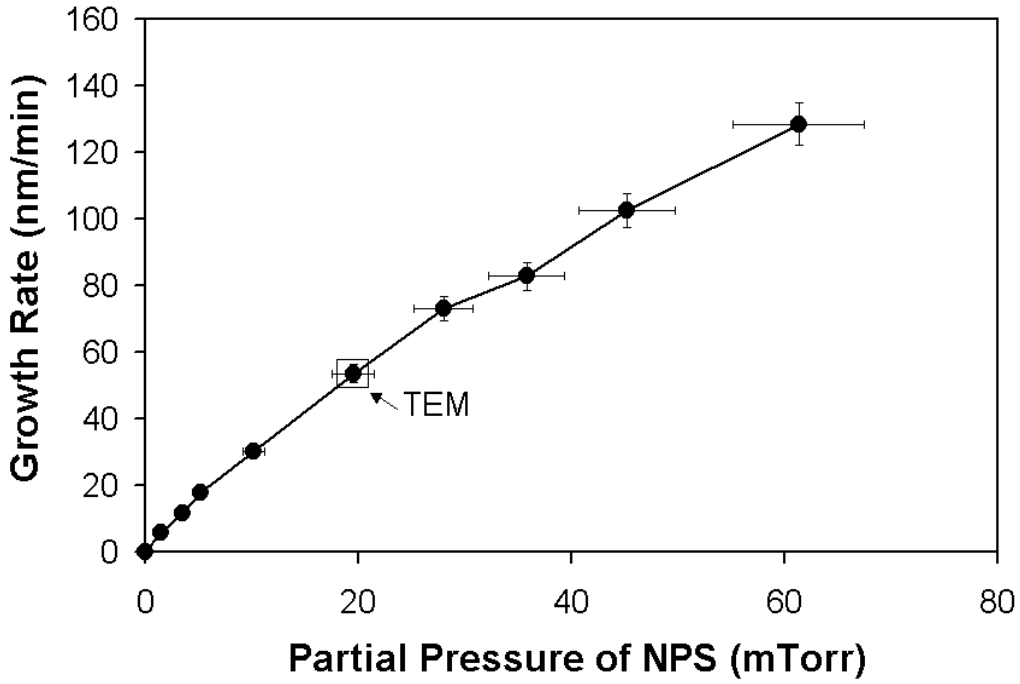

Figure 2.10. Growth rate at 600 ^{o}C in 6 torr hydrogen ambient vs. the partial pressure of neopentasilane (NPS). Error bars are shown to be 10% in growth rate and 10% in partial pressure. Partial pressure assumes flow through the bubbler is saturated. TEM of the indicated sample will be described in Chapter 3.

We have yet to observe any saturation of the growth rate with neopentasilane partial pressures. Classically, the growth rate at high partial pressures saturates because growth becomes limited by desorption of hydrogen [2.12]. A growth rate of 130 nm/min was achieved at the highest possible NPS partial pressure. To the best of our knowledge, this is the highest reported growth rate of crystalline silicon by a thermal process at 600 ^{o}C.

2.4 Growth on Oxide Substrates

2.4.1 Amorphous Silicon Growth with NPS

Growth of layers using NPS at 600 ^{o}C as the source gas was conducted on silicon wafers with patterned silicon dioxide on the surface. This was done mainly because reflectance spectroscopy allows rapid measurement of the thickness of silicon layers on silicon dioxide. UV reflectance was used to determine the crystallinity of the film. A plot of reflectance versus wavelength is shown in Figure 2.11 below:

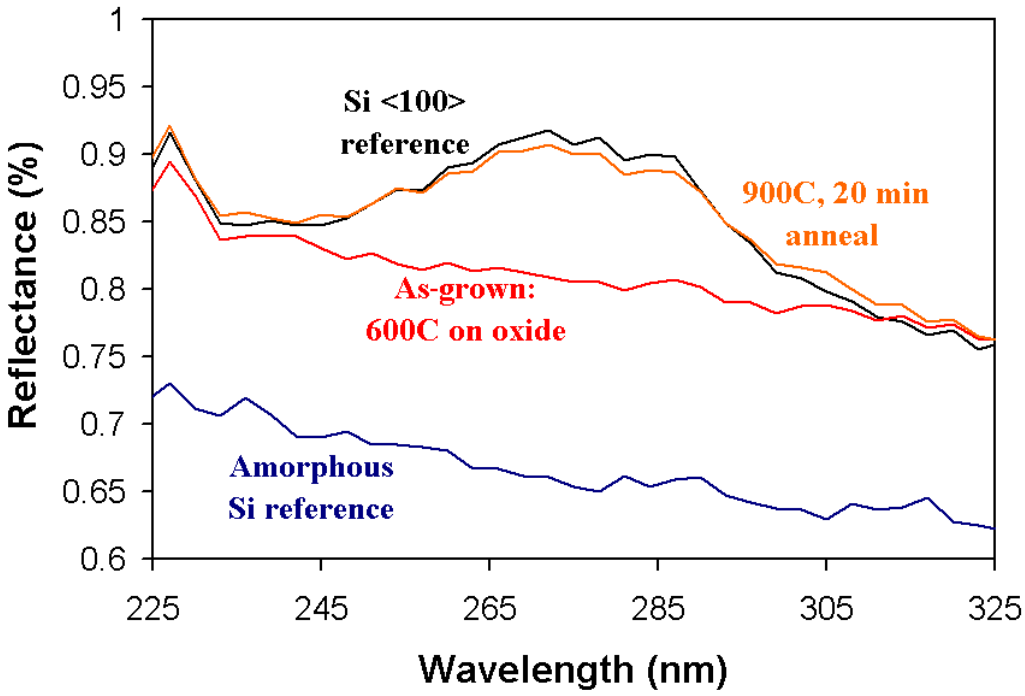

Figure 2.11. Plot of UV reflectance vs. wavelength. A Si <100> reference wafer, and an amorphous silicon reference wafer were used to compare the silicon layers grown on top of oxide substrates.

A silicon layer grown with NPS on top of oxide was compared with both a bare silicon substrate reference and an amorphous silicon sample. The UV reflectance plot of the

silicon layer grown on oxide with NPS is similar to that of the amorphous silicon reference. It lacks the peaks at 276 nm coming from the band structure of crystalline silicon [2.13]. The sample was then annealed at 900^{o}C for 20 minutes at atmospheric pressure in nitrogen. UV reflectance was then conducted on the annealed sample. From the plot we observe that the 276 nm peak can now be observed. This indicated that the crystalline structure has changed from amorphous to polycrystalline upon annealing. Furthermore, we found that unlike grown with silane on oxide, where there is a transition temperature (T > 580 ^{o}C) [2.14][2.15] between amorphous grown films and polycrystalline films, all silicon films grown on oxide using NPS were amorphous, up to a growth temperature of 700 ^{o}C. This maybe due to the combination of high growth rate and low surface mobility of adatoms.

2.4.2 Growth Rate of Amorphous Silicon versus Epitaxial Silicon

Patterned wafers with both oxide and bare silicon surfaces were used to determine the growth rate for both the epitaxy and the amorphous layer. The oxide thickness is determined using a surface profiler and is doubled checked using spectral reflectometry (Nanospec) before deposition. After deposition, the thickness of amorphous silicon is then determined using Nanospec. The epitaxy thickness is determined by from the step height using a surface profiler. The step height is then subtracted from the sum of the oxide and amorphous silicon thickness to give the thickness of the epitaxial layer. Figure 2.12a depicts the picture of the starting wafer and 2.12b illustrates a cross section after growth.

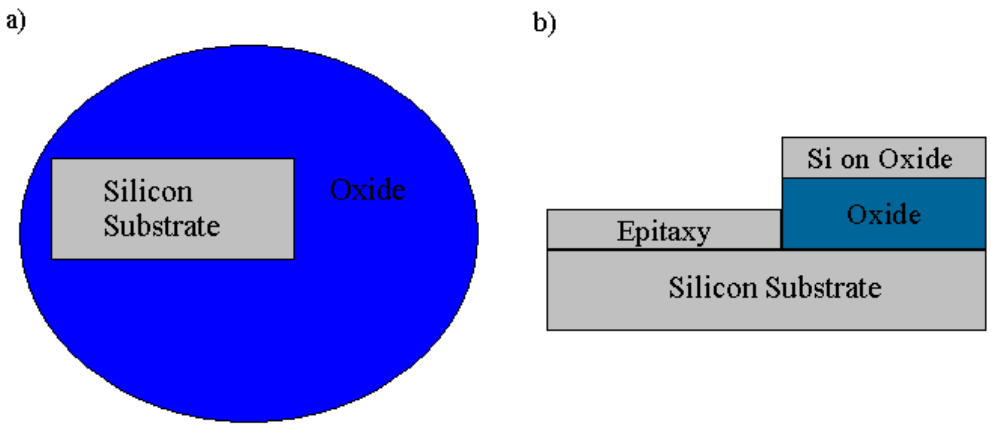

Figure 2.12a. Schematic diagram of the top view of the patterned wafers used in our growth experiments. 2.12b. Cross-sectional view of silicon deposition on both the silicon and the oxide part of the patterned wafer

2.4.3 Growth Patterns and Possible Gas Depletion

Typically in our system the growth thickness pattern is concentric circles, with the center of the wafer having the most growth and the edges having the least growth. This is due to the fact that the temperature is not uniform across the wafer, with the center at the highest temperature and the edge being the coldest. This implies that the source gas partial pressure is the same on the leading and trailing edge of the wafer. Shown in Figure 2.13 below are two samples of growth with NPS on an patterned oxide wafers with same pattern as Figure 2.12:

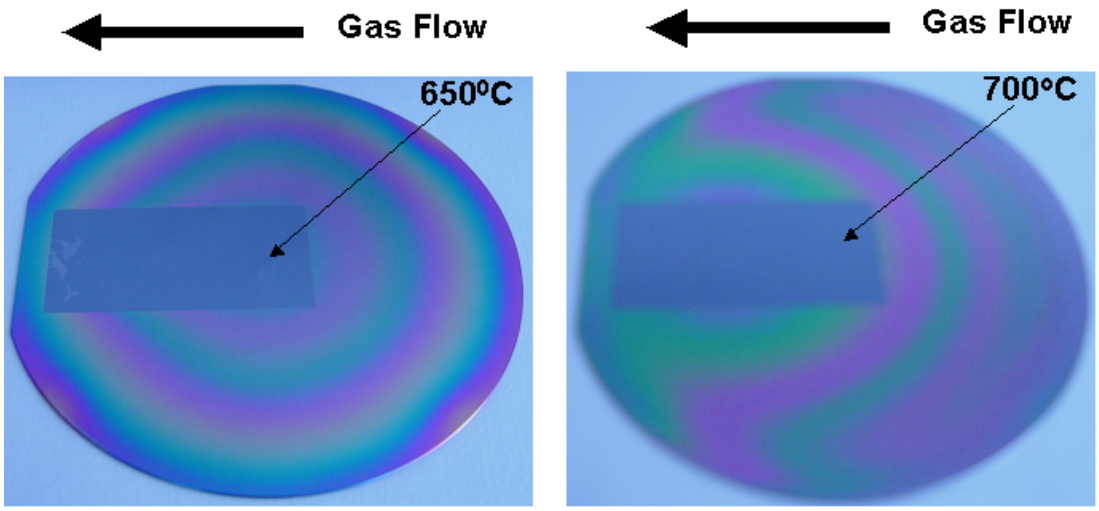

Figure 2.13. Pictures of the growth of two different temperatures (650 ^{o}C & 700 ^{o}C) on the patterned samples using the pattern shown in Figure 2.12. The growth temperature is measured at the center of the wafer. The colored patterns on the oxide are due to variations in growth temperature and NPS gas flow. The bubbler flow was 300 sccm and the growth time was 60 seconds.

The color variations of the rings are due to different thickness of amorphous silicon on oxide. We observed concentric rings in the left sample grown with NPS at 650 ^{o}C. In the right sample, we observed that the highest growth rate was not at the center of the wafer, but towards the edge (right) of the sample. The gas flow direction is from right to left. This indicated that the gas source is depleting as is moves across the surface of the wafer. In CVD processes where the gas reaction rates are very high, the source gas may be "depleted" as it moves across the wafer, causing the deposition rate in the center to be less than the deposition rate at the leading edge of the wafer. Due to this gas depletion and depressed NPS partial pressure in experiments conducted above 650 ^{o}C, experiments to understand fundamental growth mechanism with NPS were limited to 650 ^{o}C or below. At 700 ^{o}C the peak deposition thickness was 391 nm at 1 cm from the leading edge. At the center the deposition was 270 nm. On the other side of the wafer the deposition was 60nm.

2.4.4 Calculation of NPS Concentration in the Gas Output from the Ampule

Assuming that no gas phase reactions occur and that the depletion of the NPS is from reactions (deposition) on the wafer surface with 100% efficiency, (i.e. every NPS molecule reaches the surface and deposits 5 silicon atoms) we can calculate the partial pressure of NPS coming from the bubbler.

To determine the total amount of NPS coming out of the bubbler, we assume that all of the NPS molecules entering the chamber deposited on the wafer for 700 ^{o}C growth. We measured the deposition thickness on every 0.5 x 0.5 cm square on the first half of the wafer as shown in Figure 2.13, and then summed their numbers to determine the total volume of silicon deposited.

Eq. 2.2 Silicon atoms deposited = volume deposited x $5x10^{22}$ atoms / cm^3

The total number of silicon atoms deposited was determined to be $6.2 * 10^{19}$ atoms. We then convert this number into moles of silicon and then moles of NPS, where one mole of NPS has 5 moles of silicon atoms, all of which would deposit onto the surface. We determined that $2* 10^{-5}$ moles of NPS were used. In standard conditions 1 mole is approximately 24 liters, so the intended flow of actual NPS through the MFC was 0.5 scc. Since we flowed a total of 300 scc of NPS and hydrogen mixture through the bubbler, we can calculate the percentage of NPS coming from the ampule. We find that 0.17% of the gas coming out of the bubbler is NPS compared with 3.6% NPS assuming that the gas source is in saturation. This calculation provides us with the lower limit to the partial pressure of the amount of NPS coming out of the bubbler. Using the aforementioned result and the earlier calculation assuming saturation of the bubbler, the range of the gas fraction of NPS coming out of the bubbler is between 0.17% and 3.6%.

2.5 Particulates from the NPS Source.

The surface roughness of layers grown with NPS on a local scale is described in chapter 4. However, particles were detected on the surface of layers grown with NPS. Atomic force microscopy (AFM) was used to analyze the surface of the films grown with NPS. An epitaxial layer grown with NPS at 600 ^{o}C and a high growth rate of 54 nm/min with growth thickness of 80nm was analyzed and shown in Figure 2.14 below where the particulates are clearly evident.

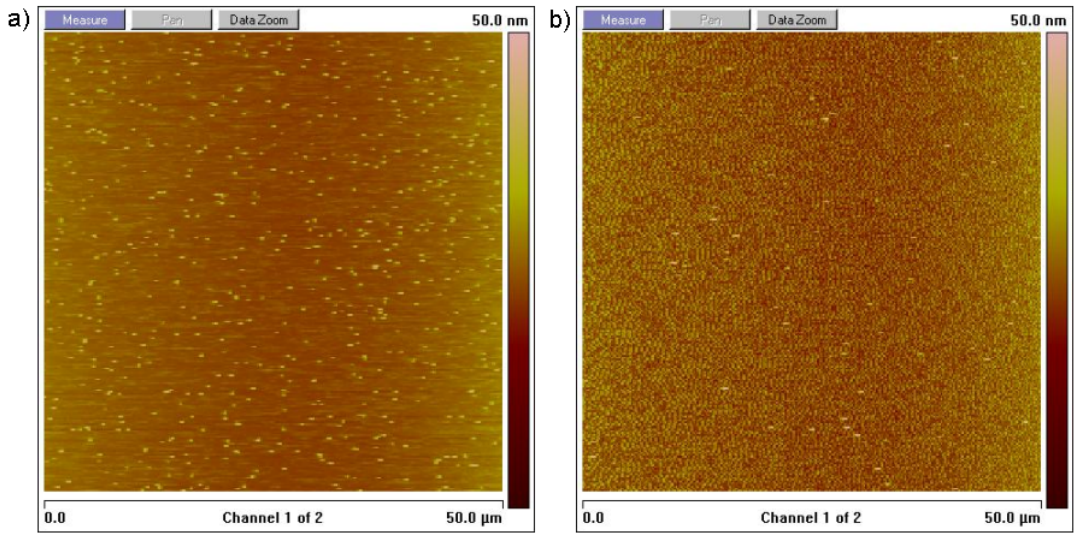

Figure 2.14. AFM scan of the surface of a wafer (polished side) with an NPS epitaxial layer grown at 600 ^{o}C with a growth rate of 54 nm/min. Shown in a) the polished side is facing upwards, in b) the polished side is facing downward. The growth thickness is 80 nm.

The surface roughness in areas without particulates is ~1nm RMS. The particulates can be either coming from the NPS source itself or due to homogenous deposition [2.16] (gas phase reactions). Furthermore, an NPS sample was grown upside down (i.e. polished side downward, etched side up) using the exact same conditions. The resulting surface was

then imaged and shown in Figure 2.14b. We observed that the number of particulates on the surface decreased significantly, indicating that something might be falling down into the surface. To differentiate between homogenous deposition and particulates raining onto the surface further experimentation was conducted.

A sample was loaded into our reactor and NPS was flowed into the chamber at room temperature without heating up the sample. Since no grown of silicon occurs at room temperature we can determine if the NPS ampule is ejecting particles, which are raining down onto the surface. The sample was then taken out of the reactor and an AFM scan of the surface was conducted. The result is shown in the Figure 2.15 below:

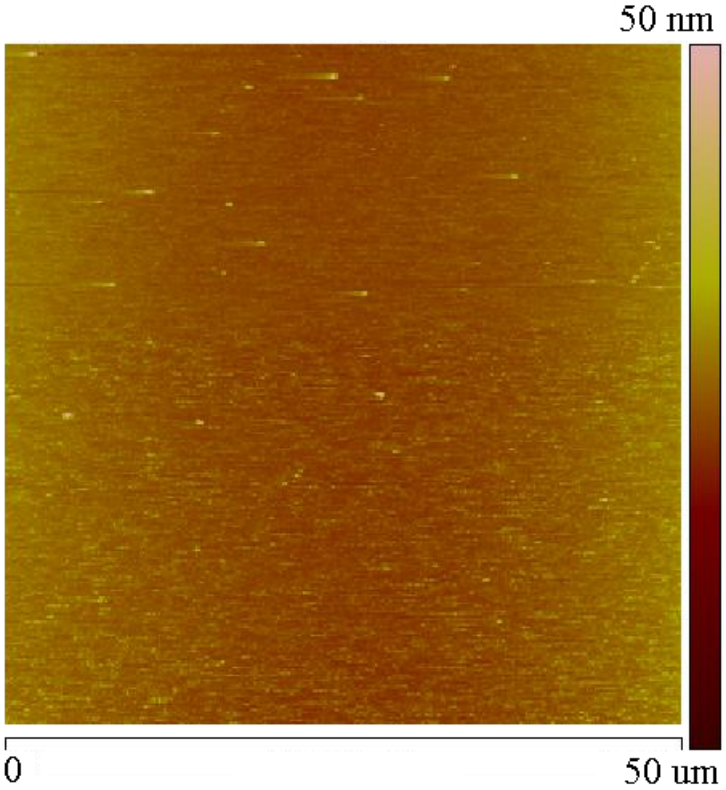

Figure 2.15. AFM of a sample loaded into the reactor chamber; NPS was then flowed at room temperature so no silicon layers were grown on the surface. The flow rate through the bubbler was 300 sccm, with 3 slpm hydrogen carrier for 90 seconds.

From the figure above we observe that particulates are raining down on the surface of the wafer without any silicon growth. This indicates that the particles observed in the previous AFM scans are coming from the NPS ampule. Based on previous evidence from the temporary clogging of the MFC in section 2.1 and the AFM scans, we speculate that the particulates may be microdroplets of liquid coming from the NPS source itself. However, data was difficult to reproduce and the results were not conclusive. A "spinner" piece, provide by Applied Materials, was temporarily inserted in front of the MFC (Figure 2.2) to eliminate the microdroplets. The piece of plumbing did not have any significant effect on the number of particulates observed on the surface and was removed.

2.6 Summary

In this chapter, we described the experimental Princeton RTCVD apparatus and the NPS cabinet and gas delivery panel. Due to the low vapor pressure of NPS, the source ampule was both heated and bubbled with hydrogen. There was also a temporary clogging of the MFC when large amounts (>50 sccm) of NPS gas are flowed for times of 5 minutes or greater. Growth with NPS leads to significant growth rate enhancement, when compared with other silanes, for similar growth conditions. CVD Silicon growth using NPS on oxide substrates were amorphous for all temperatures. Gas source depletion was observed at growth temperatures above 650 ^{o}C inhibiting our ability to conduct experiments at elevated temperatures. A calculation of the amount of NPS entering the chamber coming from the ampule when it is bubbled with hydrogen was conducted based on gas source depletion. Based on AFM surface scans, there are particulates arising from the NPS gas source.

Chapter 3
Characterization of Epitaxial Silicon Layers Grown with Neopentasilane

3.1 Introduction

In this chapter we will evaluate the crystal quality of the layers grown with NPS. Cross sectional transmission electron microscopy (x-TEM) was used to examine crystal structure. Secondary Ion Mass Spectrometry (SIMS) was used to evaluate the background impurities of the layers grown with NPS. Photoluminescence (PL) was used to characterize the minority carrier lifetimes. Field Effect Transistors (FETs) were fabricated with epitaxial layers grown with NPS and analyzed.

Silicon layers with NPS can be grown at very high growth rates and low temperatures (>650^{o}C). For instance, at 600 ^{o}C and 6 torr, using a NPS partial pressure of 20 mtorr, and a deposition time of 90 seconds, the growth rate is 54 nm/min. This growth rate is significantly faster than the growth rate using conventional gases such as dichlorosilane (DCS) and silane. For comparison, to obtain similar growth rates using silane and DCS in our reactor system, we would need to raise the temperature to 750 ^{o}C and 800 ^{o}C respectively. This is a reduction of 150-200 ^{o}C thermal budget for the same growth rate.

At such high rates and low temperatures the layers grown may not be crystalline. In the past with MBE studies, it has been shown that there is a concept of a maximum epitaxial thickness for a given growth temperature and growth rate [3.1]. Incoming adatoms have to diffuse to the proper surface sites in order to maintain crystalline growth.

This surface diffusion is affected by the growth temperature. In Figure 3.1a below, for a given growth rate of 0.7 Å/s by MBE, the maximum epitaxial thickness prior to the breakdown of epitaxy and transition to an amorphous film is shown. This indicates that for higher growth temperatures one can grow a thicker epitaxial layer prior to the transition to an amorphous growth.

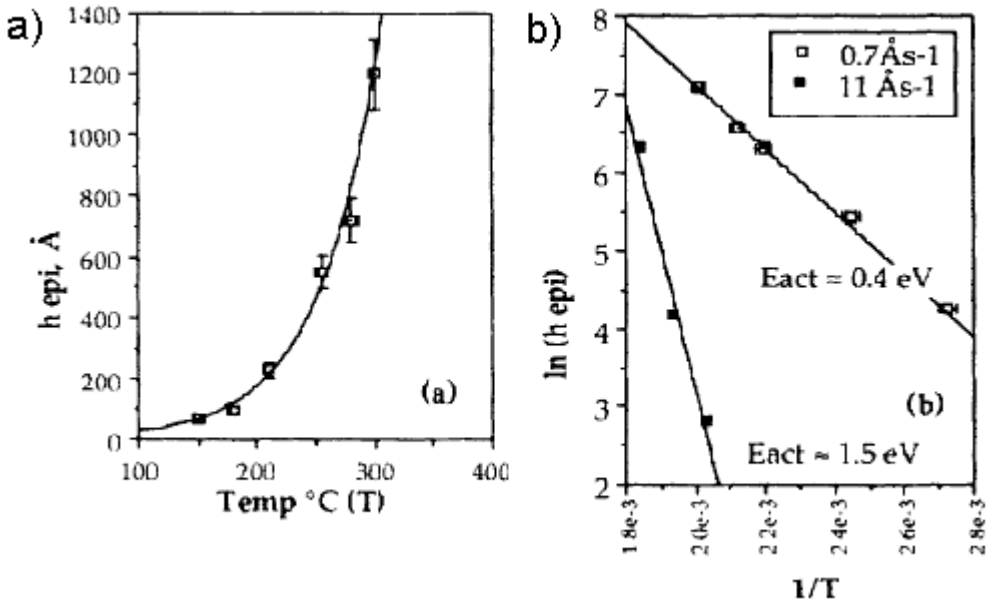

Figure 3.1a. Temperature dependence of the limiting epitaxial thickness h_{epi} along with (b) the same data plotted in Arrhenius form at growth rates of both 0.7 and 11 Å / s. The Figures are from reference [3.1] for MBE. The very steep increase near 200 ^{o}C in (a) explains why previous reports of an epitaxial temperature [3.2][3.3][3.4] usually close to this value. The activation energy suggested by the Arrhenius plot is 0.4 eV at 0.7 Å / s and 1.5 eV at 11 Å / s.

Furthermore, it was found that for the same temperature, a higher growth rate led to a thinner epitaxial layer prior to the transition to amorphous growth (Figure 3.1b). This implies that if either the growth rate is too high or if the temperature is too low, then the surface adatoms do not have enough time to diffuse to the proper growth sites. As a result the growing surface will increase in disorder and the epitaxy would breakdown into an

amorphous layer [3.1]. It was previously thought that there was a limiting epitaxial temperature (i.e. epitaxy can only be grown above a certain temperature) at roughly 200 ^{o}C [3.2][3.3][3.4]. This was due to the steep increase in the limiting epitaxial thickness at 200 ^{o}C. Since our growth rates with NPS are orders of magnitude higher than that with conventional gases (DCS and silane), we would like to observe if there are any limit of epitaxial growth rates with CVD.

3.2 Cross Sectional Transmission Electron Microscopy

We will examine the crystal quality using cross-sectional transmission electron microscopy (X-TEM) of an epitaxial layer with NPS at 600 ^{o}C and 6 torr with growth rate of 54 nm/min and thickness of 80 nm. The X-TEM micrograph is shown in the Figure 3.2 below:

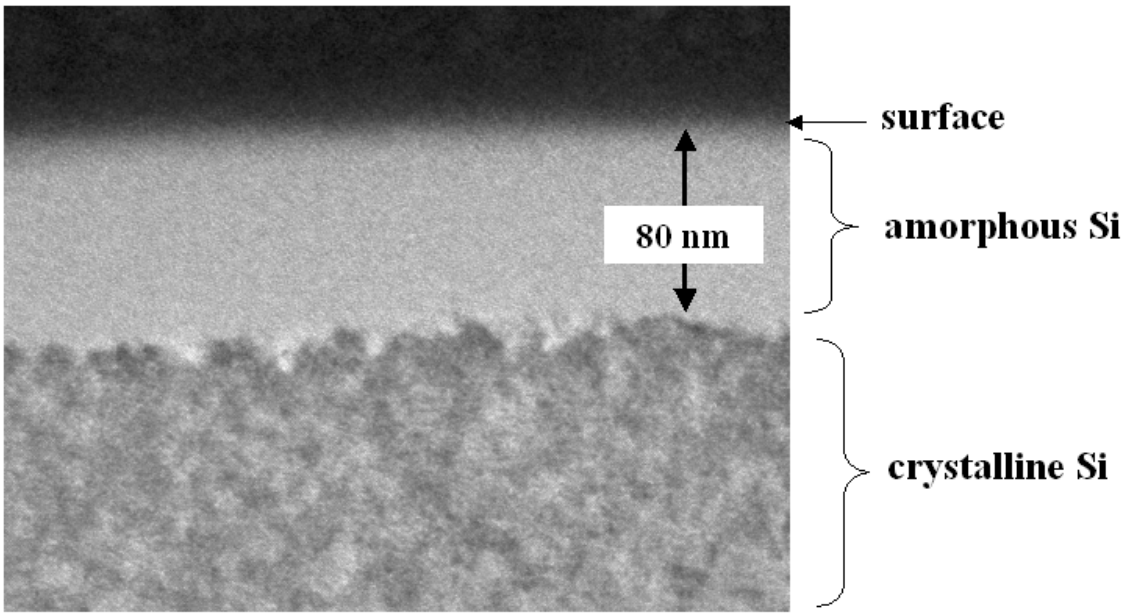

Figure 3.2. Initial cross-sectional transmission electron microscopy (X-TEM) of a sample grown with NPS at 600 ^{o}C, 6 torr, with growth rate of 54 nm/min. The grown layer was estimated to be ~80 nm from growth rates as well. Sample preparation and image courtesy of Dr. Nan Yao.

In the cross-sectional transmission electron microscopy above, we observed that our layer grown with NPS was an amorphous layer. This led us to believe that there might be limiting epitaxial thickness in CVD similar to the aforementioned phenomena with MBE. However, we later discovered that our TEM sample preparation (which involved Pt deposition in a focused ion beam at high energy directly on the silicon surface) was causing the top layer to become amorphous. We switched to a different sample preparation technique and took another TEM image (Figure 3.3).

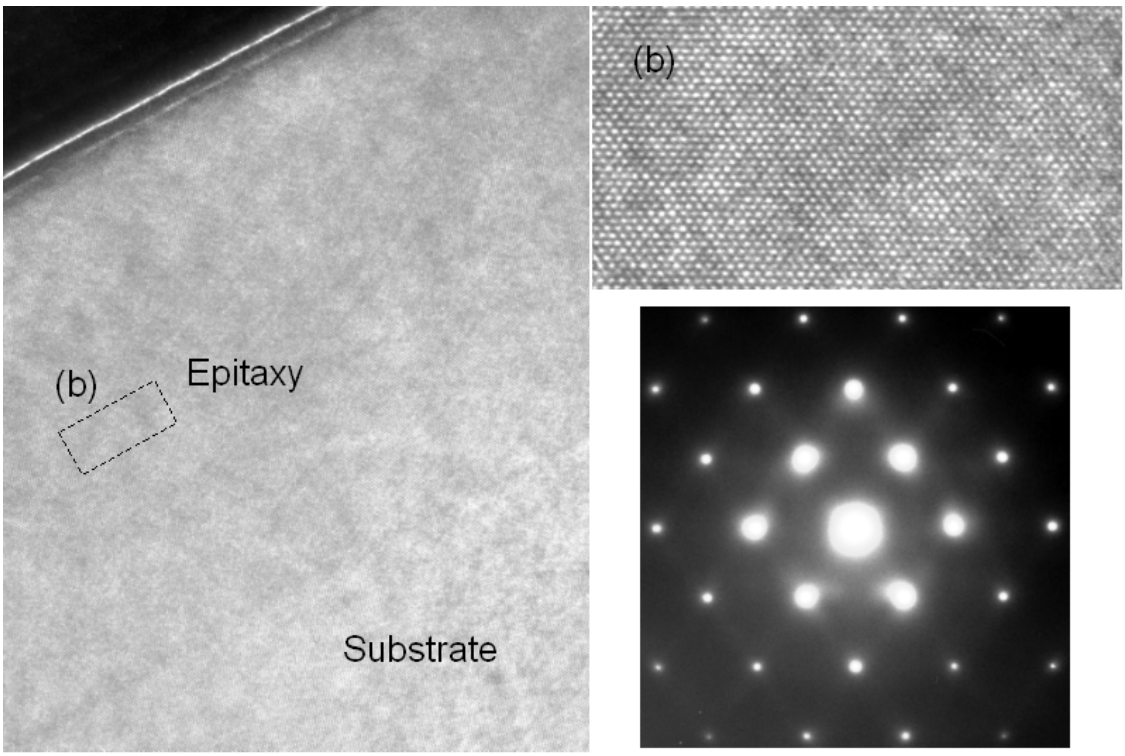

Figure 3.3. Cross sectional transmission electron microscopy of a sample grown with NPS at 600 ^{o}C, 6 torr, with growth rate of 54 nm/min prepared without platinum deposition along with closeup of region (b) and electron diffraction pattern. The epitaxy layer thickness was 80 nm.

As observed from the high resolution image (b), from the selected region of (b) the growth is single crystalline. Shown in the inset is an electron diffraction pattern, indicating good crystalline quality despite the high growth rates and reduced epitaxy temperatures. Thus, the limit of the epitaxial thickness, if any, at 54 nm/min and 600 ^{o}C, is greater than 90 nm.

3.3 Secondary Ion Mass Spectrometry

Next we will check the impurity concentrations in epitaxial layers arising from our NPS gas source. Secondary ion mass spectrometry (SIMS) was used to determine the background contaminants in the epitaxial layers. The SIMS result of the sample corresponding with the TEM shown above is shown in Figure 3.4 below:

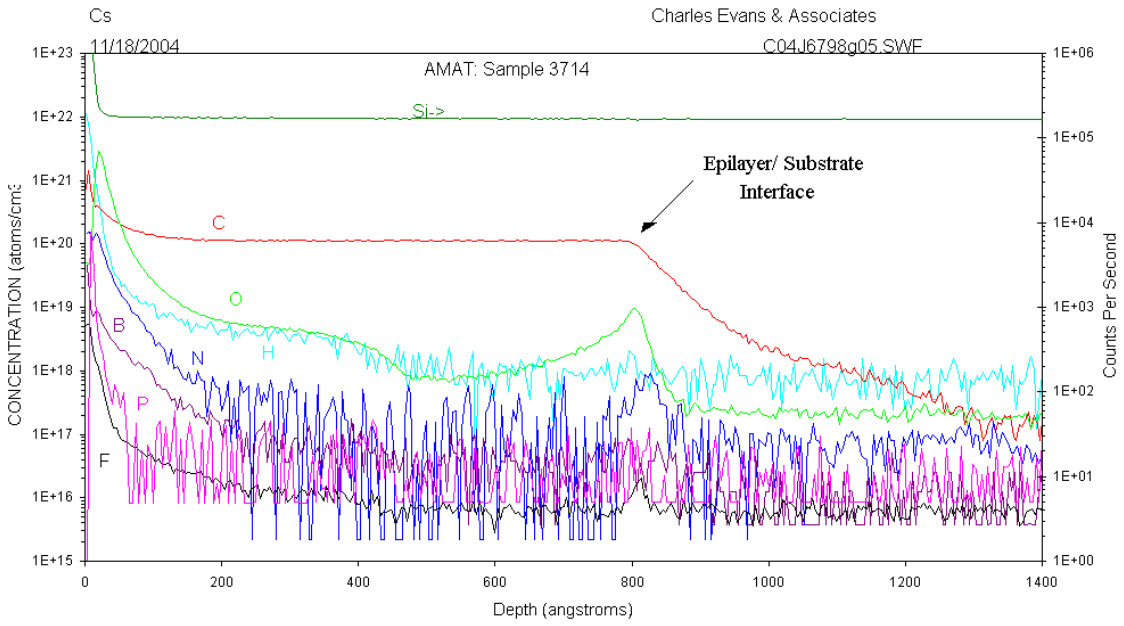

Figure 3.4. SIMS of an NPS sample grown at 600 ^{o}C with a growth rate of 54 nm/min. The oxygen peak at the start of growth interface due to a lack of in-situ cleaning prior to growth.

No in-situ cleaning was conducted prior to epitaxy growth. As a result we can observe an oxygen peak at the interface between the substrate and the epitaxial layer. The phosphorus, boron, and fluorine concentrations in the epitaxial layer are below the SIMS resolution limit of $5x10^{16}/cm^3$. The oxygen concentration is on the order of $10^{18}/cm^3$, and the carbon level is high, $\sim10^{20}/cm^3$. We believe that the carbon and the oxygen levels are due to an impure NPS source.

In the table below we compare the background impurities of silicon layers grown at different temperatures (ranging from 550 ^oC to 700 ^oC) using four different precursors (DCS, silane, disilane and NPS) available in our reactor system. Of special note is the phosphorus background level. With DCS as the silicon source the phosphorus level for layers grown in our system is usually around $10^{17}/cm^3$. Dopant incorporation using high-order silanes will be discussed in chapter 7. Also, the oxygen concentration in the epitaxial layers grown with NPS is increasing with decreasing temperature. This is due oxygen being more stable at the lower temperatures [1.13] and an impure NPS source.

Table 3.1. Comparison of the background impurity levels of silicon layers grown with different precursors and temperatures in our RTCVD system.

Precursor	Temp	Growth Rate (nm /min)	Oxygen	Carbon	Phosphorus	Boron
NPS	**550**	**2**	**10^{18}**	**$2 * 10^{20}$**	**$< 5 * 10^{16}$**	**$< 5 * 10^{16}$**
NPS	**575**	**6**	**$7 * 10^{17}$**	**$2 * 10^{20}$**	**$< 5 * 10^{16}$**	**$< 5 * 10^{16}$**
NPS	**600**	**54**	**$8 * 10^{17}$**	**$1.2 * 10^{20}$**	**$< 5 * 10^{16}$**	**$< 5 * 10^{16}$**
NPS	**650**	**130**	**$4 * 10^{17}$**	**$1.2 * 10^{20}$**	**$< 5 * 10^{16}$**	**$< 5 * 10^{16}$**
NPS	**700**	**270**	**$2 * 10^{17}$**	**$1.5 * 10^{20}$**	**$< 5 * 10^{16}$**	**$< 5 * 10^{16}$**
Disilane	**550**	**2**	**$\sim 10^{17}$**	**$\sim2 * 10^{17}$**	**$< 5 * 10^{16}$**	**$< 5 * 10^{16}$**
Disilane	**575**	**6**	**$\sim 10^{17}$**	**$\sim2 * 10^{17}$**	**$< 5 * 10^{16}$**	**$< 5 * 10^{16}$**
Disilane	**600**	**12**	**$\sim 10^{17}$**	**$\sim2 * 10^{17}$**	**$< 5 * 10^{16}$**	**$< 5 * 10^{16}$**
Disilane	**625**	**20**	**$\sim 10^{17}$**	**$\sim2 * 10^{17}$**	**$< 5 * 10^{16}$**	**$< 5 * 10^{16}$**
Silane	**625**	**0.8**	**$\sim 10^{17}$**	**$\sim2 * 10^{17}$**	**$< 5 * 10^{16}$**	**$< 5 * 10^{16}$**
Silane	**700**	**8.5**	**$\sim 10^{17}$**	**$\sim2 * 10^{17}$**	**$< 5 * 10^{16}$**	**$< 5 * 10^{16}$**
DCS	**700**	**3**	**$\sim 10^{17}$**	**$2 * 10^{17}$**	**$\sim10^{17}$**	**$< 5 * 10^{16}$**

3.4 Photoluminescence of NPS Epitaxial Layers

To further characterize the quality of epitaxial layers grown at high growth rates with neopentasilane, photoluminescence (PL) experiments at 77K were conducted. Photoluminescence is widely used as a tool for determining the quality of epitaxial heterostructures. A laser (514 nm) was used to generate free carriers into the silicon epitaxy layers. The adsorption depth is about 1 micron in silicon [3.5]. The free carriers then diffuse into the SiGe quantum well where they can recombine radiatively (luminesce). If either the silicon layer or the SiGe layer has many defects (midgap states) the free carriers would recombine non-radiatively and the luminescence intensity would be substantially decreased or non-existent. The luminescence is illustrated in the schematic shown in Figure 3.5 below:

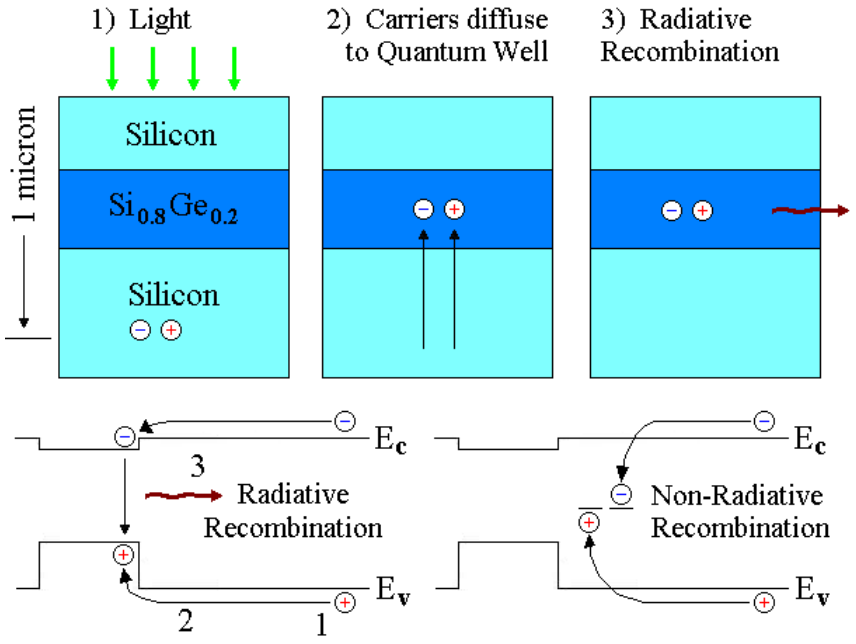

Figure 3.5. Schematic of the cross-section for a Si / SiGe /Si quantum well and its corresponding band diagram illustrating the photoluminescence technique. Carriers are generated from a green light source at 514nm, at an average depth of 1 micron. The carriers can then diffuse into the quantum well where they can recombine radiatively and luminesce. If the epitaxy layer were highly defective, the carriers would recombine non-radiatively.

The typical structure that we used for our PL experiment is comprised of a 20% SiGe layer sandwiched in between two Si layers as shown a) of Figure 3.6 below:

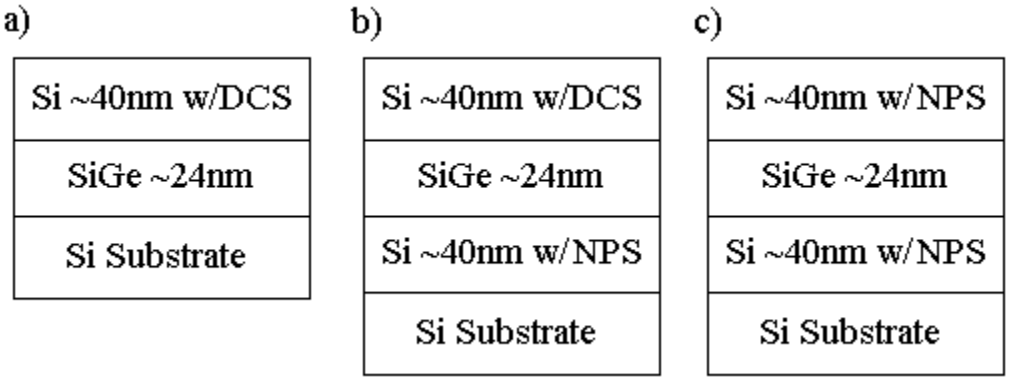

Figure 3.6. The PL structures used for the comparison of epitaxy quality of DCS versus NPS. The top silicon cap prevents carriers in the SiGe layers from recombining at the surface.

The growth temperatures for the silicon layer (except the layers grown with NPS) and SiGe layer are 700 ^{o}C and 625 ^{o}C respectively. Unless noted in Figure 3.6, DCS was used as the silicon source in all layers. In structures b and c, an underlying silicon layer is grown with NPS at 600 ^{o}C with growth rate of 54 nm/min right before the growth of the SiGe layer. Structure (a) is a control sample with all silicon layers grown with DCS. In our experiments all the SiGe layers were grown with DCS and germane, as we were unable to grow SiGe layers with 20% germane using NPS as the silicon source. In structure b) only the layer below the SiGe layer is grown with NPS, and in structure c) both the Si underlayer and the Si cap layer were grown with NPS. The photoluminescence results are plotted in Figure 3.7 below:

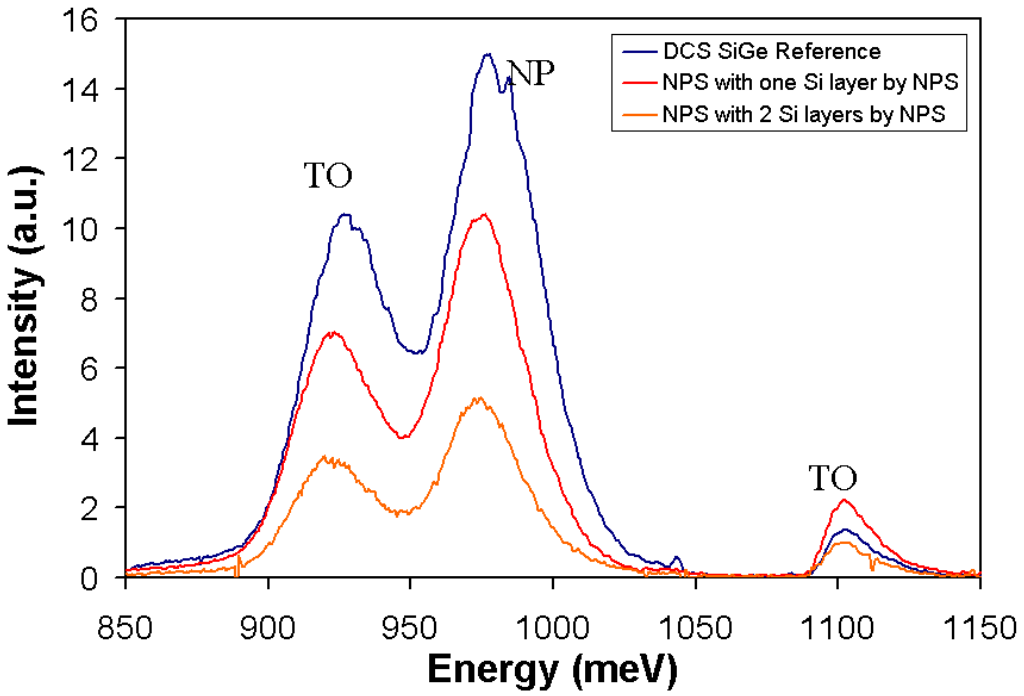

Figure 3.7. Photoluminescence of Si/SiGe/Si quantum wells grown using DCS and NPS as the silicon source The SiGe layer was grown at 625 ^{o}C using DCS and germane. The transverse optic (TO) phonon peak are shown for both the SiGe and Si layers. There is also a no-phonon (NP) peak in the SiGe layer due to alloy scattering [3.6][3.7].

We observe that there are 3 peaks arising at peaks heights of 925, 980 and 1100 meV respectively. These 3 peaks correspond to the TO (transverse optical) phonon replica and the NP (no-phonon) transitions of $Si_{0.8}Ge_{0.2}$, and TO phonon transition of the silicon substrate, respectively. The NP of SiGe is due to random alloy scattering and is used as a measure of the band gap [3.6]. The intensity of these peaks corresponds to the lifetime of the carriers in the layers. Comparing the height of the SiGe TO peak to that of the silicon TO peak in the reference sample, we observe a ratio of 8 to 1. In the two NPS samples the ratio was only 3 to 1. This indicates that the quality of the silicon epitaxy grown with NPS is not as good as the epitaxy grown with DCS at 700 ^{o}C. Since we have observed earlier from TEM that the crystalline quality of NPS is excellent, the decrease is possibly

related to the high oxygen and carbon concentrations (10^{18} cm^{-3} and 10^{20} cm^{-3}) in the films. Oxygen and interstitial carbon can lead to midgap states in crystalline silicon, which can lead to non-radiative recombination and decrease the PL intensity in the NPS samples.

3.5 Surface Roughness of Silicon Epitaxial Layers grown with Silanes

Due to the high growth rates, the resulting surface of the epitaxial layers grown may be rough. The surface roughness of the epitaxial layers grown with NPS were examined by atomic force microscopy (AFM). We observed smooth surfaces between regions with particulates of unknown origin lying on the surface. The surface roughness (not including the particulates is approximately 0.3 nm RMS for a sample with a growth rate of 54 nm /min at 600 ^{o}C. The surface of epitaxial layers between the particulates is surprisingly smooth despite the ultra-high growth rates. This data is examined in detail along with the proposed growth mechanism in chapter 4 of this thesis.

3.6 Fabrication of FET's with Silicon Epitaxial Layers Grown with NPS

To characterize the quality of the epitaxial layers grown with neopentasilane, p-channel and n-channel field effect transistors (FETs) were fabricated using a self-aligned polysilicon gate process. Approximately 200 nm of epitaxy using the neopentasilane precursor was grown on blanket n-substrate and p-substrate <100> silicon wafers by chemical vapor deposition (CVD) at 600 ^{o}C and 650 ^{o}C. Prior to loading into the reactor,

the wafers were cleaned using a chemical mixture of sulfuric acid and hydrogen peroxide followed by a 2-minute dilute HF dip [3.8]. The samples were then cleaned in-situ via 900 ^{o}C, 2-minute bake in hydrogen (5 torr) prior to the start of growth to remove any residual oxygen and carbon on the surface [3.9][3.10]. The growth rates were 55 and 75 nm/min at 600 ^{o}C and 130 and 180 nm/min at 650 ^{o}C. The epitaxial layers were not intentionally doped. As shown previously in section 3.3, the background doping levels are below the SIMS resolution limit of ~5x10^{16}/cm^{3} for both boron and phosphorus doping levels. FETs were also fabricated directly on n-type (10^{15}/cm^{3}) and p-type (5x10^{14}/cm^{3}) <100> silicon substrates as control samples.

The FET's were made using a ring geometry to avoid the need for field isolation; i.e. all the current from the source to drain has to pass through under the gate. Figure 3.8 shows top and cross sectional views of the fabricated ring-FET.

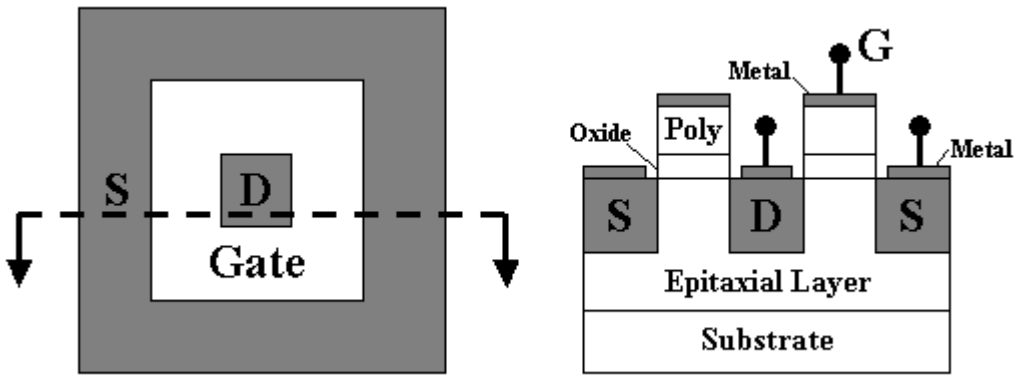

Figure 3.8. Top view (left) and cross section (right) of the fabricated ring-FET.

After epitaxy, a thermal gate oxide (~25 nm) was grown at 900 ^{o}C. The FETs were made using a self-aligned polysilicon-gate process. Sources and drains for p-channel devices were implanted using a BF_2^+ dose of 2x10^{15}/cm^{2} at 35 keV and n-channel source and drains were implanted using an As^+ dose of 10^{15}/cm^{2} at 100 keV through a sacrificial

screen oxide of 25 nm. The sacrificial oxide was then stripped and PECVD field oxide of 300 nm thickness was deposited. The implant damage was then annealed for 30 minutes at 900 ^{o}C for the boron doped (p-channel) samples and 30 minutes at 950 ^{o}C for the arsenic doped (n-channel) samples. Contact holes for the source and drain were patterned and aluminum was sputtered to form the gate and source/drain contacts. The channel width, defined as the perimeter at the midpoint of the square of the gate, was 300 microns, and the channel length was 10 microns. Four devices from each sample were measured.

3.7 FET Mobility

We seek to determine if there is any degradation in silicon quality, as measured by mobility, due to either the ultra-high epitaxial growth rates or the high background carbon levels (~ 10^{20} cm^{-3}). Saturation curves of drain current vs. drain-source voltage of FETs fabricated in an epitaxial layer grown with NPS and growth rate of 180nm/min at 650 ^{o}C, are shown in Figures 3.9a and 3.9b for n-channel and p-channel devices respectively.

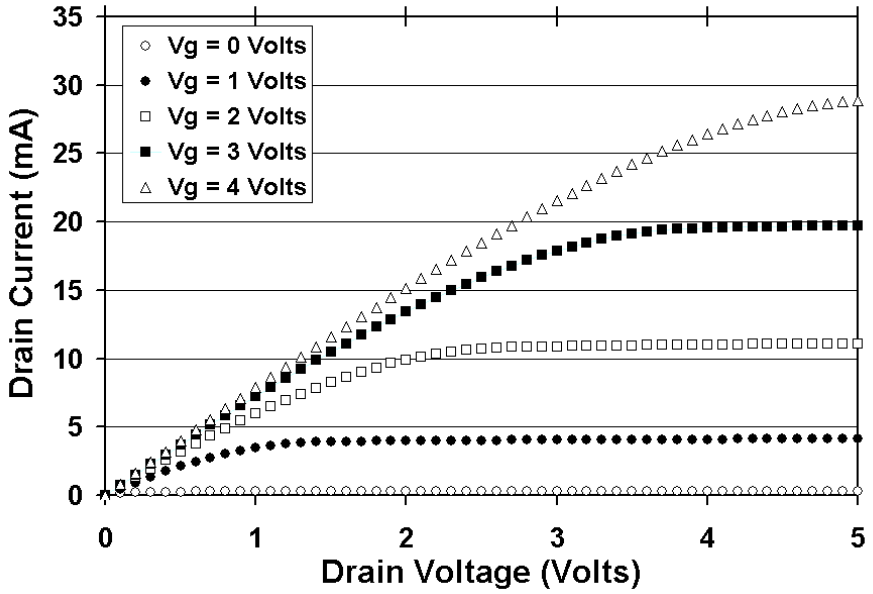

Figure 3.9a. Drain current vs. drain voltage for n-channel FETs fabricated with NPS epitaxial layers

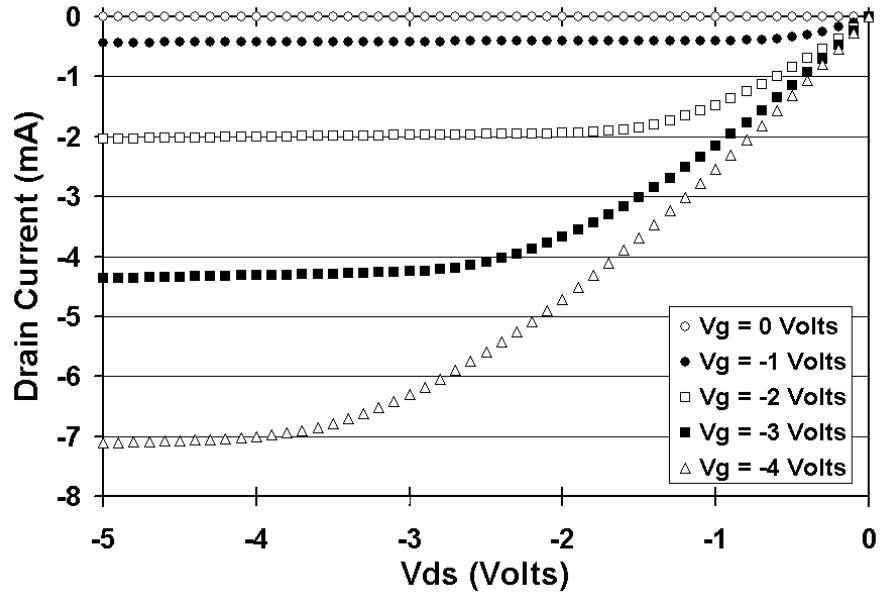

Figure 3.9b. Drain current vs. drain voltage for p-channel FETs fabricated with NPS epitaxial layers

The gate voltage was stepped from 0 to ± 4 volts, and the source was grounded in all measurements. The FETs with NPS epitaxial layers exhibit similar saturation device characteristics as the control samples for both p-channel and n-channel devices.

The linear and saturation mobilities for both the NPS epitaxial layers and the control samples are plotted in Figures 3.10a (electron mobility) and 3.10b (hole mobility). The saturation mobilities were determined from the slope of a plot of the square root of I_{DS} vs. V_{DS} for different growth rates. The saturation electron mobilites for the nFETS with NPS epitaxial layers ranged from 570 to 770 cm^2/Vs compared with 590 to 630 cm^2/Vs for the control sample. The saturation hole mobilities for the pFETS with NPS epitaxial layers ranged from 200 to 260 cm^2/Vs compared to 170 to 190 cm^2/Vs for the control samples.

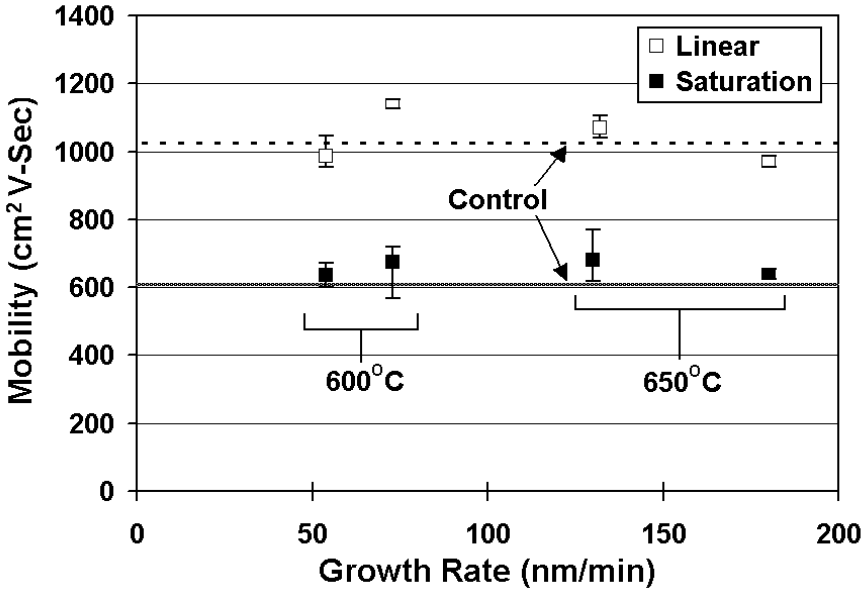

Figure 3.10a. Electron mobility vs. growth rate in the saturation (solid squares) and linear (open squares) regions of operation. The average mobility of the control samples in the saturation (dashed) and linear (solid) regions of operation are also shown. The error bars indicate the high and low values of the mobilities found out of 4 devices.

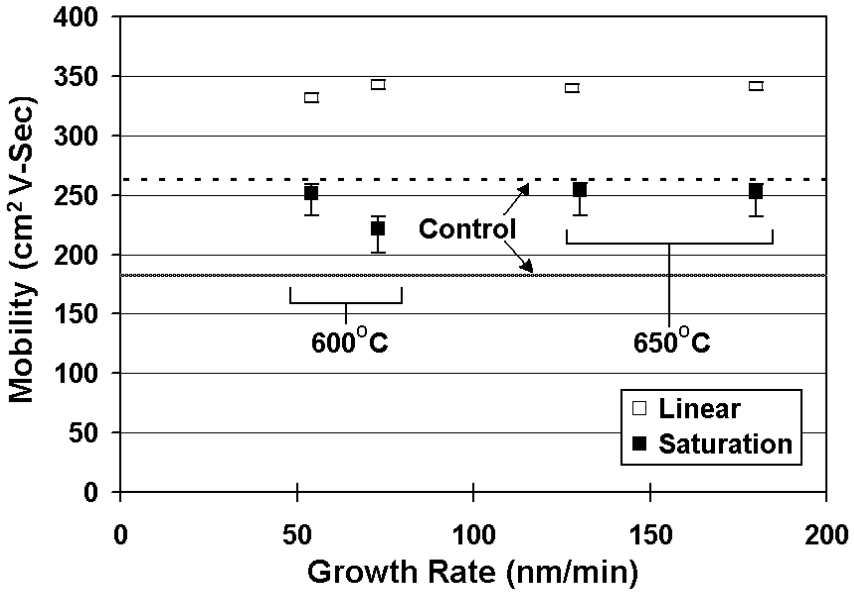

Figure 3.10b. Hole mobility vs. growth rate in the saturation (solid squares) and linear (open squares) regions of operation. The average mobility of the control samples in the saturation (dashed) and linear (solid) regions of operation are also shown. The error bars indicate the high and low values of the mobilities found out of 4 devices.

The linear carrier mobility (V_{DS} = ± 0.1 V) at the onset of inversion, was determined as a function of gate voltage (Figures 3.11a and 3.11b). We define the mobility using the following equation:

Eq. 3.1
$$\mu = \frac{L}{WC_{Ox}V_{DS}}\frac{dI}{dV_{DS}}$$

The peak electron and hole mobilities (from Figures 3.11a and 3.11b) were plotted versus growth rate in Figures 3.10a and 3.10b respectively. The linear electron mobilities for the nFETS with NPS epitaxial layers ranged from 950 to 1150 cm^2/Vs compared to 1000 to 1050 cm^2/Vs for the control samples. The linear hole mobilities for the pFETS with NPS epitaxial layers ranged from 330 to 350 cm^2/Vs compared with 260 to 270 cm^2/Vs for the control samples.

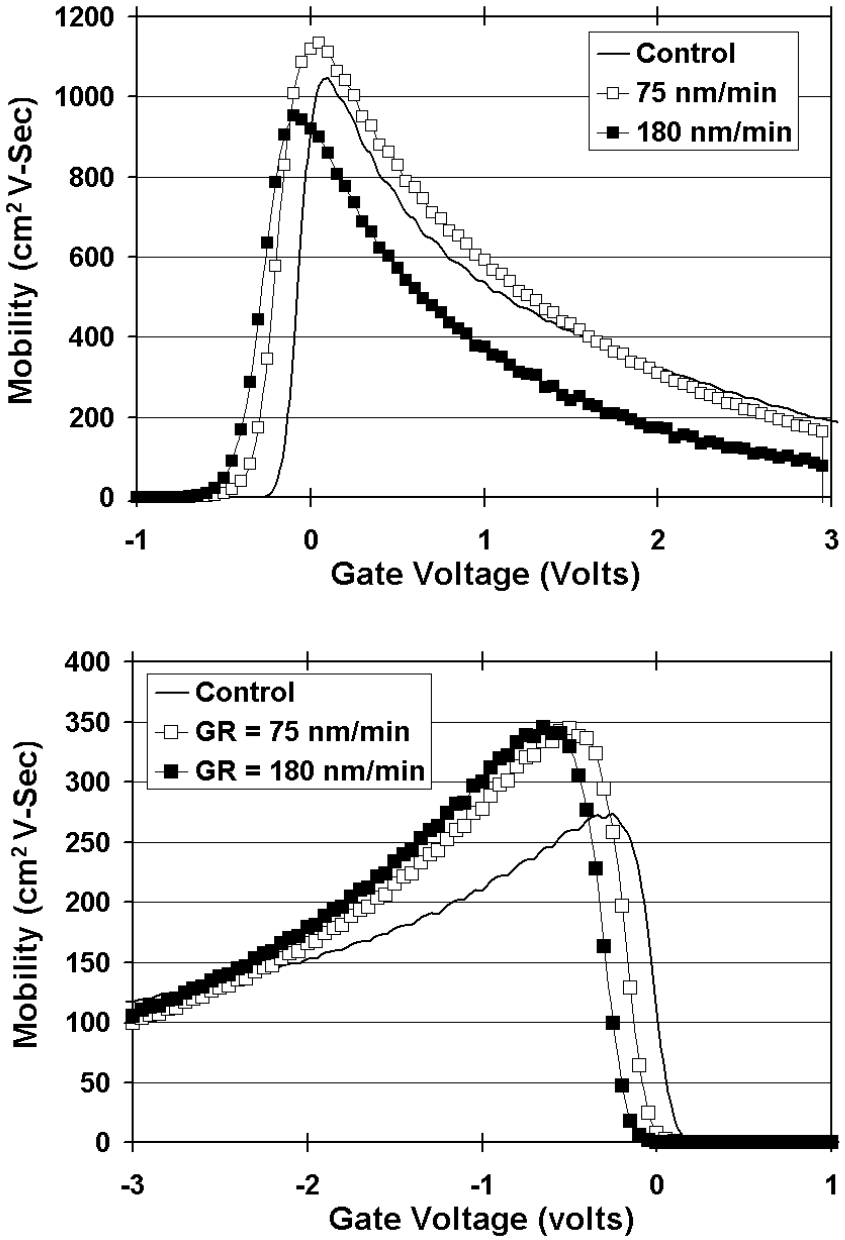

Figure 3.11a&b. Electron (top) & hole (bottom) mobility vs. gate voltage in the linear region of operation. The control sample is represented with a solid line. Open diamonds and squares are for the NPS epitaxial layers grown at 600 ^{o}C, and filled diamonds and squares are for the NPS epitaxial layers grown at 650 ^{o}C.

In both cases the measured linear mobilities are higher than the saturation mobilities (which are measured at lower average gate field). There was no significant difference in the electron mobility between the control sample and the NPS epitaxial layers, in both the linear and saturation regimes of operation, implying high quality in the epitaxial layers grown with NPS. The hole mobility for the NPS epitaxial layers are about 20% higher than the mobility of the control sample in both the linear and saturation operation regimes for reasons which are not known. A possibility is that the channel is biaxially tensile strained due to the high carbon content of $10^{20}/cm^{-3}$. This would cause a tensile strain of 0.12%. This amount of strain is predicted to give a 10% enhancement to hole mobility [3.11], which is of the same order as the observed enhancement. There was also little variation in the mobilities among the samples with NPS epitaxial layers at the different growth rates indicating that the high growth rates at 600-650 ^{o}C did not have any detrimental effect on FET mobility.

3.8 FET Threshold Voltage

The threshold voltages both the linear and saturation regions were plotted vs. the growth rate for n-channel and p-channel devices (Figure 3.12a & Figure 3.12b respectively). The threshold voltages for the n-channel FET's with NPS epitaxial layers obtained from the saturation region of operation (intercept of square root of drain current vs. gate voltage) varied from 0.48 to -0.91V compared to –0.46V for the control sample. The threshold voltages for the n-channel FET's with NPS epitaxial layers obtained from the linear region of operation varied from -0.23 to -0.36V compared to –0.11V for the control sample.

The threshold voltages for the p-channel FET's with NPS epitaxial layers obtained from the saturation region of operation (intercept of square root of drain current

vs. gate voltage) varied from 0.26 to -0.16V compared to 0.28V for the control sample. The threshold voltages for the p-channel FET's with NPS epitaxial layers obtained from the linear region of operation varied from –0.1 to -0.31V compared to -0.04V for the control sample.

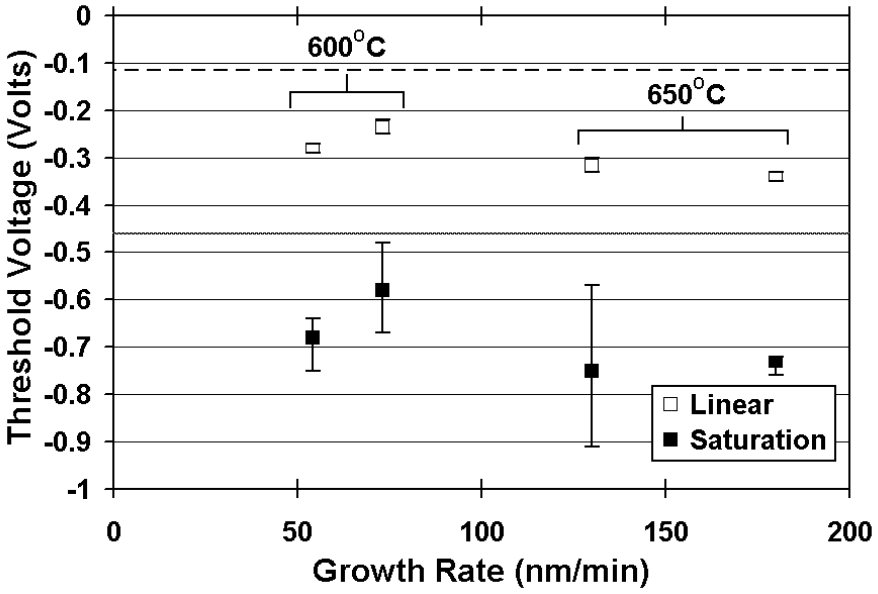

Figure 3.12a. Threshold voltage vs. growth rate for n-channel FETs in the saturation (solid squares) and linear (open squares) regions of operation. The average threshold voltage in the saturation (dashed line) and linear (solid line) region of the control devices are also plotted. The error bars indicate the high and low values of the threshold voltages calculated.

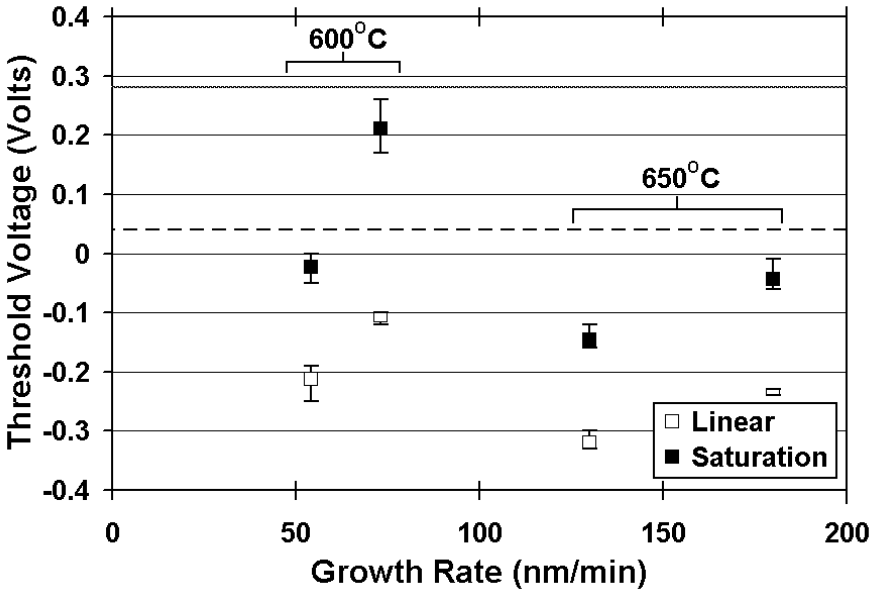

Figure 3.12b. Threshold voltage vs. growth rate for p-channel FETs in the saturation (solid squares) and linear (open squares) regions of operation. The average threshold voltage in the saturation (dashed line) and linear (solid line) region of the control devices are also plotted. The error bars indicate the high and low values of the threshold voltages calculated.

The threshold voltages determined in both the saturation and linear region of operation for the NPS epitaxial layers were more negative than the control samples for both n-channel FETs and p-channel FETs. Assuming that the interface and oxide charges are the same for both the control wafers and the NPS epitaxial layers, this implies that the NPS epitaxial layers have an n-type background doping.

Numerical simulation using MEDICI shows for an epitaxial layer of 200nm, an n-type doping density of $4x10^{15}/cm^3$ decreases the threshold voltage by ~0.2V for both the n-channel and p-channel devices. Thus we conclude that the background doping of the epitaxy was of this value.

3.9 Subthreshold Characteristics

Typical device turn-off characteristics are shown in Figure 3.13 below.

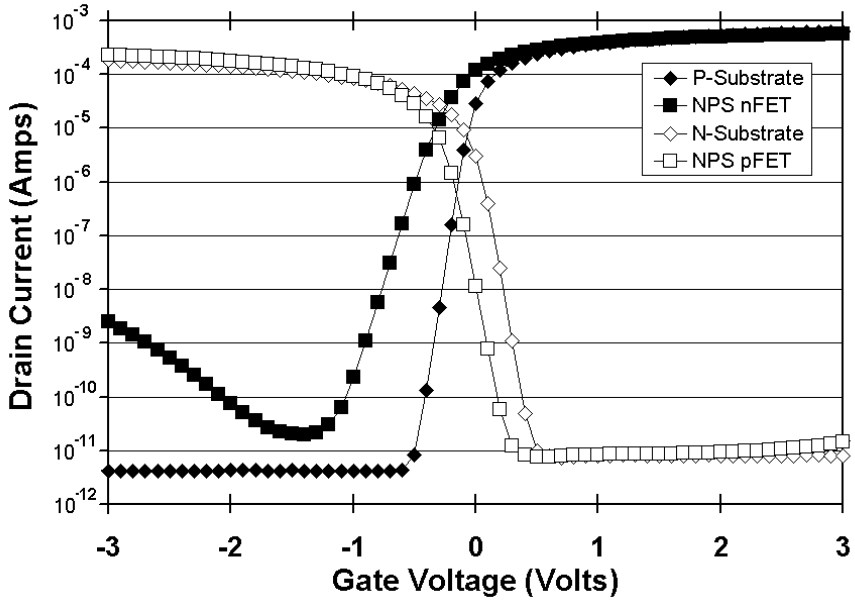

Figure 3.13. Drain current vs. gate voltage for n-channel FET devices (solid squares) and pFET devices (open squares). The control sample (circles) and a sample with an epitaxial layer grown using neopentasilane at 650 ^{o}C at a rate of 180 nm/ min (squares) were compared.

For p-channel devices, the substhreshold slope with NPS epitaxial layers were slightly worse than the control (80 to 92 meV/dec compared with 63 to 67 meV/dec). For n-channel devices the substhreshold slopes with NPS epitaxial layers were also consistently worse than that of the control devices (100 to 205 meV/dec vs. 63 to 67 meV/dec). We also observed that the drain current increased in the n-channel devices at negative gate voltage (~1 nA) and in p-channel devices for positive gate voltage (to a lesser degree, ~20 pA) in the NPS devices. This was found to be a drain to gate leakage, not a drain to source or drain to substrate current, as shown in Figure 3.14 below.

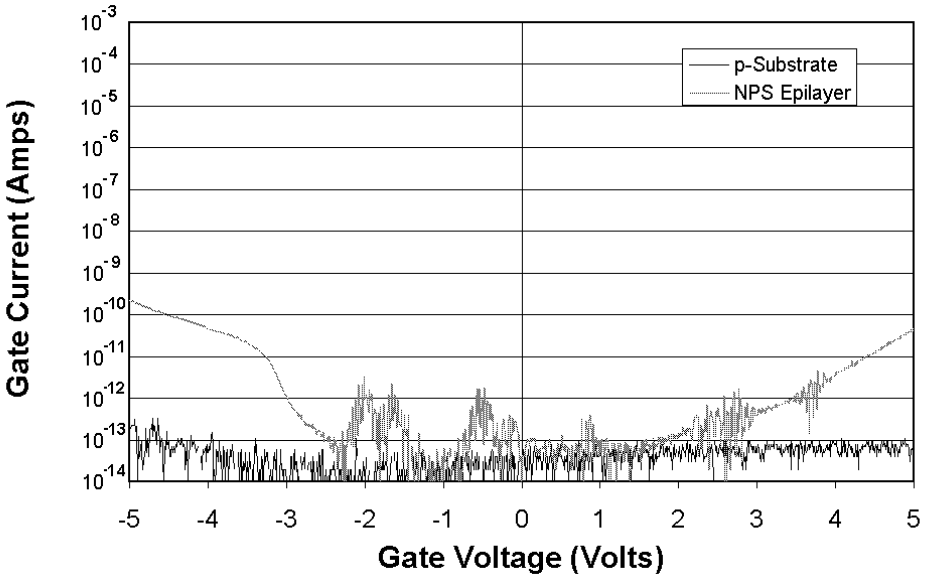

Figure 3.14. Plot of gate current vs. gate voltage. The n-channel control sample (circles) and an sample with an epitaxial layer grown using neopentasilane at 650 ^{o}C at a rate of 180 nm/ min (squares) was compared.

The control sample does not exhibit any gate current from –5 to 5 volts. The expected breakdown voltage for the control sample is 20 volts. The sample with an NPS epitaxial layer exhibits gate current at 3 volts. This leakage current is believed to be due to particles on the surface of epitaxial layers grown with NPS described in more detail in chapter 2.5. As observed with AFM, (Figure 2.x in chapter 2) there are particles on the surface with a size on the order of 20 nm with density up to ~10^6 cm^{-2}. The gate oxide thickness is ~25nm. The particles probably cause the gate leakage (due to a rough surface) and could also cause the poor subthreshold slopes, due to a high number of interface states near the particle. We note that subthreshold slope degradation may also be due to interstitial carbon levels in silicon.

3.10 Summary

In this chapter we have evaluated the quality of silicon epitaxy with high growth rates at 600 ^{o}C and 650 ^{o}C by chemical vapor deposition using neopentasilane. In spite of high-growth rates and low growth temperatures, epitaxial layers grown with NPS are crystalline as shown by x-TEM. SIMS measurements show that the epitaxial layers grown with NPS have low background impurities concentrations of boron and phosphorus (~5 x 10^{16}/cm^{3}), but high carbon concentrations of ~10^{20}/cm^{3}. The oxygen background is around 10^{18}/cm^{3}. Photoluminescence experiments indicate that the epitaxial layers grown with NPS at 600 ^{o}C are close in quality to those grown with a conventional silicon source (DCS) at a higher temperature of 700 ^{o}C. Ring-FETs were fabricated on epitaxial layers grown with NPS and analyzed. Saturation and linear mobilities for both electrons and holes show no detrimental effect from the high growth rate or high carbon levels. Mobilities of FETs with NPS epitaxial layers are comparable with the control samples for n-channel devices and have a 20% enhancement in the p-channel devices. NPS devices have significantly worse turn-off characteristics and all NPS devices had excess gate leakage current. Gate leakages in the devices were caused by particulates of unknown origin.

Chapter 4
Mechanism of Growth Rate Enhancement of Silicon Epitaxy due to Higher-Order Silanes

4.1 Epitaxial Growth Introduction

4.1.1 Chemical Vapor Deposition Growth Steps

Chemical vapor deposition is an extremely complicated process. There are many different mechanisms and steps to the deposition process. We will group all mechanisms that are taking place into six steps. The first step (i) is the transport of precursor molecules from the chamber inlet to the proximity of the wafer. This is done by flowing gas and pumping the gas in a particular direction. The second step (ii) is the transport of the precursor to the surface of the wafer, via diffusion through a boundary layer. We will digress to discuss a little on boundary layers and gas flows before going on to describe the third step. A boundary layer occurs due to the "drag" on the gas flow near the wafer surface. This separates the rapidly moving gas from the stationary gas next to the surface. Figure 4.1 below illustrates this concept.

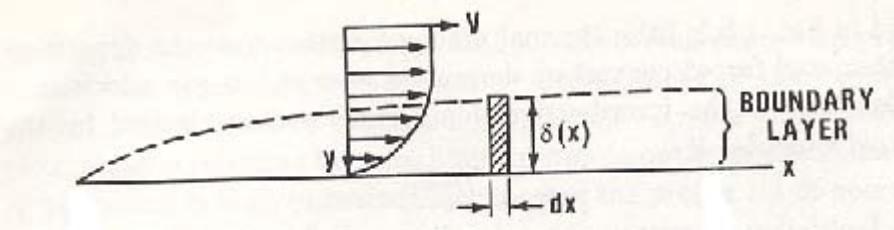

Figure 4.1. Diagram illustrating the boundary layer created by gas flow across a solid surface. In the boundary layer the gas velocity ranges from 0 to v. [4.1]

In CVD processing it is important to have laminar (streamline) gas flow. What this means is that is it flows in steady state fashion without turbulence. The Reynolds number (Re) is use to characterize the type of flow regime, laminar or turbulent. A low Reynolds number (<2000) corresponds to laminar flow [4.1a], while turbulent flow is obtained at high Reynolds numbers. Both the boundary layer thickness and the Reynolds number are calculated for the Princeton RTCVD reactor. The thickness of the boundary layer is calculated using the following equation:

Eq. 4.1 $$\delta(x) = \text{sqrt}\ (\ x\ \mu\ )/\ (\ D_t\ v\ \rho\ ))$$

The Reynolds number (dimensionless) was calculated using the following equation:

Eq. 4.2 $$Re\ = D_t\ v\ \rho\ /\ \mu$$

where D_t is the characteristic dimension of the reactor chamber (0.2 meters), v is the gas velocity, ρ is the gas density (hydrogen), μ is the viscosity, and x is the distance across the wafer (5 cm at the center).

The boundary layer thicknesses were calculated for our reactor system (ignoring the chamber wall location) using hydrogen at 3 lpm and 6 torr with a chamber cross section of 20 centimeters, corresponding to a gas velocity of 6.3 cm/s at 600 ^{o}C. Typical

parameters at T=600^{o}C are ρ = 2.2 x 10^{-4} grams/liter and μ = 1.7 x 10^{-2} centipoise in hydrogen and ρ = 3.1 x 10^{-3} grams/liter and μ = 3.6 x 10^{-3} centipoise in nitrogen [4.1b][4.1c]. The calculated boundary layer thickness ranged from 24.9 to 44.5 cm (hydrogen) and 9.56 to 17.2 cm (nitrogen) for the temperatures of 1100 ^{o}C to 600 ^{o}C and a chamber pressure of 6 torr. The Reynold's numbers ranged from 0.16 to 0.05 (hydrogen) and 1.09 to 0.34 (nitrogen) for the temperatures of 1100 ^{o}C to 600 ^{o}C respectively, indicating that the gas flow in our system is laminar throughout our growth temperatures. (These are only order of magnitude estimates, since the reactor geometry limits the boundary layer to a few cm.)

The third step (iii) involves both the surface reaction between the gas and the surface and other reactions on the surface. This is the actual growth step of CVD and will be examined in detail in this chapter. The last three steps are (iv) desorption of the gaseous by-products from the surface reactions, (v) the transport of the by-products away from the surface of the wafer across the boundary layer, and finally (vi) the transport of the by-products from the reactor.

In conventional CVD there are two growth regimes, mass-transport-limited (limited by steps ii and iv) and reaction-rate-limited (limited by step iii). The former occurs at high growth temperatures and the latter occurs at low growth temperatures. Figure 4.2 illustrates the change in concentration of silane vs. distance above the wafer for different temperatures.

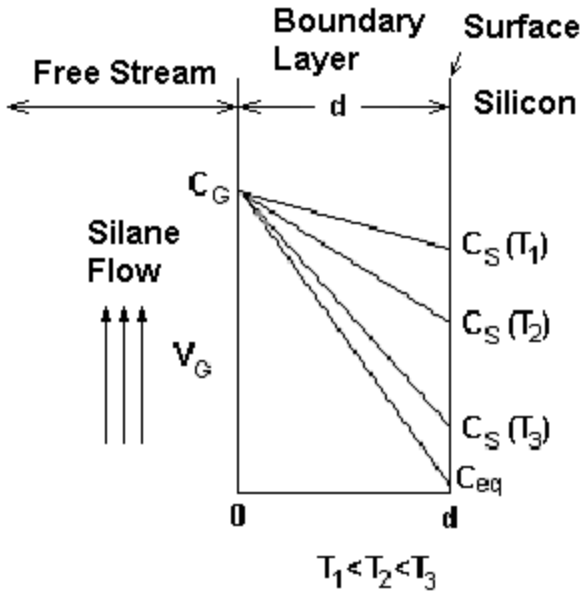

Figure 4.2. Silane flow concentration in free stream (x=0) and on the silicon surface (x=d) versus height above the wafer for different temperatures. Also schematically shown is the gas flow, perpendicular to the wafer surface in the free stream. [4.1a]

In the figure the precursor gas is silane, but the theory is the same for all gases. On the x-axis, 0 represents the interface between the boundary layer and the free stream. In the free stream, gas flow is perpendicular to the surface with velocity V_G. d is the thickness of the boundary layer between the silicon surface and the free stream. The gas concentration in the free stream shown in the diagram is C_G. The gas then diffuses a distance d through the boundary layer to the surface. Shown on the silicon surface are the concentrations of the precursor C_S on the surface at different temperatures with $T_1 < T_2 < T_3$. As the temperature increases surface reactions occur more readily, decreasing the surface concentration. When the temperature is high enough the surface concentration becomes near zero (i.e. any gas molecule reaching the surface reacts immediately). The diffusion rate across the boundary layer also increases with temperature, but depends weakly on temperature (steps (ii) and (iv)). The surface reactions typically increase exponentially with temperature, in Arrhenius fashion, so they are much faster at high

temperatures. Therefore, at high temperature the growth rate is limited not by surface reactions on the growing surface, but by diffusion through the boundary layer. This is known as the "mass-transport" regime.

As the temperature is reduced the surface reactions decrease faster than the diffusion through the boundary layer and the surface concentration increases with decreasing temperature. We plot the growth rate versus inverse temperature in Figure 4.3 below, illustrating the two growth regimes.

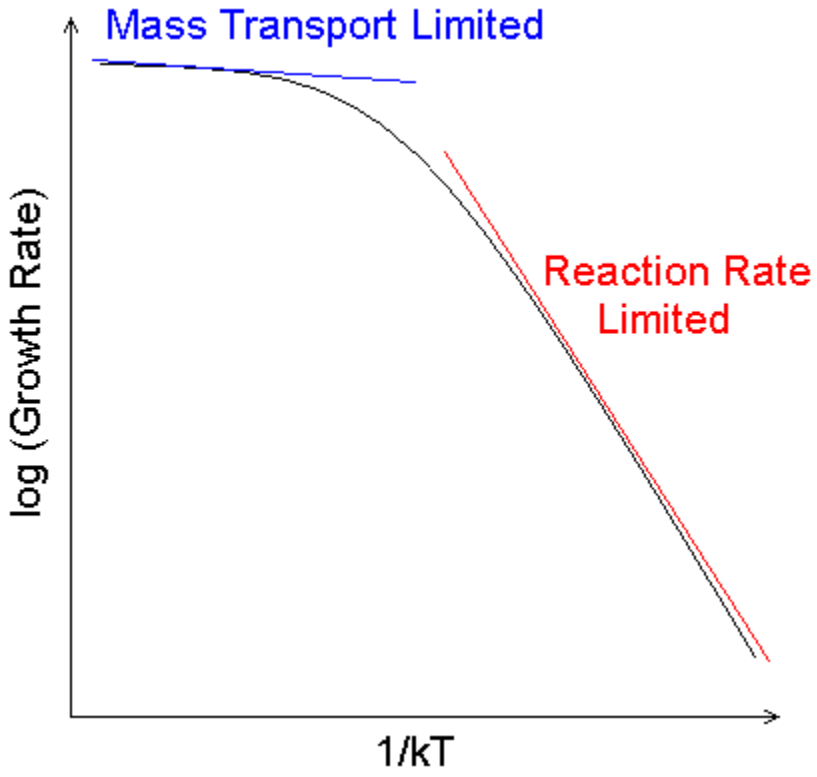

Figure 4.3. Plot of growth rate versus inverse temperature of the mass transport limited and reaction rate limited growth regimes.

In the reaction-rate-limited regime (at low temperature), the growth rate is dominated not by the gas flow but by the surface reactions, which are very slow. Thus the surface concentration is about equal to the free stream concentration. The reaction-rate

coefficient of the surface reactant is a strong function of temperature (exponential). This causes the growth rate (proportional to the reaction-rate) to depend strongly with temperature in the reaction-rate-limited regime.

4.1.2 The Silicon Surface: 2x1 Reconstruction and Hydrogen Passivation

Silicon has a diamond lattice where each silicon atom has four nearest neighbors. For a clean (unpassivated) (001) silicon surface, the surface silicon atoms (1 and 1' in Figure 4.4) are left with two dangling bonds. The surface reconstructs itself (i.e. the atoms on the surface assume a different structure than the bulk) into a lower energy structure. The resulting structure has a 2 x 1 periodicity structure shown in Figure 4.4 below:

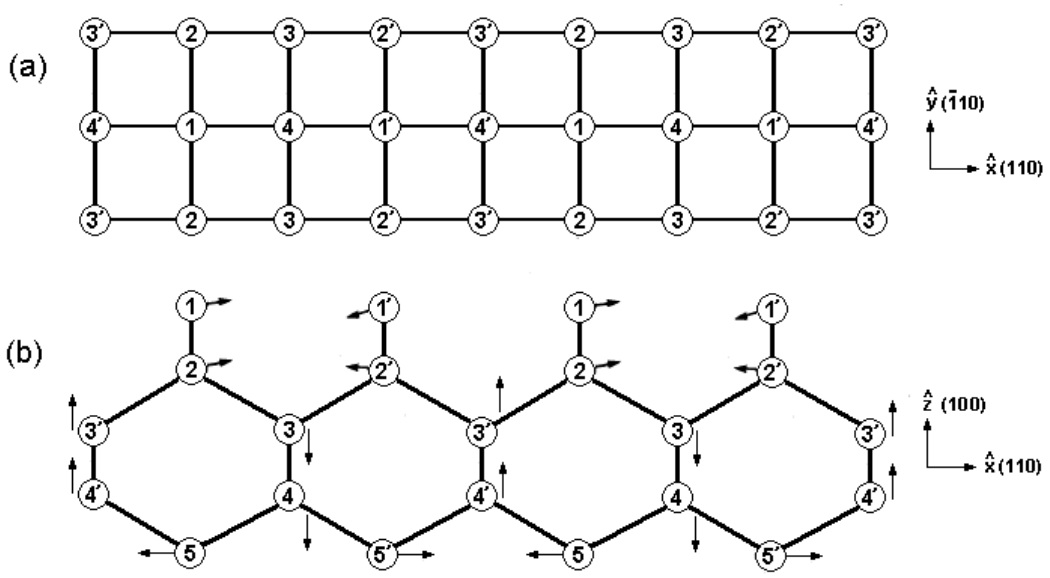

Figure 4.4. Top (a) and side (b) view in the indicated directions of an ideal Si(100) surface. The atoms denoted by 1 and 1' are surface-layer atoms, 2 and 2' are second-layer atoms, etc. The dimerization (1 and 1') of the surface leads to the formation of strong bonds between atoms 1 and 1'. Directions of atomic displacements from ideal positions are shown in (b). [4.2]

In the reconstructed surface, the calculated atomic displacements are found to be (in Angstroms): $\Delta x_1 = 0.46$, $\Delta x_{1'} = -1.08$, $\Delta z_1 = 0.04$, $\Delta z_{1'} = -0.435$, $\Delta x_2 = -\Delta x_{2'} = 0.115$, $\Delta z_2 = \Delta z_{2'} = 0.014$, $\Delta z_3 = -0.12$, $\Delta z_{3'} = 0.11$, $\Delta z_4 = -\Delta z_{4'} = -.007$, $\Delta x_5 = -\Delta x_{5'} = 0.034$ [4.2]. The surface is called a 2 x 1 reconstructed surface due to the dimerization of every two rows of silicon atoms. Note that the displacement is only along one axis (x-axis) and there are distortions in the lattice.

For our typical growth temperatures, (500 ^{o}C to 700 ^{o}C) and pressure (6 torr hydrogen) the majority of the surface is hydrogen passivated. Experimental studies have shown that adsorption of atomic H on the Si(100) 2x1 surface at temperatures above 350 ^{o}C (625K) leads to a 2x1 Si:H monohydride phase in which the asymmetric (2x1) dimers become symmetric and each Si atom's single-dangling bond is terminated with only one H [4.3][4.4][4.5]. The other dangling bond is consumed by the formation of the dimers. Shown in Figure 4.5 below is the resulting 2x1 reconstructed, hydrogen passivated silicon surface (2x1 Si:H).

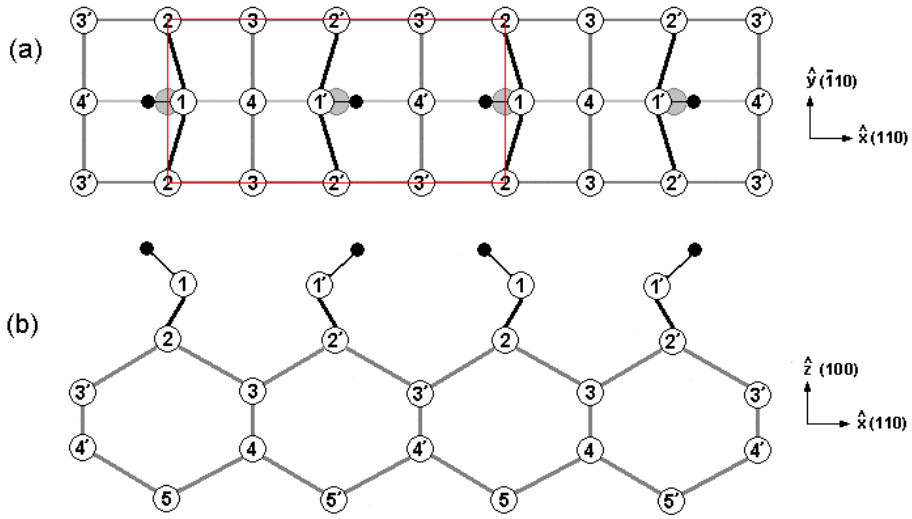

Figure 4.5. Top (a) and side (b) view in the indicated directions of a 2x1 Si (100) reconstructed surface that is passivated with hydrogen (solid circle without number) . The atoms denoted by 1 and 1' are surface-layer atoms, 2 and 2' are second-layer atoms, etc. 1 and 1' form a dimerized pair on the silicon surface with one hydrogen atom attached per silicon atom on the surface. The unit cell is boxed in red in (a).

The silicon atoms 1 and 1' bond to form a dimer pair in the direction without the hydrogen atom (solid circle without number). The spacing between the two silicon atoms is 2.42 Angstroms for the same dimer pair and 5.28 Angstroms for the inter-dimer pair [4.6]. The distance between two atoms on the same plane (i.e. 2 and 2', or 3 and 3') is 3.85 angstroms. The unit cell is 3.85 x 7.70 angstroms, and can be drawn by forming a rectangle around four atoms on the same plane (shown in red in Figure 4.5).

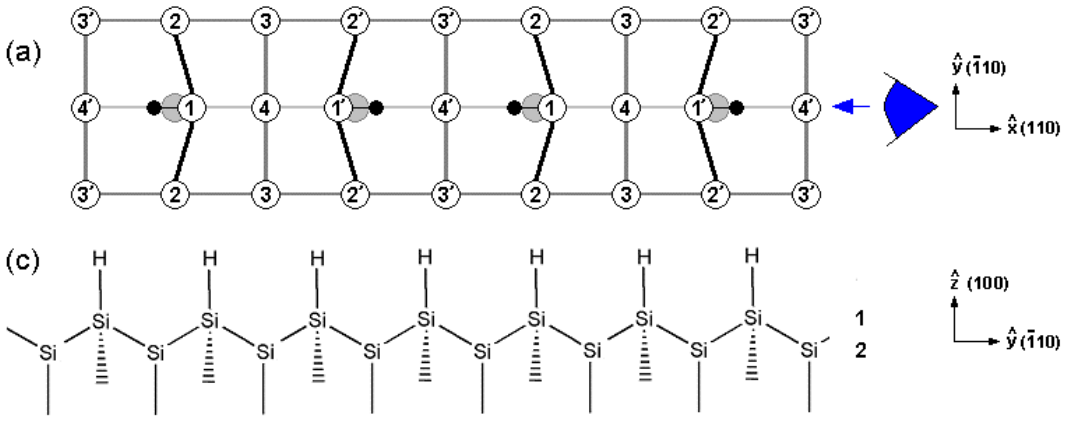

Figure 4.6. Top view (a) and side view (c) along the (110) direction of a 2x1 reconstructed surface that is passivated with hydrogen (solid circle). In the side view (c), the first silicon two layers are shown with the numbers corresponding to the layer shown in the top view (a). The dashed triangle underneath the silicon surface represents the reconstruction of the surface silicon atoms in/out of the plane of the figure.

If we look in direction (blue eyeball) along the (110) direction of the silicon and draw a schematic representation of the 2x1 reconstructed, hydrogen passivated surface, we would see the silicon cross section shown in Figure 4.6(c). We will use the schematic representation (Figure 4.6c) for ease of describing our microscope model later on in the chapter.

4.1.3 Hydrogen Desorption Model

In most of our growth experiments we use hydrogen as a carrier gas. This effect leaves our surfaces in a 2 x 1 reconstructed silicon surface passivated with one hydrogen atom per surface silicon atom (as shown in Figure 4.5 above), known as a monohydride surface. We assume that the hydrogen desorption reaction follows first-order kinetics [4.7] and a Langmuir-type adsorption model. We can determine the equilibrium number of open sites using the following Equation:

Eq. 4.3
$$\theta_H = \frac{\left(K_{eq} P_{H_2}\right)^{1/2}}{(1 + K_{eq} P_{H_2})^{1/2}}$$

where θ_H is the number of hydrogen-terminated surface sites, p is the pressure (Pascal), and K_{eq} is given by the following Equation:

Eq. 4.4
$$K_{eq} = k_a / k_d = \exp(-\Delta G / k_B T)$$

where, k_a and k_d, are the adsorption and desorption rate coefficients respectively, ΔG is the Gibb's free energy difference, and k_B is Boltzmann's constant. Both the rate coefficients has the form of $k = v * \exp(-E_a/k_B T)$. The activation energy and the pre-exponential factor of the desorption rate coefficient are 47 ± 3 kcal/mol and 7.9 x 10^{11} s^{-1} respectively [4.7][4.8]. Furthermore, $\Delta G = \Delta H - T\,\Delta S$, where ΔH is the enthalpy of reaction ~ 47 kcal/mol (~2 eV) and ΔS is the entropy (~1.2meV / K) [4.9][4.10].

Using Equation 4.4 the open site fraction was calculated for typical low-pressure (6 torr) and ultra-high vacuum growth (10 mtorr) pressures, assuming only hydrogen gas. The open site fraction (total open sites / total surface sites) is plotted in Figure 4.7 below:

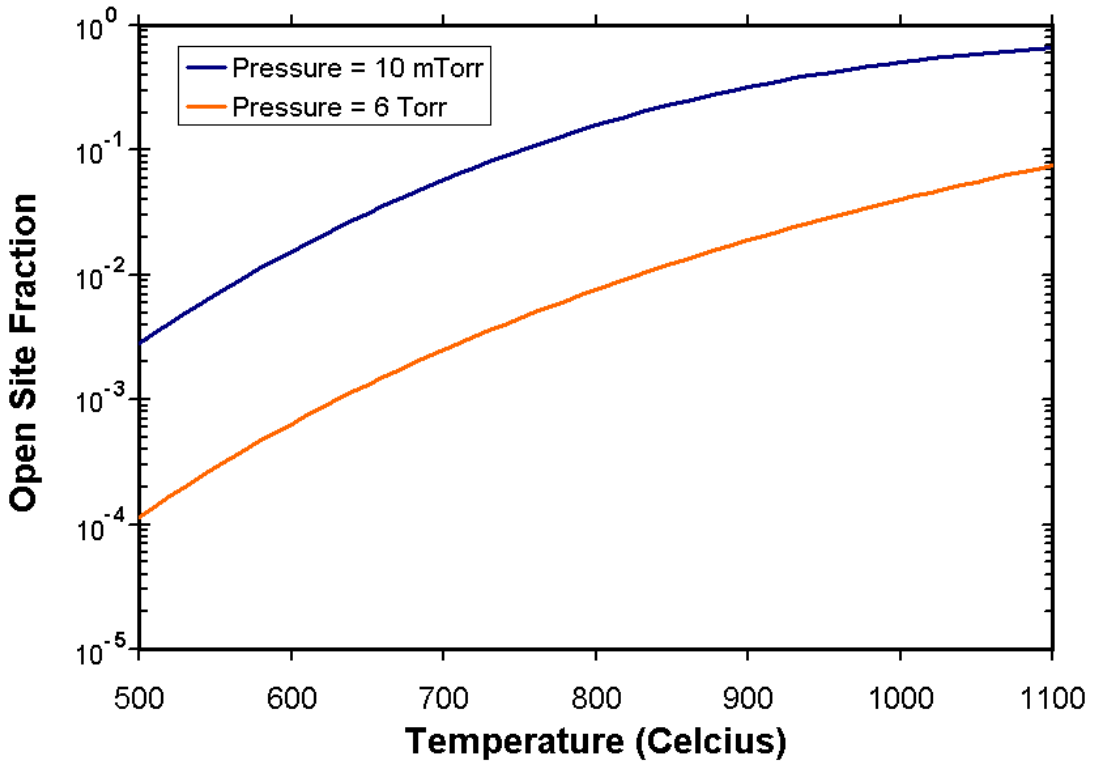

Figure 4.7. Fraction of open sites vs. temperature calculated using Equation 4.4. The open site fraction is plotted for 6 Torr and 10 mtorr, of hydrogen.

At low growth temperatures (T < 700 ^{o}C), growth rates are typically limited by surface reaction rates. We will consider the conventional hydrogen desorption model [4.11] for the deposition rate using silane as the silicon source. This model shows that the growth rate increases linearly with the silane partial pressure at low partial pressures and saturates at high silane partial pressures. The adsorption of silicon adatoms onto the surface on the open sites depends on the rate constant and silane pressure. Therefore, the growth rate (GR) of silicon can be expressed using the following Equation:

Eq. 4.5 $$GR = C\, k_g\, pp_{SiH4^*}(1-\theta_H)$$

where θ_H is the hydrogen coverage, $(1-\theta_H)$, is the number of open sites, k_G is the reaction constant for growth (adsorption reaction constant for silane) and pp_{SiH4} is the partial pressure of silane and C is a constant taking into atomic volume and the surface site density. We note that this is a first-order process instead of a second order process even though the growth with silane requires the formation of two adjacent open surface sites [4.12]. The reason is due to a preferential pairing of open sites at high surface coverage, $\theta_H \sim 1$, (See Appendix C). The adsorption rates (A) of H_2 and silane and desorption rate (D) of H_2 are given by the following Equations:

Eq. 4.6
$$A = \frac{d\theta_H}{dt} = [1-\theta_H]k_a pp_{H_2} + [1-\theta_H]k_G pp_{SiH_4}$$

Eq. 4.7
$$D = -\frac{d\theta_H}{dt} = -k_d \theta_H$$

where $d\theta_H / dt$ is the change in hydrogen coverage over time, k_a and k_d are the adsorption and desorption reaction constants for hydrogen respectively, k_G is the adsorption rate of silane, pp_H and pp_{SiH4} are the partial pressures of hydrogen and silane respectively. Equating the two Equations using an equilibrium of adsorption and desorption gives us the following:

Eq. 4.8
$$[1-\theta_H]*(k_a pp_{H_2} + k_G pp_{SiH_4}) = k_d \theta_H$$

Substituting $k_{eq} = k_a / k_d$ and $k_1 = k_G / k_d$, we can rewrite Equation 4.8 as the following:

Eq. 4.9
$$[1-\theta_H]*(k_{eq} pp_{H_2} + k_1 pp_{SiH_4}) = \theta_H$$

Eq. 4.10
$$[1-\theta_H] = \frac{\theta_H}{(k_{eq} pp_{H_2} + k_1 pp_{SiH_4})}$$

We now substitute the Equation back into the original growth rate Equation 4.5 above:

Eq. 4.11 $$GR = \frac{k_G pp_{SiH_4} \theta_H}{(k_{eq} pp_{H_2} + k_1 pp_{SiH_4})} \cong \frac{k_G pp_{SiH_4}}{(k_{eq} pp_{H_2} + k_1 pp_{SiH_4})}$$

We assume that the hydrogen surface coverage is essentially fully covered ($\theta_{H2} = 1$). We observe that the growth mode is dependent on the partial pressure of silane atoms. When the silane pressure is low ($k_1\ pp_{SiH4} << k_{eq}\ pp_{H2}$), the growth rate Equation is dominated by the top term and the growth rate increases linearly with increasing silane partial pressure. At high silane partial pressures ($k_1\ pp_{SiH4} >> k_{eq}\ pp_{H2}$) the growth rate saturates and does not further increase with increasing partial pressure. This is plotted in Figure 4.8 below:

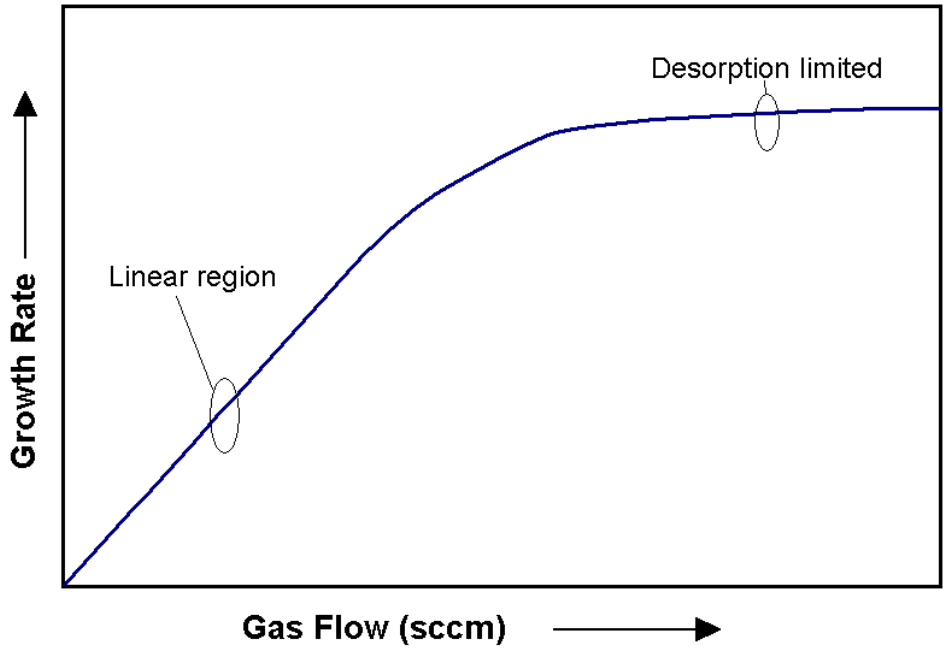

Figure 4.8. Plot of growth rate vs. silane partial pressure (gas flow) when the growth is limited by the surface reaction. In the first region, (the linear region) the open site fraction is constant. Hence the growth rate increases linearly with silane partial pressure. In the second region (desorption-limited) the growth rate saturates and is limited by the formation of open sites (hydrogen desorption).

On a microscopic level, in the linear (low partial pressure) region, the equilibrium open site fraction for silicon adatom adsorption is constant. In this regime the adsorption of the silicon adatom is only reducing the equilibrium open site fraction by an insignificant amount (i.e. the open sites can regenerate at a rate faster than the silicon adsorption. For instance if 1000 sites are generated and consumed every second by hydrogen desorbing and readsorbing, and only one site is consumed per second by silane adsorption, the equilibrium and open site density are little changed. Hence the growth rate is increasing linearly with increasing silane partial pressure (i.e. silane gas flow). As the gas flow (silane partial pressure) is continually increased, at some point the adatom adsorption will begin to reduce the equilibrium open site fraction until every open site generated will immediately be adsorbed by an incoming silicon adatom. In this case the growth rate will saturated as the growth rate is now determined by the hydrogen desorption rate. Even if we were to remove the hydrogen carrier gas entirely, say in UHV-CVD, the growth rate would be enhanced but the hydrogen desorption limit still apply as the surface will be covered with hydrogen, coming from the silane gas itself. This model (requiring open sites to be created via hydrogen desorption) is the accepted model for growth with silane. We will observe in Section 4.4 that this model fails to explain the growth rate enhancements for high-order silanes.

4.2 Model of Silicon Surface Reactions

4.2.1 Comparison of the Bond Strengths of Different Silanes

In this section we will examine the surface reactions that contribute to the growth of epitaxy on a microscopic level. First we will compare the bond enthalpies of silanes

and alkanes, given in Table 4.1 below. The bond with the lowest bond enthalpy is likely to be the bond that is cleaved when reacting with the silicon surface during epitaxial growth. The header of each column is the detached fragment from the parent silane molecule.

Table 4.1. Calculated bond enthalpies (kJ/mol) of linear silanes [4.13]. The header of each column indicated the detached fragment.

Silanes	**-H**	**-SiH_3**	**-SiH_3SiH_2**	**-$SiH_3(SiH_2)_2$**	**-$SiH_3(SiH_2)_3$**
SiH_4	**383.37**	**383.37**			
Si_2H_6	**371.66**	**317.55**	**371.66**		
Si_3H_8	**369.32**	**313.44**	**313.44**	**369.32**	
Si_4H_{10}	**368.94**	**312.69**	**310.92**	**312.69**	**368.94**
Si_5H_{12}	**368.63**	**312.49**	**310.36**	**310.36**	**312.49**
Si_6H_{14}	**368.51**	**312.41**	**310.37**	**310.01**	**310.37**

From the table we observe that it is easier to break the Si-Si than to break a Si-H bond, assuming the activation barriers follow the bond energies. Furthermore, as we increase in silane order, the energy to break off a SiH_3 decreases and saturates. The easiest bond to break in the linear silanes is the central Si-Si bond, since it has the lowest enthalpy. We do not know if the energy barrier in the surface reaction with the high-order linear silanes correlates linearly with the bond enthalpy. If it does, increasing the silane chain length past tetrasilane (Si_4H_{10}) will not provide a significant enhancement in the epitaxial growth rate.

4.2.2 Conventional Surface Reactions for Silane

In this chapter we wish to further explore the surface reaction that governs the growth process, starting from the precursor as a gas and ending with solid silicon deposition on the growth surface. We will explain the surface reactions that occur starting

from adsorption of the silicon adatom on the surface to the incorporation of the silicon atom into the bulk. Since silane is a well-studied precursor gas, we will begin with the accepted growth model explanations for silicon growth using silane. Silane undertakes the following reactions for CVD growth in ultra-high vacuum (UHV) conditions (clean silicon surface) [4.14]:

Eq. 4.12a	$SiH_4(g) \Rightarrow Si(s) + 2H_2(g)$	[total mechanism]
Eq. 4.12b	$SiH_4\ (g) + 2\ (*) \Rightarrow H^* + SiH_3\ (a)$	[silane adsorption]
Eq. 4.12c	$SiH_3\ (a) + (*) \Rightarrow H^* + SiH_2\ (a)$	[H decomposition]
Eq. 4.12d	$2SiH_2\ (a) \Rightarrow H_2\ (g) + 2SiH\ (a)$	[H decomposition, H desorption]
Eq. 4.12e	$2SiH\ (a) \Rightarrow H_2\ (g) + 2\ Si\ (a)$	[H decomposition, H desorption]
Eq. 4.12f	$2H\ (a) => H_2\ (g) + 2\ (*)$	[H desorption]
Eq. 4.12g	$Si\ (a) \Rightarrow Si\ (s) + (*)$	[surface migration]

where (*) denotes an open site (a dangling bond) for adsorption, (g) represents gas phase, H* is an adsorbed surface hydrogen atom, and (a) represents an adsorbed species. Equation 4.12a is the overall surface reaction for the growth process with silane. Equations 4.12b through 4.12g are the individual reaction steps.

If we balance Equations 4.12b-4.12g (divide Equations 4.12d and 4.12e by 2) we end up with the original reaction (Equation 4.12a). Equation 4.12b is the silane adsorption step. Equations 4.12b-e are the hydrogen decomposition steps. Equation 4.12f is the open site generation step via mono-hydride desorption. Equation 4.12g is the surface diffusion step for silicon.

According to Gates, [4.12][4.14][4.15], Equation 4.12b is the rate-limiting step when there are open sites available (i.e. the growth rate is limited by silane ($SiH_4(g)$) adsorption, controlled by the number of open sites (*)). Figure 4.9 shown below,

illustrates Equation 4.12b describing how silane adsorbs onto the hydrogenated 2x1 reconstructed silicon surface.

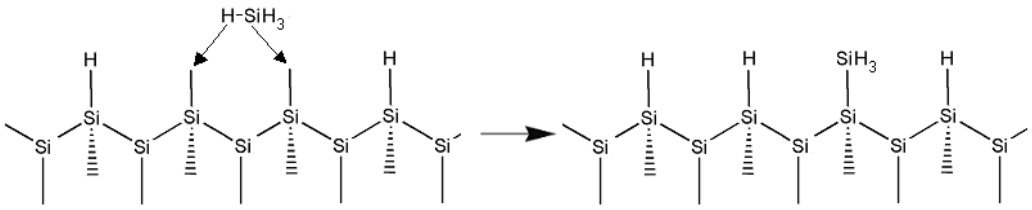

Figure 4.9. Side view of silane adsorption reaction on a (2 x 1) reconstructed silicon surface. The silane dissociatively adsorbs onto the surface using two open sites. H and SiH_3 then occupy the two sites on the surface. The dashed triangle underneath the silicon surface represents the reconstruction of the surface silicon atoms in/out of the plane of the figure.

In order for silane to adsorb on the surface, it also requires two adjacent open sites to be generated. In Figure 4.9, only the adsorption on two adjacent open sites from separate dimer rows is shown. The silane adsorption can occur on any two adjacent open sites. Silane dissociatively adsorbs, splitting a Si-H bond and forming SiH_3 on one site and an H on another open site. The need for open sites explains why the silane growth rate in low pressure CVD with a hydrogen carrier is much smaller than that of UHV-CVD for the same silane partial pressure; the open site fraction is significantly less in a hydrogen environment. Figure 4.10 below illustrates the adsorption steps for silane on a hydrogenated 2x1 reconstructed silicon surface. Equations 4.12b to 4.12d and Equation 4.12f are illustrated in the figure. Note that in Figure 4.10, the adsorption of silane is shown along the dimer row as opposed to adsorbing on two separate dimer rows in Figure 4.9.

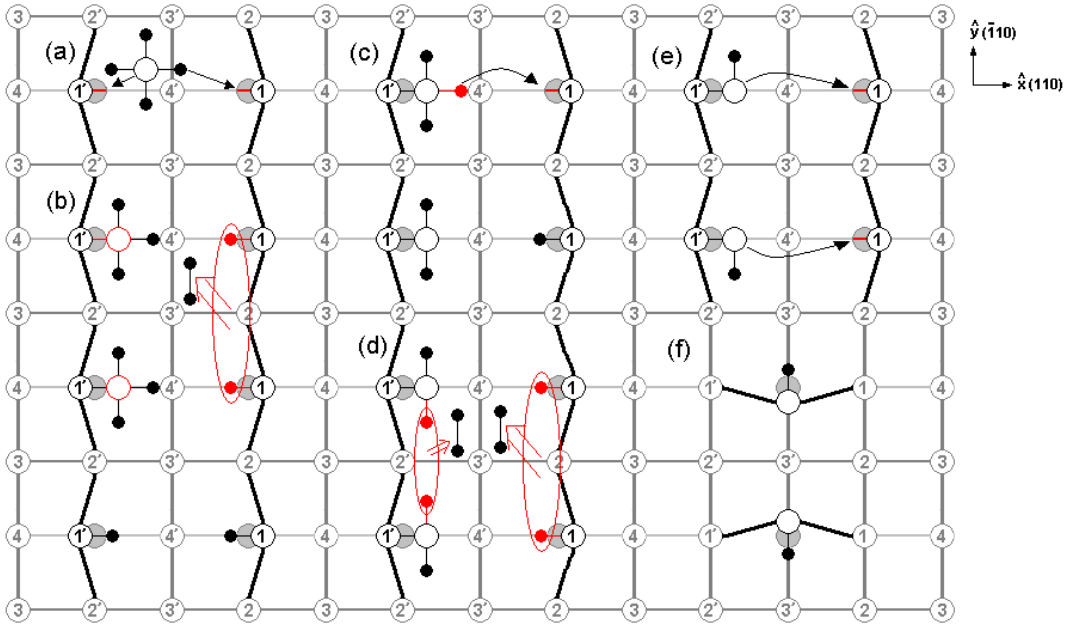

Figure 4.10(a - f). Top view of the adsorption process of silane onto a Si:H (100) (2x1) reconstructed surface based on references [4.14][4.15]. (Refer to Figures 4.4 and 4.5 for meaning of Si atoms (1,2,3,4)). Red circles indicate the change, and a red line indicates an open surface site. (a) Illustrates the adsorption of silane as an SiH_3 and a hydrogen atom (Equation 4.12b). (b) Depicts hydrogen desorption (Equation 4.12f) to form two open sites for (c) the SiH_3 to split into SiH_2 (Equation 4.12c). Another two hydrogen desorption step occurs in (d) to create two open sites and for SiH_2 to be reduced to SiH (Equation 4.12d). Step (e) shows the SiH bonding with its two nearest neighboring silicon atoms (i.e. incorporated into the solid) and the new reconstruction (f) on the surface.

4.2.3 Conventional Surface Adsorption Reaction for Disilane

The widely accepted initial step in disilane decomposition on Si(100)-(2 x 1) surface is dissociation adsorption to yield two adsorbed SiH_3 fragments, according to the following reaction [4.15][4.16]:

Eq. 4.13 $Si_2H_6\ (g) + 2(*) \Rightarrow 2SiH_3\ (a)$

Note that this Si-Si bond is expected to break much easier than a Si-H bond in disilane (Table 4.1). Equation 4.13 is based on thermally-programmed desorption (TPD) experiments on clean silicon surfaces [4.14][4.17][4.18]. This is also assumed to be the reaction for the growth of disilane on hydrogen-terminated surfaces. Similar to the silane growth model of section 4.2.2, it requires two adjacent open sites, and thus the growth rate should be proportional to $(1-\theta_H)^2$. This is illustrated from a side view on a hydrogenated silicon surface in Figure 4.11 below:

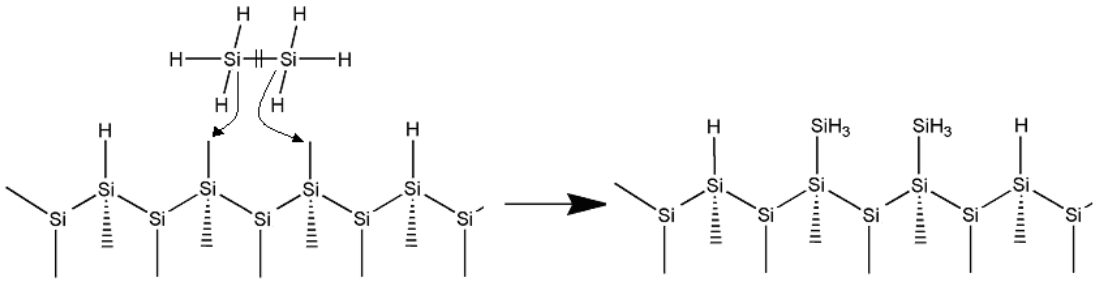

Figure 4.11. Disilane adsorption reaction on a (2 x 1) reconstructed silicon surface. The disilane dissociatively adsorbs onto the surface using two open sites. Two SiH_3 then occupy the two sites on the surface. The dashed triangle underneath the silicon surface represents the reconstruction of the surface silicon atoms in/out of the plane of the figure.

On a microscopic level, disilane adsorption on the (2 x 1) surface can occur in four different orientations along different dimer rows on the surface [4.17], which will not be discussed in this thesis. We will assume that disilane adsorbs on all four possible dimers rows with equal probability. It is easier to split the Si-Si bond in disilane then to split a Si-H bond in silane (Table 4.1). This could explain the reason why the growth rate is higher for disilane than silane under the same growth conditions, since the rate of reaction for disilane would be faster than the rate of reaction for silane.

4.3 Growth Rates of Different Silicon Sources in Nitrogen vs. Hydrogen Ambient

As shown Equation 4.5 above (GR =C k_g $pp_{SiH4*}(1-\theta_H)^2$), the more open sites there are on the surface, the higher the growth rate will be (prior to the hydrogen desorption limit). We will examine the dependence of growth rate versus hydrogen coverage experimentally for the precursor gases available in our system. By switching the carrier gas from hydrogen to nitrogen, the hydrogen coverage on the surface decreases significantly (i.e. $pp_{H2} \sim 0$). Previous work found that growth in a nitrogen ambient leads to a growth rate enhancement by a factor of ten compared to growth in hydrogen ambient [4.19]. Growth rate experiments are done with hydrogen and nitrogen ambients using the precursors of silane, disilane, and NPS are plotted in Figure 4.12 below.

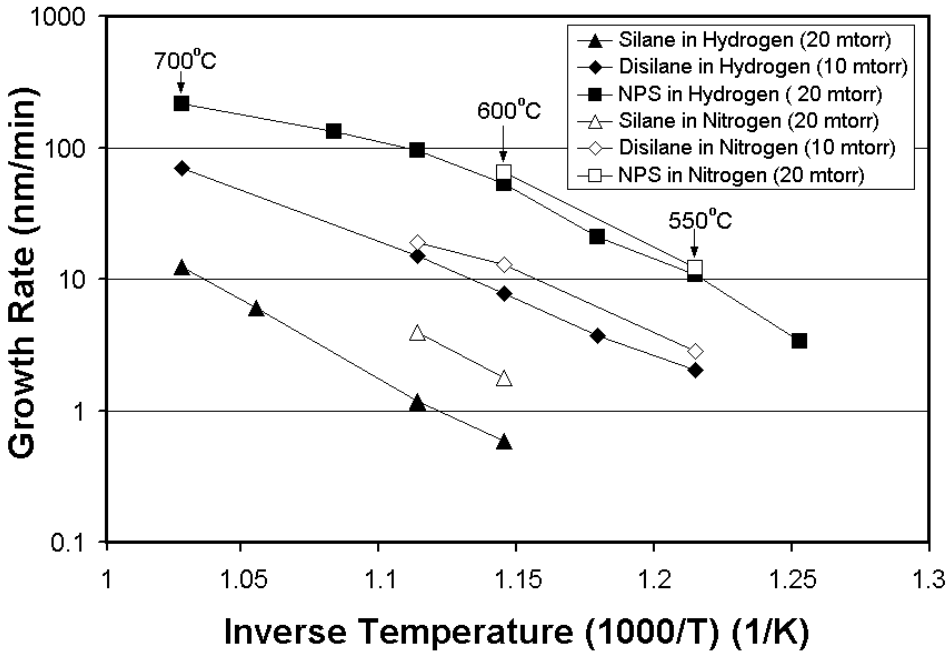

Figure 4.12. Comparison of epitaxial growth rates vs. inverse temperature for the precursors of silane, disilane and neopentasilane (NPS) (squares) on (100) silicon substrates in hydrogen and nitrogen ambient. The chamber pressure in all experiments was set to 6 torr with 3 slpm of either hydrogen or nitrogen carrier gas flow. The partial pressures are 20 mtorr of silane, 10 mtorr of disilane, and 20 mtorr (estimated upper limit) of NPS. [4.20]

Over the range of our experiments, the growth rate was still increasing linearly with partial pressure of the source. Because of the equilibrium between the hydrogen on the silicon surface and that in an ambient (hydrogen desorbs and adsorbs), the switch from hydrogen ambient to nitrogen ambient is thought to reduce the hydrogen coverage on the surface (Figure 4.7). This increases the number of open sites on the silicon surface for chemical adsorption of the growth species and increases the growth rate in the case of silane [4.19]. (It is assumed that the temperature range of our experiments (525 ^{o}C to 700 ^{o}C) nitrogen does not interact with the silicon surface.) Both the growth rate and open-site enhancement factors in switching from hydrogen to nitrogen are plotted in Figure 4.13 below:

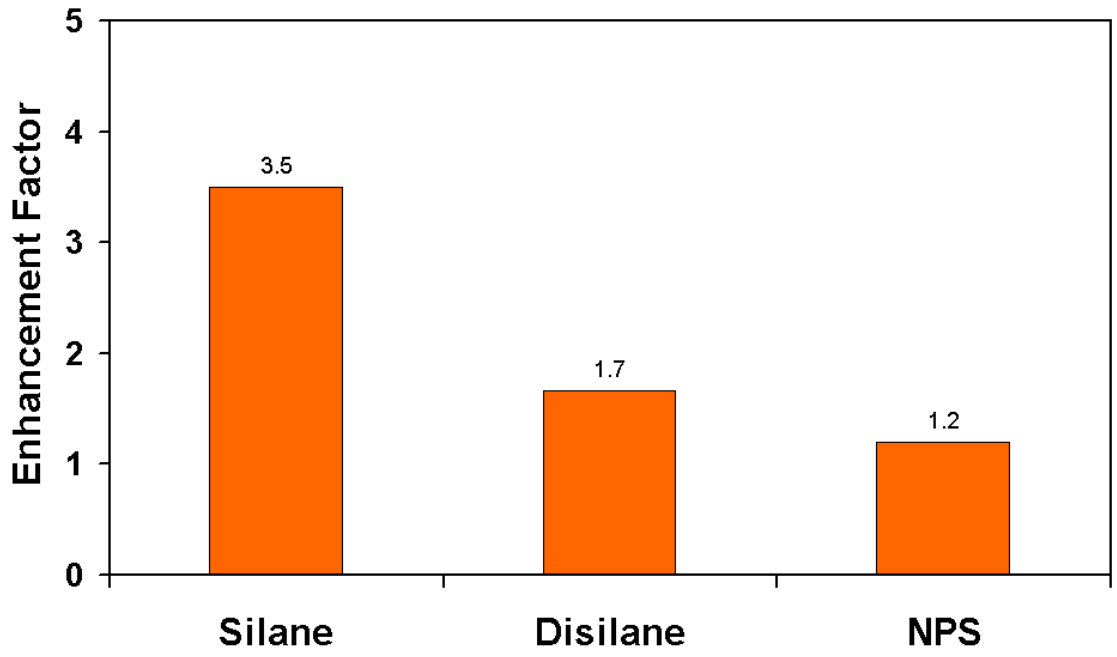

Figure 4.13. Epitaxial growth rate enhancement factor for the growth in nitrogen vs. hydrogen ambients for silane, disilane and NPS at 600^{o}C. Note the decreasing growth rate enhancement factor upon switching to a nitrogen ambient for disilane and NPS compared to silane.

The lack of increase in rate from hydrogen to nitrogen ambient suggests that open sites from the hydrogen ambient-surface equilibrium play a small role in determining the growth rate with NPS, and play a smaller role with disilane than with silane. There are two possibilities to explain this affect. The first is that higher-order silanes can somehow adsorb without open surface sites. The second is that the growth cycle with higher-order silanes can create its own open surface sites, without relying on conventional hydrogen desorption to create them. In this mechanism the growth process uses an open site to start the growth process but does not consume the site (i.e. it regenerates the used site so the reaction does not depend on hydrogen desorption for every adsorbing neopentasilane molecule). Both mechanisms could also be occurring simultaneously in the growth process with high-order silanes. The rest of the chapter is largely used to examine which of the two mechanisms is more likely.

4.4 Surface Adsorption Mechanisms of High-Order Silanes for Epitaxial Growth

4.4.1 Surface Adsorption Mechanisms with Alkanes

We will attempt to draw an analogy between high-order silane reactions and the cracking mechanisms of alkanes of zeolites (silicon-aluminum surfaces) and surface-catalyzed cracking of alkanes on metal catalysts. Alkanes are linear molecules that are carbon-based, analogous to the silicon-based silanes. Ethane (C_2H_6) is the carbon-based equivalent to the silicon-based disilane, Si_2H_6. Based on previous studies of alkanes, we propose that there are two possible mechanisms that could explain the lack of dependence of pre-existing open surface sites.

The first is that the high-order silane molecule can adsorb onto the surface via a concerted surface reaction (simultaneous forming and breaking of 2 or more bonds). Our theory for a concerted model arises from the well-studied cracking of linear and branched hydrocarbons on catalytic hydrogen covered metal surfaces. As the branching of the hydrocarbon increases, the carbon-carbon bond weakens and cracks more readily [4.21][4.22][4.23]. This thus promotes a "concerted" reaction of simultaneous bond breaking and bond forming. In this case, a carbon-carbon bond breaks and a hydrogen-metal surface bond breaks, and they are replaced by a carbon-hydrogen bond and a carbon-metal surface bond [4.21][4.22][4.23]. The reaction is given in Equation 4.14 below (Figure 4.14a):

Eq. 4.14 $C_2H_6 + H^* \Rightarrow CH_3^* + CH_4\ (g)$

Due to the significantly lower energy of the Si-Si bond (317.55 KJ/mol) compared with the C-C bond (370.91 KJ/mol), such reactions occurring with silanes are even more likely than with alkanes. Note that in this reaction, there is no need for a pre-existing surface site which is free from hydrogen.

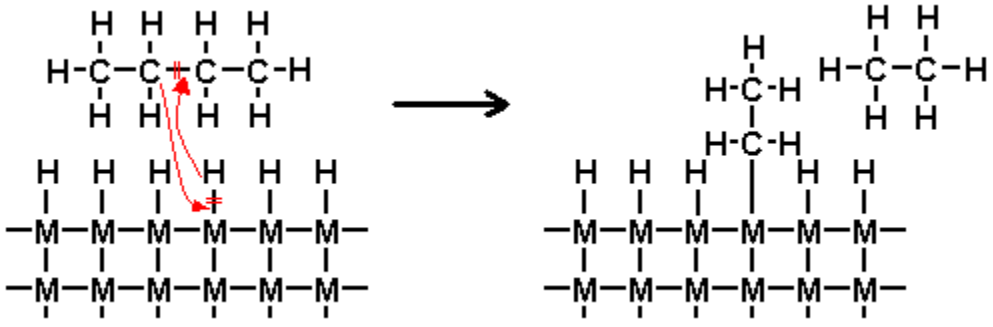

Figure 4.14a. Butane concerted reaction on a metal catalytic surface without the need for open sites. The C-C bond of the butane molecule is broken by the insertion of a surface hydrogen onto the surface, while the other side of the C-C bond is then attached onto an open site on the surface. In this reaction the number of open sites are preserved.

The second possible mechanism is that the high-order silane adsorbs onto the surface via an existing open site and enhances desorption of hydrogen similar to the hydrogenoylsis of alkanes on metal surfaces. Hydrogenolysis is defined as the breaking of C-C bonds by the uptake of surface hydrogen [4.24]. In Figure 4.14b we show a schematic of the hydrogenolysis of butane (C_4H_{10}). In the reaction first the butane is adsorbed dissociatively onto the surface. The C-C bond of the remaining ethyl on the surface is then broken by the insertion of a neighboring hydrogen atom. Methane is then desorbed off the surface leaving CH_2 on the surface and creating an open site. The remaining CH_2 will then react further with hydrogen and desorb off as CH_4 (not shown in Figure 4.14b). We note that in hydrogenolysis open sites are generated.

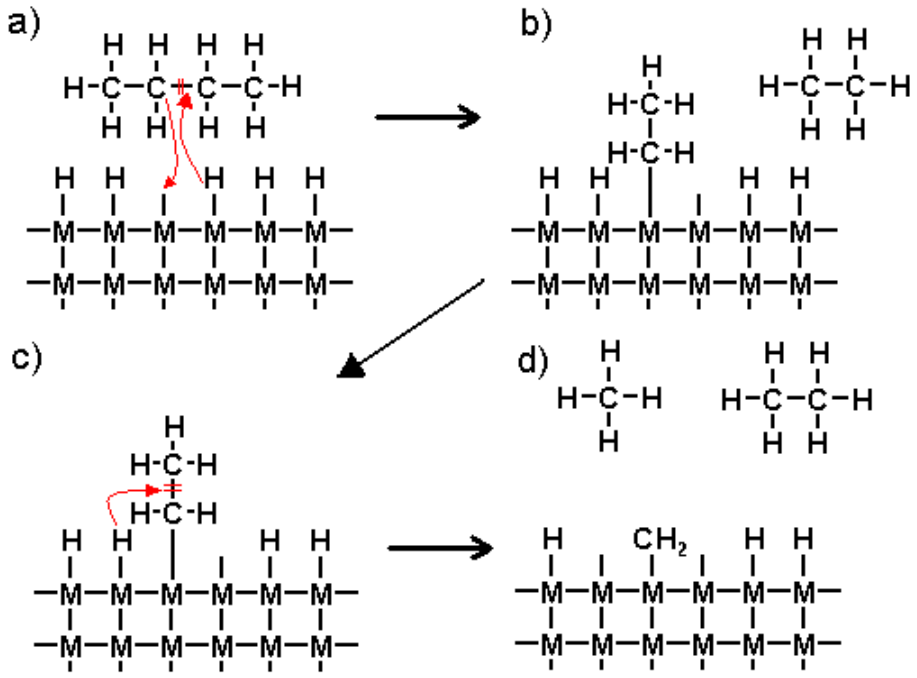

Figure 4.14b. The cracking of butane on a metal surface by hydrogenolysis. The butane is adsorbed dissciatively onto the surface leaving an ethyl on the surface. The C-C bond of the ethyl is then broken by the insertion of surface hydrogen. The methane is desorbed off leaving CH_2 and an open site.

We can formulate similar reactions for high order silanes such as disilane and NPS instead of alkanes. The disilane and NPS surface adsorption mechanisms will be covered in the next two subsections. These mechanisms will involve either the conventional growth using two open sites, concerted processes requiring one or zero open sites, and hydrogenolysis. Note that in practice all of these mechanisms could take place simultaneously.

4.4.2 Proposed Disilane Surface Adsorption Mechanisms

There have been many experiments conducted to determine the disilane adsorption mechanism on silicon surfaces [4.15][4.16][4.18][4.25][4.26]. On clean surfaces free of hydrogen, it is agreed upon that disilane adsorbs dissociatively.

In CVD, when the surface is largely hydrogen covered, the conventional model for dissociative disilane adsorption requires two adjacent open sites (Section 4.2.3). This conventional model fails to explain why the there is little growth rate enhancement when more open surface sites are available as shown experimentally in Section 4.3. In order to explain the growth rate enhancement observed by disilane compared with silane in hydrogen, and to explain the lack of significant growth enhancement upon switching to nitrogen, we will propose that disilane can adsorb via a different surface reaction than the conventional one. In these surface reactions, the incoming disilane can either adsorb without open sites or regenerate them during the adsorption cycle. We will examine all possible mechanisms in which disilane can adsorb onto the surface. The mechanisms may involve two, one, or zero initial open sites. The six possible reaction processes labeled A-F are shown in Figures 4.15A-F below:

Process A:

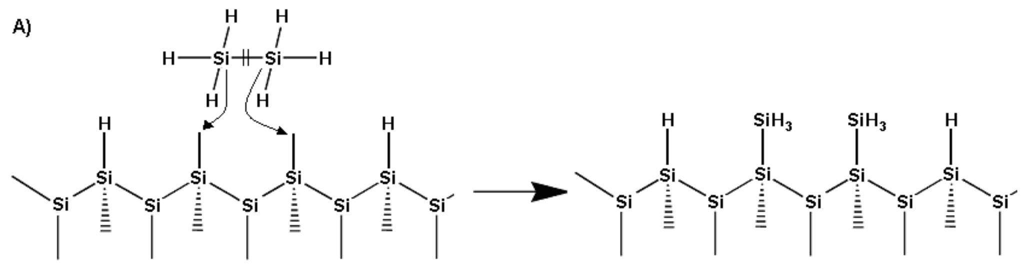

Figure 4.15A. *Process A*: Disilane adsorption reaction on a (2 x 1) reconstructed silicon surface. The disilane dissociatively adsorbs onto the surface using two open sites (Same as Figure 4.11). Two SiH_3 fragments then occupy the two sites on the surface.

In *Process A* (Figure 4.15A) the disilane adsorbs dissociatively by the breaking of the central Si-Si bond (317.55 KJ/mol). The two SiH_3 species then adsorb using two open surface sites. This is the conventionally accepted growth mechanism as shown earlier in Figure 4.10 and Equation 4.13.

Process B:

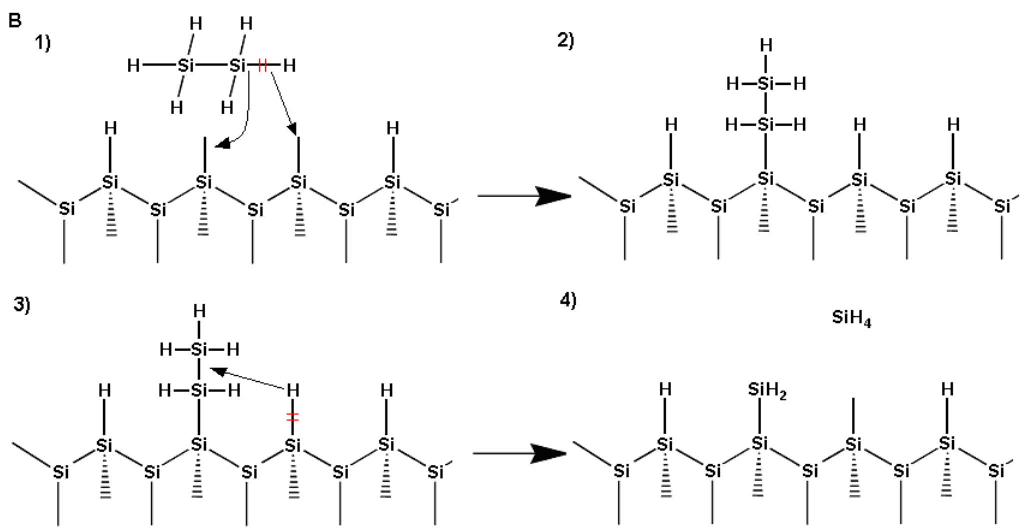

Figure 4.15B1. *Process B:* Disilane adsorption reaction on a (2 x 1) reconstructed silicon surface. The disilane dissociatively adsorbs onto the surface using two open sites. In this reaction a Si-H bond is broken and Si_2H_5 and a single H is adsorbed onto the surface. Another surface hydrogen can then attack the Si-Si bond of the adsorbed Si_2H_5 molecule. This mechanism is similar to hydrogenolysis of alkanes via surface catalyzed cracking (See Figure 4.14). SiH_4 is then desorbed off and SiH_2 and an open site are left on the surface.

In *Process B* (Figure 4.15B) the disilane adsorbs onto two open surface sites by the breaking of a Si-H bond (371.66 KJ/mol) instead of the central Si-Si bond (317.55 KJ/mol). Si_2H_5 and H are then adsorbed onto the surface (Equation 4.15a), each occupying one of the open sites.

Eq. 4.15a $H_3Si\text{-}SiH_3 + 2\_ \Rightarrow H_2Si^*\text{-}SiH_3 + H^*$

The surface hydrogen can then attack the Si-Si bond of the Si_2H_5 in a manner similar to the hydrogenolysis of alkanes. A SiH_4 molecule is then desorbed off the surface and a SiH_2 is left on the surface along with an open site from the uptake of the surface hydrogen to form the silane molecules (Equation 4.15b)

Eq. 4.15b $H_2Si^*\text{-}SiH_3 + H^* \Rightarrow H_2Si^* + \_ + SiH_4\ (g)$

The total reaction is then:

Eq. 4.15c $H_3Si\text{-}SiH_3 + 2\_ \Rightarrow H_2Si^*\text{-}SiH_3 + H^* \Rightarrow H_2Si^* + \_ + SiH_4\ (g)$

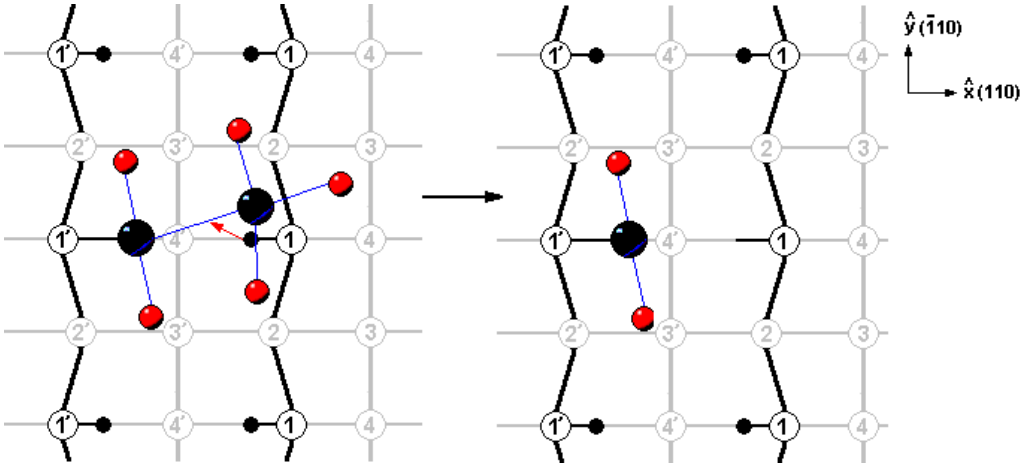

Figure 4.15B2. *Process B:* Top view of the reaction of surface-bonded H_2Si-SiH_3 molecule with a surface hydrogen molecule. The surface hydrogen inserts itself into the Si-Si bond and forms a silane molecule which desorbed from the surface (not shown in diagram). Note that the H_2Si^*-SiH_3 can also react with the surface hydrogen along the dimer row instead of the hydrogen on the intra-dimer.

The reaction steps in Equation 4.15b are illustrated from a top view in Figure 4.15B1. Note that the H_2Si^*-SiH_3 can also react with the surface hydrogen along the dimer row instead of the hydrogen on the intra-dimer. In either case, in this growth reaction only one open site is consumed and a SiH_2 is left on the surface along with an open surface site. The SiH_2 can then either pass off one of its hydrogen atoms into the open site, or the silicon atom can bond with the open site, so that it forms two bonds with the silicon surface. In either case the SiH_2 is closer to being incorporated into the solid than SiH_3.

Process C

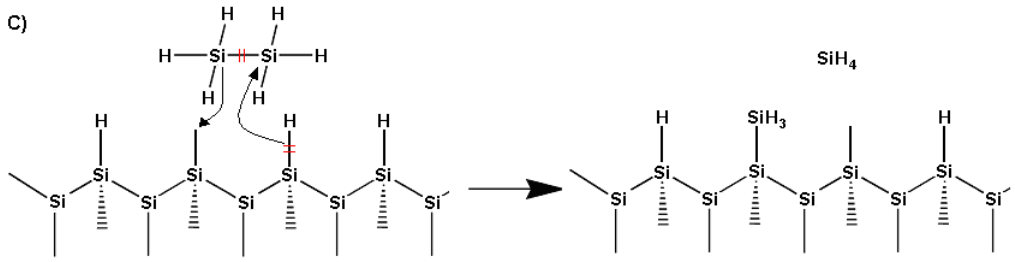

Figure 4.15C. *Process C:* Disilane adsorption reaction on a (2 x 1) reconstructed silicon surface using only one site. The disilane adsorbs via a concerted reaction where the Si-Si bond of the disilane molecule is broken by the insertion of a surface hydrogen onto the surface, while the other side of the Si-Si bond is then attached onto an open site on the surface. In this reaction the number of open surface sites are preserved.

In *Process C* (Figure 4.15C), we propose that the disilane molecule adsorbs via a concerted reaction with only one open site. In this reaction then Si-Si bond of the disilane is broken when the disilane molecule comes into proximity of surface hydrogen and an open site (Equation 4.16).

Eq. 4.16 $H_3Si\text{-}SiH_3 + \_ + H^* \Rightarrow SiH_3^* + \_ + SiH_4\ (g)$

The surface hydrogen inserts itself onto one side of the SiH_3, forming silane, which is then desorbed away from the surface. The other SiH_3 is then adsorbed onto the surface. In this reaction process the total number of open sites is preserved.

Process D:

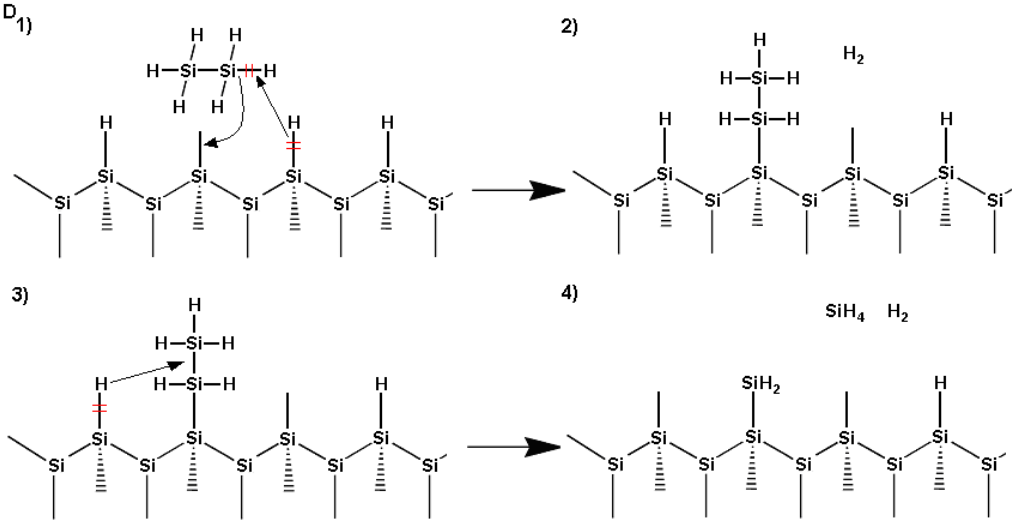

Figure 4.15D. *Process D:* Disilane adsorption reaction on a (2 x 1) reconstructed silicon surface using only one open site. The disilane adsorbs via a concerted reaction where the Si-Si bond of the disilane molecule is broken by the insertion of a surface hydrogen onto the surface, while the other side of the Si-H bond is then attached onto an open site on the surface. In this reaction a total of one open site is generated.

In *Process D* (Figure 4.15D), again the disilane can adsorb via a concerted reaction onto the surface using only one open site as in *Process C*. Unlike *Process C,* in *Process D* the Si-H bond is broken instead of the Si-Si bond. H_2 is desorbed and Si_2H_5 is adsorbed onto the surface (Equation 4.17a)

Eq. 4.17a $\quad H_3Si\text{-}SiH_3 + \_ + H^* \Rightarrow H_2Si^*\text{-}SiH_3 + \_ + H_2\ (g)$

The Si-Si bond of the Si_2H_5 is then attacked by surface hydrogen to desorb off one side of the Si-Si bond as SiH_4, leaving an open site and SiH_2 on the surface (Equation 4.17b).

Eq. 4.17b $\quad H_2Si^*\text{-}SiH_3 + H^* \Rightarrow H_2Si^* + \_ + SiH_4\ (g)$

Adding the two steps together gives Equation 4.17c.

Eq. 4.17c $H_3Si\text{-}SiH_3 + \_ + 2H^* \Rightarrow H_2Si^* + 2\_ + SiH_4\,(g) + H_2\,(g)$

The net total reaction is then,

Eq. 4.17d $H_3Si\text{-}SiH_3 + 2H^* \Rightarrow H_2Si^* + \_ + SiH_4\,(g) + H_2\,(g)$

In this reaction mechanism an open site is generated on the surface along with the by products of silane and hydrogen (Equation 4.17d). Again SiH_2 is left on the surface instead of the usual SiH_3.

Process E:

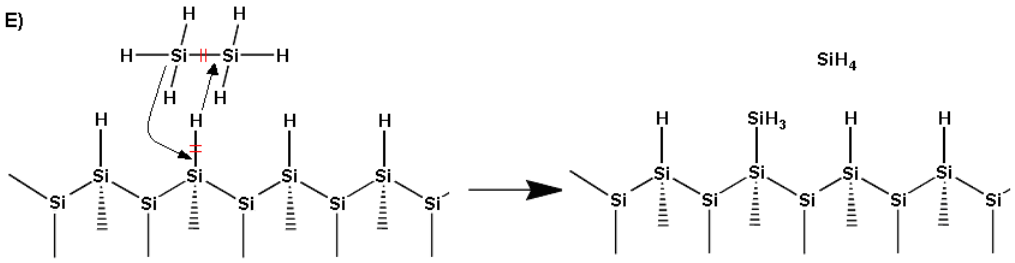

Figure 4.15E. *Process E:* Disilane adsorption reaction on a (2 x 1) reconstructed silicon without the need for open sites. The disilane adsorbs via a concerted reaction where the Si-Si bond of the disilane molecule is broken by the insertion of a surface hydrogen onto the surface, while the other side of the Si-Si bond is then attached onto an open site on the surface. In this reaction the number of open sites are preserved.

In *Process E* (Figure 4.15E), we propose that the disilane can adsorb via a concerted reaction without the need for open sites.

Eq. 4.18 $H_3Si\text{-}SiH_3 + H^* \Rightarrow SiH_3^* + SiH_4\,(g)$

As the disilane approaches the surface the Si-Si bond breaks, along with a hydrogen-surface bond. The previously surface-bonded hydrogen is inserted into one side of the silicon-silicon bond (desorbing off as SiH_4 (g)), while the other side of the silicon-silicon bond is adsorbed onto the freed surface site as SiH_3 (Equation 4.18). Such a "concerted" mechanism for disilane was also proposed as a possibility for the growth of disilane of (111) Si surfaces [4.27]. Although no desorption of silane was measured in their experimental data, the author did find that incoming disilane caused a reduction in the required temperature of the desorption of hydrogen from 400 ^{o}C to 250 ^{o}C. This result leads us to the possibility of *Process F*, where a concerted growth process of a Si-H bond-breaking instead of a Si-Si bond breaking is taking place (Figure 4.15F).

Process F:

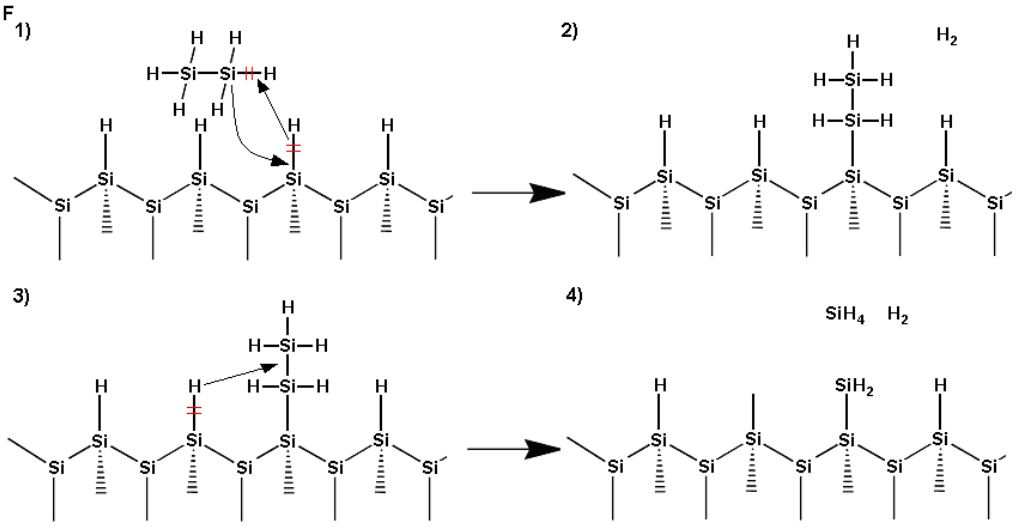

Figure 4.15F. *Process F:* Disilane adsorption reaction on a (2 x 1) reconstructed silicon without the need for open sites. The disilane adsorbs via a concerted reaction where the Si-H bond of the disilane molecule is broken by the insertion of a surface hydrogen, while the other side of the Si-H bond is then attached onto an open site on the surface. In this reaction a total of one open site is generated and SiH_2 is left on the surface.

In Figure 4.15F, the disilane adsorbs via a concerted reaction where the Si-H bond is broken by the insertion of surface hydrogen. Si_2H_5 is inserted onto the surface as a hydrogen from the surface forms H_2 gas with a hydrogen from the silane (Equation 4.19a).

Eq. 4.19a $H_3Si\text{-}SiH_3 + H^* \Rightarrow H_2Si^*\text{-}SiH_3 + H_2\ (g)$

The Si-Si bond of the Si_2H_5 is then attacked by a surface hydrogen, forming SiH_4 (g) which desorbs off the surface.

Eq. 4.19b $H_2Si^*\text{-}SiH_3 + H^* \Rightarrow H_2Si^* + \_ + SiH_4\ (g)$

In the total reaction SiH_2 is left on the surface along with a generated open surface site and the by products of silane and hydrogen which can then re-adsorb onto other open surface sites.

Eq. 4.19c $H_3Si\text{-}SiH_3 + 2H^* \Rightarrow H_2Si^* + \_ + SiH_4\ (g) + H_2\ (g)$

Discussion:

The six possible mechanisms are summarized in Table 4.2 below:

Table 4.2: Possible surface reaction mechanisms for the adsorption of disilane onto a silicon surface.

Process	Bond	Surface Reaction	Uptake of H*	# of Open Sites Required	Final Surface Species	# of Net Sites
A (Disilane)	**Si-Si**	**$H_3Si\text{-}SiH_3$ + 2_ => 2 SiH_3***	**No**	**2**	**2SiH_3**	**+1**
B (Disilane)	**Si-H**	**$H_3Si\text{-}SiH_3$ + 2_ => Si_2H_5* + H***	**SiH_4**	**2**	**SiH_2**	**-1**
C (Disilane)	**Si-Si**	**$H_3Si\text{-}SiH_3$ + _ + H* => SiH_3* + SiH_4(g) + _**	**No**	**1**	**SiH_3**	**0**
D (Disilane)	**Si-H**	**$H_3Si\text{-}SiH_3$ + _ + H* => Si_2H_5* + H_2(g)+_**	**SiH_4**	**1**	**SiH_2**	**+1**
E (Disilane)	**Si-Si**	**$H_3Si\text{-}SiH_3$ + H* => SiH_3* + SiH_4(g)**	**No**	**0**	**SiH_3**	**0**
F (Disilane)	**Si-Si**	**$H_3Si\text{-}SiH_3$ + H* => Si_2H_5* + H_2(g)**	**3SiH_4**	**0**	**SiH_2**	**+1**

The "bond" column is the initial bond that breaks when the disilane molecule is adsorbed onto the surface. The "Uptake of Hydrogen" column is the attacking of a Si-Si bond by hydrogen similar to hydrogenolysis of alkanes. The "# of Open Sites Required" column denotes the number of open surface sites to start the reaction process. The "Final Surface Species" column is the silicon species remaining on the surface when the reaction process is completed. The "# of Net Sites" column describes the net generation of surface on the original surface free of hydrogen. Adsorbed SiH_2 is not counted in this total. *Process A* and *Process B* requires two open surface sites to take place and both are net consuming of open sites. *Process C* and *Process D* only require one open site to begin the reaction and can regenerate the open site (C) or create an additional open site (D). (Note: SiH_2 surface species are not counted as an open site.) Note *Process E* and *Process F* may take place without the need for a prior open site. Thus as the hydrogen pressure was decreased, leading to more open sites, the growth rate would not increase for these last two processes.

Recall from experiments (Section 4.3) that with disilane, the growth rate enhancement was small compared with silane when the hydrogen partial pressure was decreased. This suggests that reactions which require open sites to start the surface reaction, and/or which consumes open sites, are not likely to be the dominant growth process. They would be expected to greatly increase as the hydrogen surface coverage decreases with decreasing hydrogen pressure, especially *Process A* and *Process B* as both requires two open sites and are net consuming of surface sites. *Process C and Process D* do not consume sites but still requires and open site to start the reaction, hence a decrease in hydrogen surface coverage should increase the growth rate if either of these were the dominant growth process. Only *Procesess E & F* are still possibilities as the dominant growth process as they do not require open surface sites for adsorption and/or generate open surface sites. In Section 4.5 we will examine surface roughness to shed further light on the question of whether the growth mechanisms using disilane can generate additional open sites.

4.4.3 Proposed NPS Surface Adsorption Mechanisms

In the previous section, we examined possible disilane growth mechanism and showed that "concerted" processes (besides usual dissociative adsorption) likely to explain the high growth rates and lack of growth rate increase in going from a hydrogen to a nitrogen ambient. Similarly for NPS, in this section, we will examine eight possible mechanisms in which NPS can adsorb onto the surface. Since NPS has multiple silicon atoms it is in principle possible for the reaction to involve as many as 5 open sites. Due to our growth being in the low temperature range with a hydrogen coverage where open site fractions are rare, we will ignore all adsorption reactions that require more than 2 open sites. Our

proposed mechanisms may involve two, one, or zero open sites. These reaction processes will be shown in Figures 4.15G-N below:

Process G:

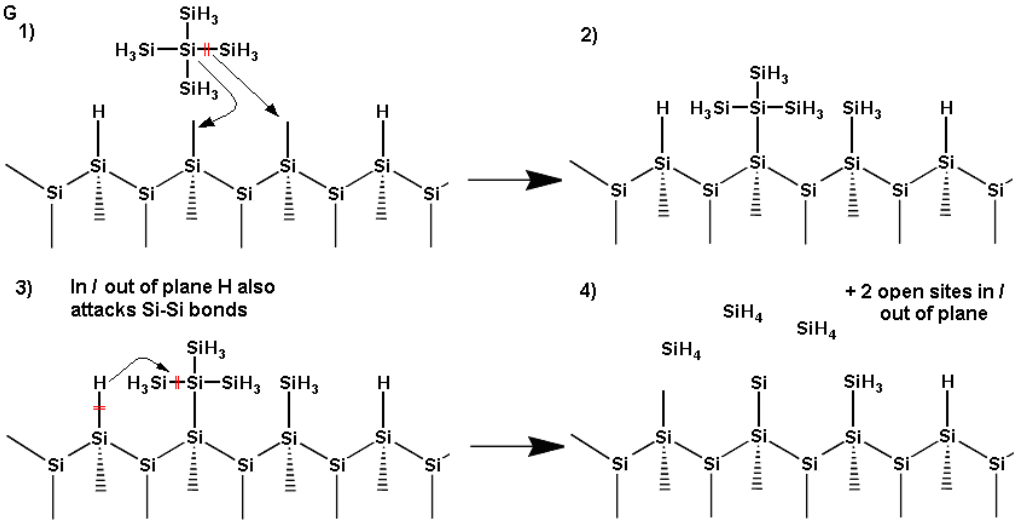

Figure 4.15G. *Process G:* NPS adsorption reaction on a (2 x 1) reconstructed silicon surface. The NPS dissociatively adsorbs onto the surface using two open surface sites. SiH_3 and Si-3SiH_3 is adsorbed onto the surface (2). Surface hydrogen atoms can attack the Si-Si bonds of the adsorbed Si-3SiH_3 molecule and desorb off the surface as SiH_4 (3). In this reaction an open site is created by the adsorption of NPS.

In *Process G* (Figure 4.15G), NPS adsorbs dissociatively by the breaking of one of its four Si-Si bonds. A SiH_3 and Si-3SiH_3 adsorb onto the surface via a Si-Si surface bond (Eq. 4.20a)

Eq. 4.20a $\qquad$ Si-4SiH_3 + 2_ => Si*-3SiH_3 + SiH_3*

The Si-Si bonds of the adsorbed Si-3SiH_3 are then attacked by surface hydrogen (3 in Figure 4.15G) to desorb off as SiH_4 (Equation 4.25b). If the Si-Si bond of the Si-3SiH_3 sees an open site instead of surface hydrogen the SiH_3 can break off and adsorb onto the surface (not shown).

Eq. 4.20b $Si^*\text{-}3SiH_3 + 3H^* \Rightarrow Si^* + 3\_ + 3SiH_4$ (g)

The net reaction of *Process G* is:

Eq. 4.20c $Si\text{-}4SiH_3 + 2\_ + 3H^* \Rightarrow Si^* + 3\_ + SiH_3^* + 3SiH_4$ (g)

In this reaction for NPS, a Si adatom is left on the surface along with the net generation of an open site and the byproducts of 3 silane molecules. Note that Si* is likely to incorporated into the solid by bonding with an in/out of plane open site to form the next surface layer.

Process H:

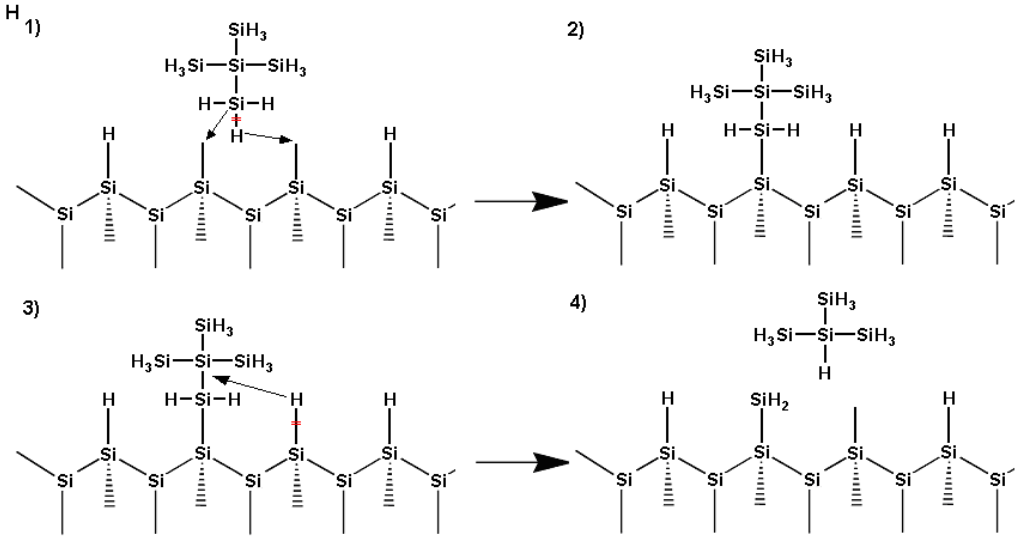

Figure 4.15H *Process H*: NPS adsorption reaction on a (2 x 1) reconstructed silicon surface. The NPS dissociatively adsorbs onto the surface using two open surface sites. SiH_2-Si-$3SiH_3$ and H is adsorbed onto the surface (2). Surface hydrogen atoms can attack the Si-Si bond of the adsorbed SiH_2-Si-$3SiH_3$ molecule (3) and desorbs off the surface as H-Si-$3SiH_3$. A total of one site is used up in this reaction (4).

In *Process H* (Figure 4.15H), NPS adsorbs dissociatively by the breaking of one of its twelve Si-H bonds. An H_2Si-Si-$3SiH_3$ adsorbs onto the surface via a Si-Si surface bond as shown in part 2 of Figure 4.15H.

Eq. 4.21a $\quad Si\text{-}4SiH_3 + 2\_ \Rightarrow H_2Si^*\text{-}Si\text{-}3SiH_3 + H^*$

The central Si-Si bond of the adsorb H_2Si^*-Si-$3SiH_3$ is then attacked by surface hydrogen (3 in Figure 4.15H) to desorb off as H-Si-$3SiH_3$ (Equation 4.21b).

Eq. 4.21b $\quad H_2Si^*\text{-}Si\text{-}3SiH_3 + H^* \Rightarrow SiH_2^* + H\text{-}Si\text{-}3SiH_3(g) + \_$

The net reaction of *Process H* is:

Eq. 4.21c $\quad Si\text{-}4SiH_3 + 2\_ \Rightarrow SiH_2^* + H\text{-}Si\text{-}3SiH_3(g) + \_$

In this net reaction for NPS, a SiH_2 is left on the surface along with the byproduct of H-Si-$3SiH_3$ and a net loss of one open site.

Process I:

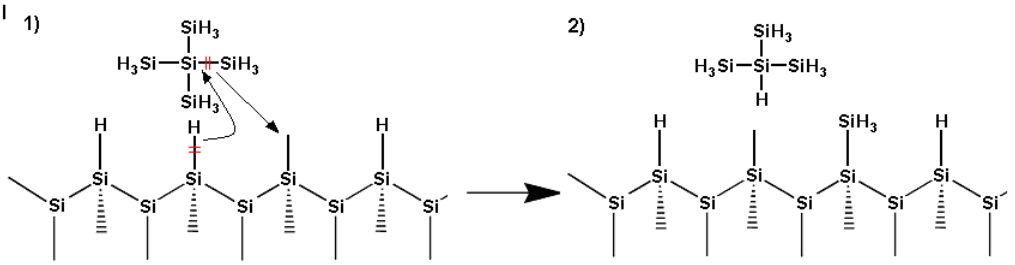

Figure 4.15I. *Process I:* NPS adsorption reaction on a (2 x 1) reconstructed silicon surface. The NPS dissociatively adsorbs onto the surface using one open surface site. A Si-Si bond of NPS is broken by the insertion of a surface hydrogen forming H-Si-$3SiH_3$. The SiH_3 from the original NPS is adsorbed onto the surface simultaneously. The total number of open sites is conserved in this reaction process.

In *Process I* (Figure 4.15I), NPS adsorbs via a concerted reaction onto the surface using only one open surface site. A Si-Si bond of NPS is broken by the insertion of surface hydrogen forming H-Si-3SiH_3 as a byproduct. The other side of the Si-Si bond, SiH_3 is adsorbed onto the open surface site (Equation 4.22)

Eq. 4.22 $\quad Si\text{-}4SiH_3 + \_ + H^* \Rightarrow SiH_3^* + \_ + H\text{-}Si\text{-}3SiH_3\ (g)$

In this reaction for NPS, a SiH_3 is left onto the surface along with an open site and the byproduct of H-Si-3SiH_3(g) is created. Note that in this reaction no net sites are gained or lost.

Process J:

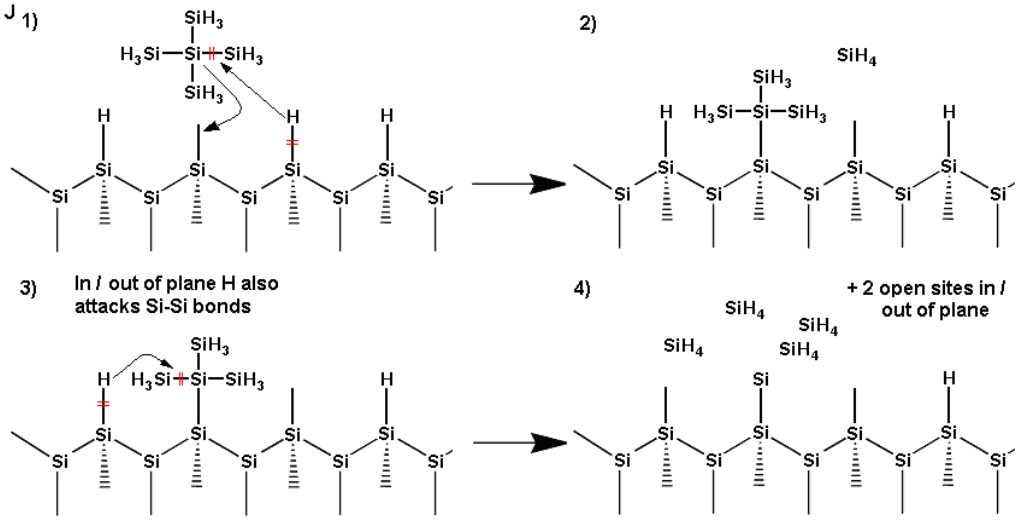

Figure 4.15J. *Process J:* NPS adsorption reaction on a (2 x 1) reconstructed silicon surface. The NPS dissociatively adsorbs onto the surface using one open surface site. An Si-Si bond of NPS is broken by the insertion of a surface hydrogen forming SiH_4. The other side of the Si-Si bond is attached to the surface as Si-3SiH_3 (2). Surface hydrogen atoms can then attack the Si-Si bonds of the Si-3SiH_3 molecule (3) and form SiH_4, which is desorbed off the surface leaving a Si atom on the surface. This reaction process creates a total of 3 open sites.

In *Process J* (Figure 4.15J), NPS adsorbs via a concerted reaction onto the surface using only one open surface site. A Si-Si bond of NPS is broken by the insertion of surface hydrogen forming SiH_4 as a byproduct. The other side of the Si-Si bond, $Si\text{-}3SiH_3$ is adsorbed onto the open surface site (Equation 4.23a)

Eq. 4.23a $\quad Si\text{-}4SiH_3 + \_ + H^* \Rightarrow Si\text{-}3SiH_3^* + \_ + SiH_4\ (g)$

Similar to *Process G*, the Si-Si bonds of the adsorbed $Si\text{-}3SiH_3$ are then attacked by surface hydrogen (3 in Figure 4.15J) to desorb off as SiH_4 (Equation 4.23b).

Eq. 4.23b $\quad Si^*\text{-}3SiH_3 + 3H^* \Rightarrow Si^* + 3\_ + 3SiH_4\ (g)$

The net reaction of *Process J* is:

Eq. 4.23c $\quad Si\text{-}4SiH_3 + \_ + 4H^* \Rightarrow Si^* + 4\_ + 4SiH_4\ (g)$

In this reaction for NPS, a Si adatom is left onto the surface along with the net generation of three open sites and the byproducts of four silane molecules. The silane byproducts may re-adsorb onto the surface.

Process K:

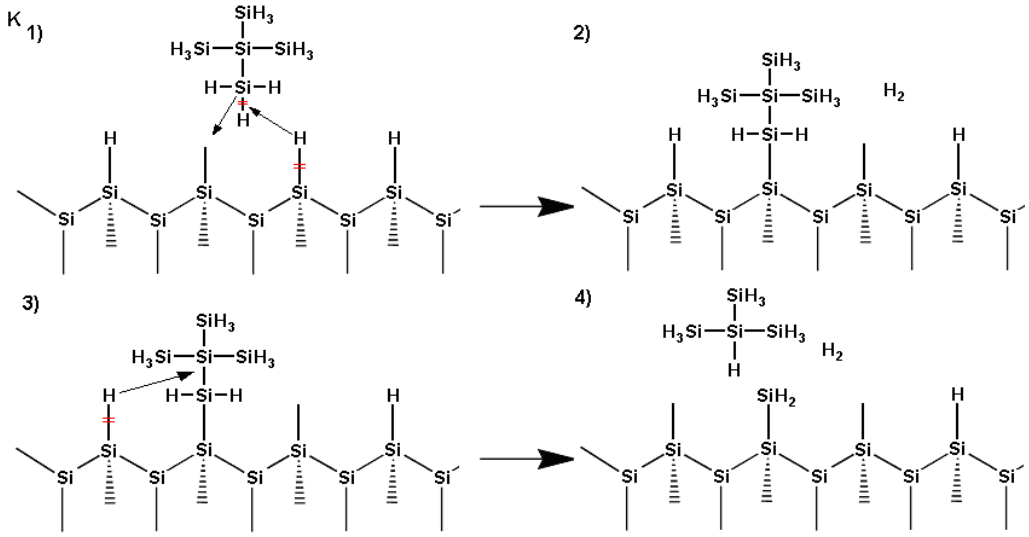

Figure 4.15K. *Process K:* NPS adsorption reaction on a (2 x 1) reconstructed silicon surface. The NPS dissociatively adsorbs onto the surface using one open surface site. An Si-H bond of NPS is broken by the insertion of a surface hydrogen forming H_2 gas. The other side of the Si-H bond is attached to the surface as SiH_2-Si-3SiH_3 (2). Surface hydrogen atoms can then attack the Si-Si bonds of the SiH_2-Si-3SiH_3 molecule (3) and form H-Si-3SiH_3, which is desorbed off the surface leaving just an Si atom on the surface. This reaction process creates an open site.

In *Process K* (Figure 4.15K), NPS adsorbs via a concerted reaction onto the surface using only one open surface site. A Si-H bond of NPS is broken by the insertion of surface hydrogen forming H_2 (g) as a byproduct. The other side of the Si-H bond, H_2Si-Si-3SiH_3 is adsorbed onto the open surface site (Equation 4.24a)

Eq. 4.24a $\quad$ Si-4SiH_3 + _ + H* => H_2Si-Si-3SiH_3* + _ +H_2 (g)

The central Si-Si bond of the adsorbed H_2Si-Si-3SiH_3 is then attacked by surface hydrogen (3 in Figure 4.15K) to desorb off as H-Si-3SiH_3(g) leaving a SiH_2 on the surface (Equation 4.24b)

Eq. 4.24b $H_2Si\text{-}Si\text{-}3SiH_3^* + H^* \Rightarrow SiH_2^* + H\text{-}Si\text{-}3SiH_3(g) + \_$

The net reaction of *Process K* is:

Eq. 4.24c $Si\text{-}4SiH_3 + \_ + 2H^* \Rightarrow SiH_2^*\ H\text{-}Si\text{-}3SiH_3(g) + 2\ \_ + H_2\ (g)$

In this reaction for NPS, a SiH_2 is left on the surface along with the generation of an open site and the byproducts of $H\text{-}Si\text{-}3SiH_3(g)$ and H_2 (g). The $H\text{-}Si\text{-}3SiH_3(g)$ byproduct may re-adsorb onto the surface.

Process L:

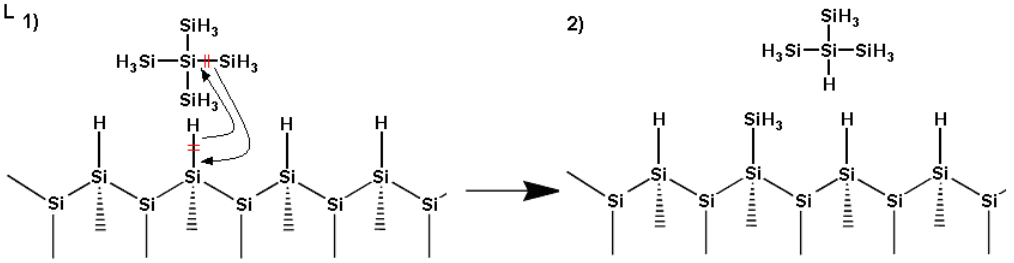

Figure 4.15L. *Process L:* NPS adsorption reaction on a (2 x 1) reconstructed silicon surface. The NPS adsorbs onto the surface without the need for an open surface site. An Si-Si bond of NPS is broken by the insertion of a surface hydrogen forming $H\text{-}Si\text{-}3SiH_3$. The SiH_3 from the original NPS is adsorbed onto the surface simultaneously. The total number of open sites is conserved in this reaction process.

In *Process L* (Figure 4.15L), NPS adsorbs via a concerted reaction onto the surface without the need for open surface sites. A Si-Si bond of NPS is broken by the insertion of surface hydrogen forming $H\text{-}Si\text{-}3SiH_3$ as a byproduct. The other side of the Si-Si bond, SiH_3 is adsorbed onto the open surface site (Equation 4.25)

Eq. 4.25 $Si\text{-}4SiH_3 + H^* \Rightarrow SiH_3^* + H\text{-}Si\text{-}3SiH_3\ (g)$

In this reaction for NPS, a SiH_3 is left onto the surface and the byproduct H-Si-3SiH_3(g) is created. Note that in this reaction no net sites are gained or lost.

Process M:

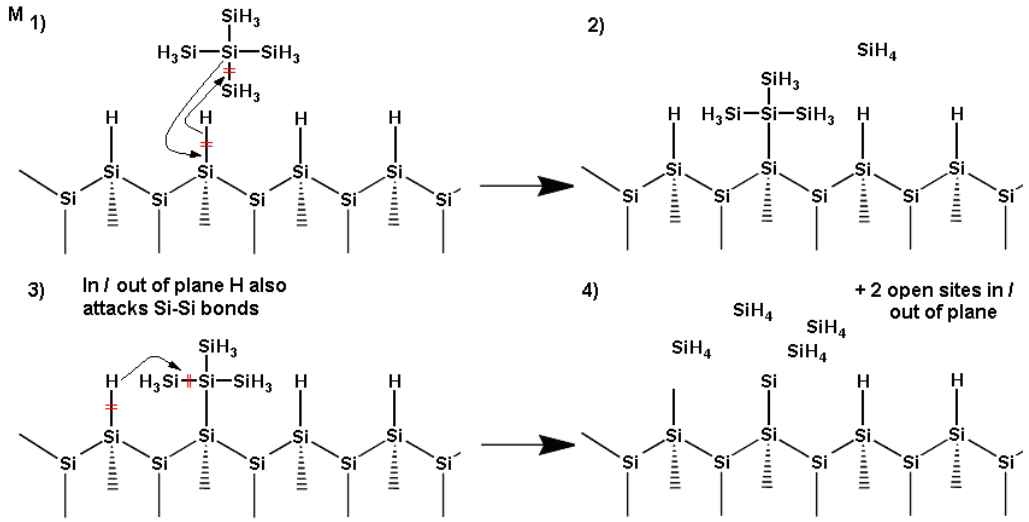

Figure 4.15M. *Process M:* NPS adsorption reaction on a (2 x 1) reconstructed silicon surface. The NPS adsorbs onto the surface without the need for an open surface site. An Si-Si bond of NPS is broken by the insertion of a surface hydrogen forming SiH_4. The other side of the Si-Si bond is attached to the surface as Si-3SiH_3 (2). Surface hydrogen atoms can then attack the Si-Si bonds of the Si-3SiH_3 molecule (3) and form SiH_4, which is desorbed off the surface leaving a Si atom on the surface. This reaction process creates a total of 3 open sites.

In *Process M* (Figure 4.15M), NPS adsorbs via a concerted reaction onto the surface using no open surface sites. A Si-Si bond of NPS is broken by the insertion of surface hydrogen forming SiH_4 as a byproduct. The other side of the Si-Si bond, Si-3SiH_3 is adsorbed onto the open surface site (Equation 4.26a)

Eq. 4.26a $\quad$ Si-4SiH_3 + H* => Si-3SiH_3* + SiH_4 (g)

The Si-Si bonds of the adsorb Si-3SiH_3 are then attacked by surface hydrogen (3 in Figure 4.15M) to desorb off as SiH_4 (Eq. 4.26b) as in *Processes G & J.*

Eq. 4.26b $\quad$ Si*-3SiH_3 + 3H* => Si* + 3_ + 3SiH_4 (g)

The net reaction of *Process M* is:

Eq. 4.26c $\quad$ Si-4SiH_3 + 4H* => Si* + 3_ + 4SiH_4 (g)

In this reaction for NPS, a Si adatom is left onto the surface along with the generation of 3 open sites and the byproducts of 4 silane molecules. The silane byproducts may re-adsorb onto the surface.

Process N:

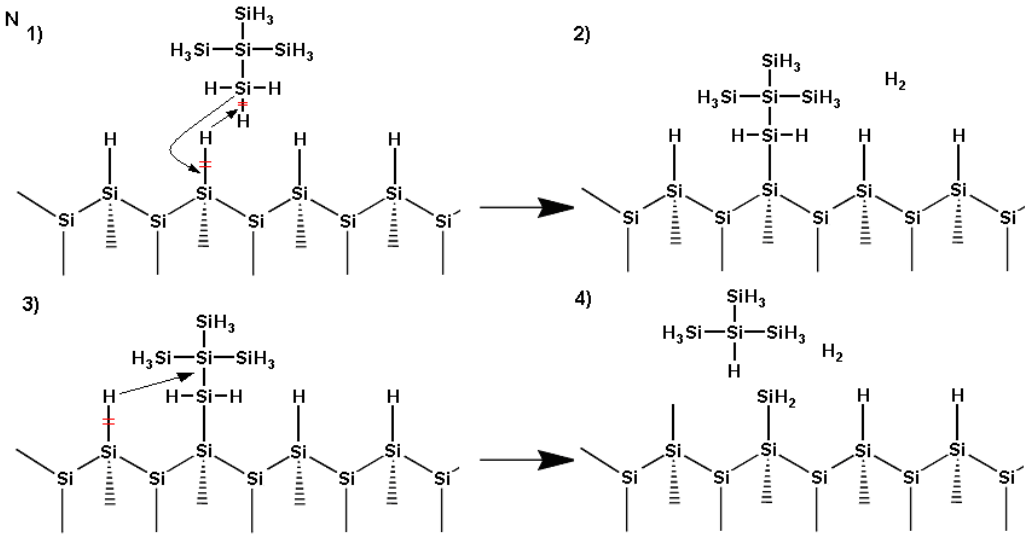

Figure 4.15N. *Process N:* NPS adsorption reaction on a (2 x 1) reconstructed silicon surface. The NPS adsorbs onto the surface without the need for an open surface site. A Si-H bond of NPS is broken by the insertion of a surface hydrogen forming H_2 gas. The other side of the Si-H bond is attached to the surface as SiH_2-Si-3SiH_3 (2). Surface hydrogen atoms can then attack the Si-Si bonds of the SiH_2-Si-3SiH_3 molecule (3) and form H-Si-3SiH_3, which is desorbed off the surface leaving just a Si atom on the surface. This reaction process creates an open site.

In *Process N:* (Figure 4.15N), NPS adsorbs via a concerted reaction onto the surface without the need for open surface site. A Si-H bond of NPS is broken by the insertion of surface hydrogen, to form H_2 (g) as a byproduct. The other side of the Si-Si bond, H_2Si-Si-$3SiH_3$ is adsorbed onto the open surface site (Equation 4.27a)

Eq. 4.27a $\quad Si\text{-}4SiH_3 + H^* \Rightarrow H_2Si\text{-}Si\text{-}3SiH_3^* + H_2\ (g)$

The central Si-Si bond of the adsorb H_2Si-Si-$3SiH_3$ is then attacked by surface hydrogen (3 in Figure 4.15N) as in *Process K* to desorb off as H-Si-$3SiH_3$(g) leaving a SiH_2 on the surface (Equation 4.24b)

Eq. 4.27b $\quad H_2Si\text{-}Si\text{-}2SiH_3^* + H^* \Rightarrow SiH_2^* + H\text{-}Si\text{-}3SiH_3(g) + \_$

The net reaction of *Process N* is:

Eq. 4.27c $\quad Si\text{-}4SiH_3 + 2H^* \Rightarrow SiH_2^* + H\text{-}Si\text{-}3SiH_3(g) + \_ + H_2\ (g)$

In this reaction for NPS, a SiH_2 is left on the surface along with the generation of an open site and the byproducts of H-Si-$3SiH_3$(g) and H_2 (g). The H-Si-$3SiH_3$(g) byproduct may re-adsorb onto the surface.

Alternate Path:

Several growth processes for NPS (G, J, & M) had large fragments of Si-$3SiH_3$ attached to the surface. We proposed that the SiH_3 units could all desorb by combining with surface hydrogen to form SiH_4, leaving a bare Si bound to the surface.

Alternatively, the SiH_3 may adsorb on the surface by a concerted reaction with adjacent surface hydrogens as shown in Figure 4.15O.

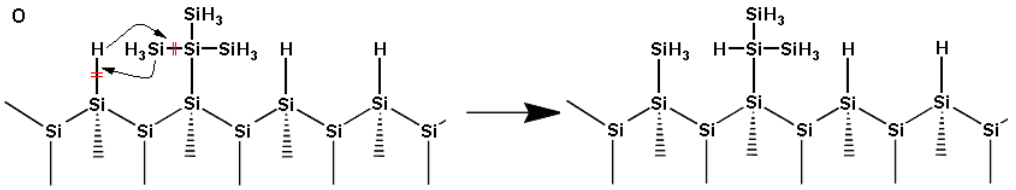

Figure 4.15O. The SiH_3 fragment of the adsorbed Si-3SiH_3 molecule (*Processes G, J & M*) swaps position with a surface hydrogen resulting in an adsorbed SiH_3 and H-Si-2SiH_3.

This will not create any new open sites and does not change the initial process leading to the Si-SiH_3 adsorption. Hence if such a reaction occurs, it will result in fewer open sites generated for *Processes G, J, & M* than originally described. Instead of a net generation of +1, +3, and +3 for the 3 processes respectively, they would now be –2, 0, and 0. Both the uptake of surface hydrogen to form SiH_4 and the swapping of the SiH_3 with the surface hydrogen could occur, resulting in an intermediate value of net open sites.

Discussion:

The eight possible mechanisms are summarized in Table 4.3 below:

Table 4.3: Possible surface reaction mechanisms for the adsorption of NPS onto a silicon surface.

Process	Bond	Surface Reaction	Uptake of H*	# of Open Sites Required	Final Surface Species	# of Net Sites
G (NPS)	**Si-Si**	**Si-4SiH_3 + 2_ => SiH_3* + Si-3SiH_3***	**3SiH_4**	**2**	**Si, SiH_3**	**+1**
H (NPS)	**Si-H**	**Si-4SiH_3 + 2_ => H_2Si*-Si-2SiH_3 + H***	**H-Si-2SiH_3**	**2**	**SiH_2**	**-1**
I (NPS)	**Si-Si**	**Si-4SiH_3 + _ + H* => SiH_3* + H-Si-3SiH_3(g) + _**	**No**	**1**	**SiH_3**	**0**
J (NPS)	**Si-Si**	**Si-4SiH_3 + _ + H* => Si*-3SiH_3+ SiH_4(g) + _**	**3SiH_4**	**1**	**Si**	**+3**
K (NPS)	**Si-H**	**Si-4SiH_3 + _ + H* => H_2Si*-Si-2SiH_3 + _ + H_2(g)**	**H-Si-2SiH_3**	**1**	**SiH_2**	**+1**
L (NPS)	**Si-Si**	**Si-4SiH_3 + H* => SiH_3* + H-Si-3SiH_3(g)**	**No**	**0**	**SiH_3**	**0**
M (NPS)	**Si-Si**	**Si-4SiH_3 + H* => Si*-3SiH_3+ SiH_4(g)**	**3SiH_4**	**0**	**Si**	**+3**
N (NPS)	**Si-H**	**Si-4SiH_3 + H* => H_2Si*-Si-2SiH_3 +H_2(g)**	**H-Si-2SiH_3**	**0**	**SiH_2**	**+1**

The "bond" column is the initial bond that breaks when the disilane molecule is adsorbed onto the surface. The "Uptake of Hydrogen" column is the attacking of a Si-Si bond by hydrogen similar to hydrogenolysis of alkanes. The "# of Open Sites Required" column denotes the number of open surface sites to start the reaction process. The "Final Surface Species" column is the silicon species remaining on the surface when the reaction process is completed. The "# of Net Sites" column describes the net generation of surface on the original surface free of hydrogen. Adsorbed SiH_2 or Si, and open sites related to them are not counted in this total. (This may be an avenue for future study.) We would like to note that due to the large size of adsorbed fragments of NPS, both concerted reactions and the combination of dissociative adsorption with hydrogenolysis are probably occurring in practice. Hydrogenolysis and the formation of gaseous silane molecules occurs in *Processes G, H, J, K, M, & N.*

If we again recall from experiments (Section 4.3) that with NPS, the growth rate enhancement was small compared with silane when the hydrogen partial pressure was decreased. This suggests that the processes that require open sites to start the surface reaction, and/or consumes open sites, are not likely to be the dominant growth process, ruling out *Process H*. While *Processes G, H, I, & J,* have either a net generation of open surface sites or no consumption of open surface sites, they all require open sites to begin the reaction process. Although this implies that when the hydrogen surface coverage is decreased these processes will lead to a significant enhancement of growth rate that is not observed in the experimental data (Figure 4.12). It is possible that H_2 gas or reaction byproducts such as SiH_4 may adsorb onto these generated open sites (via hydrogenolysis and the formation of silane preventing significant growth rate enhancement. All three of the concerted reaction *Procesess L, M, & N,* remain as possibilities as the dominant growth process. These processes do not require open surface sites for adsorption and/or generate open surface sites.

We will examine two more things to further aid in the determination of the dominant growth mechanism. First, the roughness of the resulting epitaxial silicon layers will give insight into the surface mobility and thus open surface sites and second, dopant adsorption, which is also related to open sites (due to adsorption) will be examined. This will help us determine if the net process reaction can generate a net number of open surface sites. The reaction processes for NPS and disilane will be discussed again later in the chapter.

4.5 Surface Roughness of Epitaxial Layers Grown with Different Silanes

4.5.1 Fundamental Considerations

In the previous section we examined models for the adsorption of the silicon adatom onto the growth surface. The adsorption is only half of the epitaxial growth process. The second half is the diffusion of adsorbed silicon species to the final growth site. On a flat surface, the ideal process is called layer-by-layer growth (also known as Frank-van der Merwe (FM) growth). However, the substrates used for all experiments in this thesis are all cut at vicinal angles. The growth mode now changes to step-layer growth, and the adsorbed silicon species diffuses into what are called "kink sites". In this section we will examine the diffusion of the silicon adatom on an atomistic level, how surface diffusion relates to surface morphology, and the implications of our surface reaction models on surface morphology.

We will first explain the structure of the silicon reconstructed surface on a vicinal substrate. We use the Terrace-Step-Kink (TSK) model, which was proposed in a classic paper by Burton, Cabrera, and Frank [4.28], and has been the basis for descriptions of atomistic growth mechanisms. It is based upon the idea that the energy of an atom's position on a crystal surface is determined by its bonding to neighboring atoms and the transitions simply involve the counting of broken and formed bonds. In the appendix, the model is shown for a simple cubic cell. For crystalline silicon surface the simple cubic cell model is not appropriate as the silicon lattice has a diamond configuration. In the previous section, we described in detail the 2x1 reconstructed silicon surface on a flat region (terrace). On a vicinal substrate the silicon reconstructed surface forms two types of domains: (2x1) and (1x2), as shown in Figure 4.16 below:

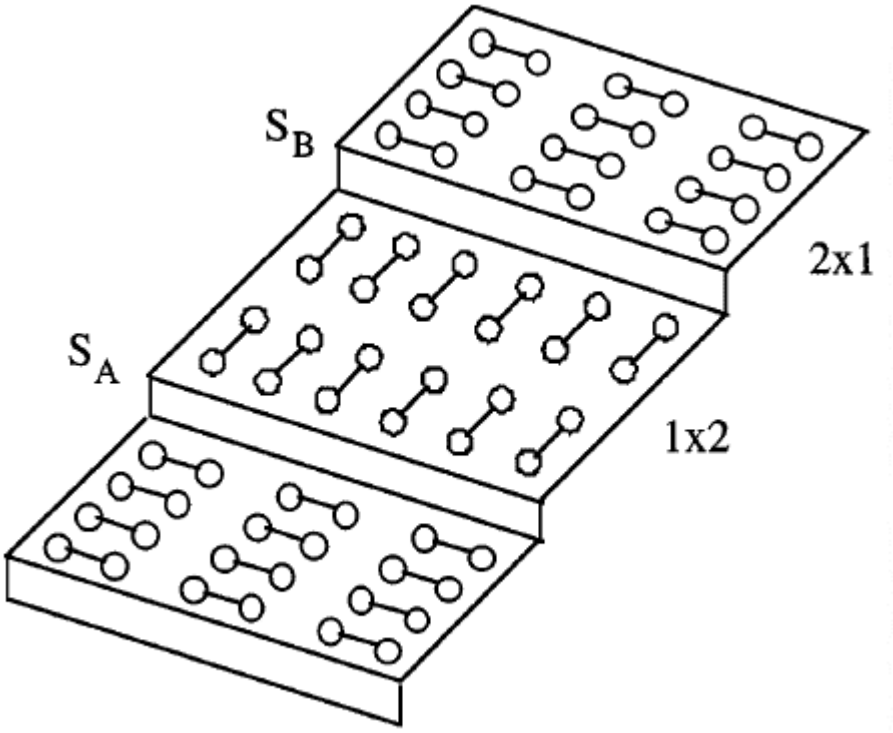

Figure 4.16. Schematic of the two types of terrace domains (2x1) and (1x2), along with the two types of terrace steps S_A going from (2x1) to (1x2), and S_B from (1x2) to (2x1) [4.29]. The circles indicate surface atoms and the bonds are the dimers.

The dimer rows rotate 90^o from one terrace domain to the next due to the diamond structure of silicon. As a result two types of monatomic steps exist. We will define S_A as the step that is parallel to the upper-terrace dimer rows and S_B as the step that is perpendicular its upper-terrace dimer rows [4.30]. Figure 4.16 above is redrawn below an atomic scale in Figure 4.17.

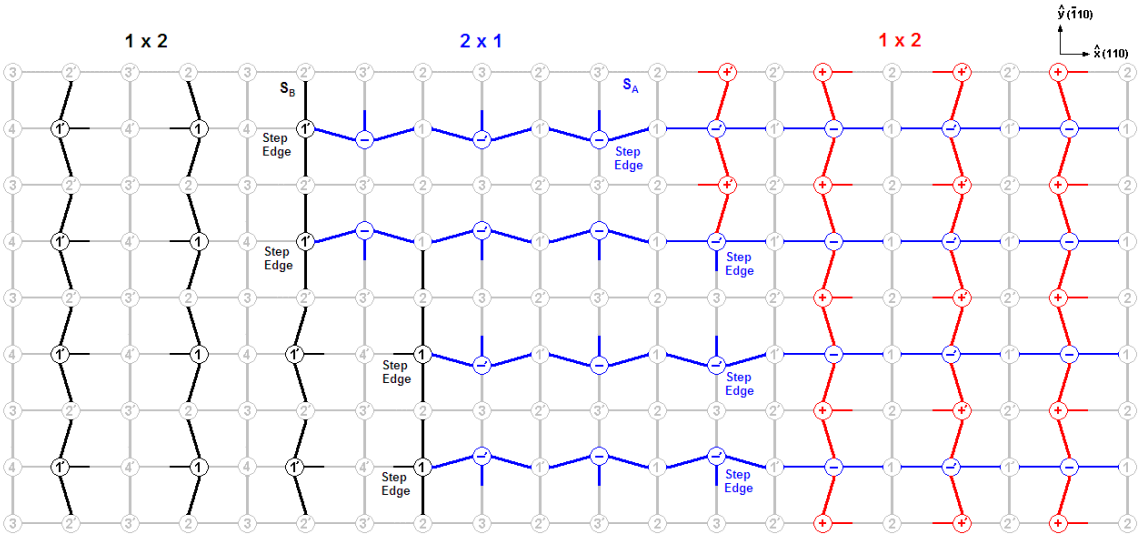

Figure 4.17. Top view of a terraced un-passivated (hydrogen-free) silicon surface. Three different terraces are shown in the diagram. The silicon atoms from the top layer to the bottom layers are from +, - , 1,2,3,4. The red (1 x 2) layer is the top terrace, the blue (2 x 1) is the layer underneath that, and the black (1 x 2) layer is the bottom terrace. Shown in the diagram are the two steps S_B and S_A, the step edges and the kink site. 1 and 1', - and - , + and +' form dimer pairs.

In Figure 4.17, three different terrace layers are shown, along with the two different types of steps S_B and S_A. The silicon atoms from top to bottom are arranged from + , - , 1 , 2 , 3, 4. From the figure you can see that the layer of atoms on top of silicon atom layer 1, (i.e. layer (-)), has a reconstruction that is rotated 90^o. Similarly the next layer of silicon atoms (layer (+)) is also rotated by 90^oC with respect to the previous layer. As a result, each terrace alternates from 1x2 to 2x1 and back to the 1x2 domain phases.

4.5.2 Silicon Adatom Diffusion

Surface smoothness is determined by the surface diffusion of the silicon adatom. An incoming adatom can land on either the 2x1 terrace or the 1x2 terrace. The adatom then has to diffuse to the step edges. Due to the 2x1 reconstruction of the silicon surface,

the diffusion is anisotropic. The adatom diffusion is faster in the direction parallel to the dimer rows than in the direction perpendicular along the dimer rows [4.29][4.31]. Note that along one of the silicon terraces the diffusion to the kink site is parallel to the dimer row and on the next terrace the diffusion is perpendicular to the dimer row.

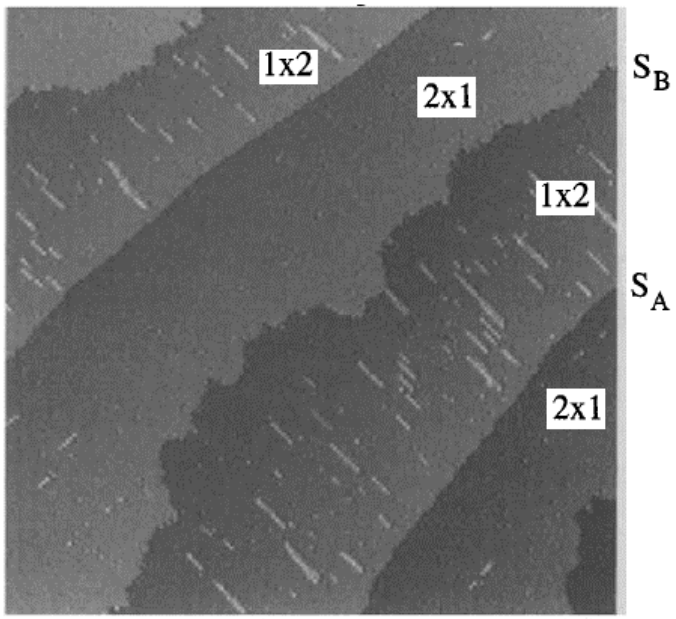

Figure 4.18. STM image of terrace domains illustrating the diffusion anisotropy of the two different terrace domains. The surface steps down from upper left to lower right. The adatoms landing on the 2 x 1 domain can diffuse to the step leading to an atomically flat layer. The adatoms on the 1 x 2 domain have a much smaller diffusion coefficient, as a result 2D island formation is observed [4.32].

Figure 4.18 provides evidence of the diffusion anisotropy on the two different terrace domains [4.32]. It is evident that the adatoms on the 2 x 1 terrace domains have a larger diffusion constant that the adatoms on the 1 x 2 terrace domains. The 2 x1 atomically smooth while the 1 x 2 domains have 2D island formation. On a bare silicon surface the activation energies of surface diffusion parallel and perpendicular to dimer rows are 0.6eV and 1eV, respectively, based on theoretical calculations [4.29][4.33]. Hydrogen is known to hinder surface diffusion. On a monohydride surface, the values increase to

1.5eV and 1.7eV respectively [4.29][4.34]. At high temperatures the adsorbed adatoms can diffuse along the terraces for substantial distances until they encounter a step edge, where they then become part of the bulk crystal [4.35]. At intermediate temperatures, growth arises from the coalescence of islands that form on the flat terraces when one or more adatoms meet [4.36]. In this case the silicon adatom cannot diffuse to the proper step edge before an incoming adatom lands on top and immobilizes it. The resulting terrace (and hence silicon surface) will be rough. Shown in Figure 4.19 below are these two different conditions:

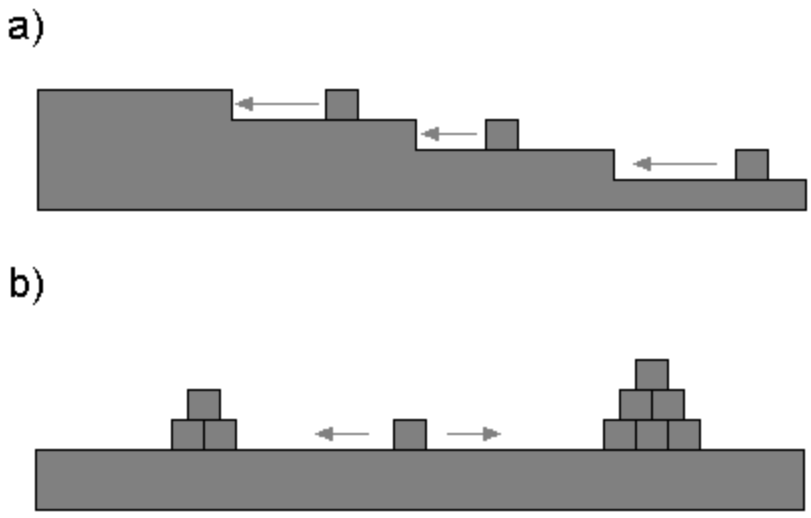

Figure 4.19. Schematic illustrating two-different growth modes, a) step-flow growth is shown and b) islanding on a terrace.

The surface diffusion is dependent on the temperature and the hydrogen pressure. We note that for the same temperature and hydrogen pressure (and thus surface conditions), increasing the growth rates (less time to diffuse) leads to an increase in surface roughness for silicon growth, as shown for silane by two separate authors [4.37][4.38].

4.5.3 Surface Smoothness of Films Grown with Various Silanes

Due to the high growth rates and low temperatures (and thus low diffusion rates), the epitaxial silicon layers grown with disilane and NPS might be expected to have rough surfaces. We compare the surface roughness of one sample grown using silane as the precursor and a second sample grown using disilane as the precursor. Shown in the Figure 4.20 below, it is evident that the disilane sample (b) is smoother than the silane sample (a). Both samples are grown under the same pressure, (6 torr hydrogen ambient), same temperature (600 ^{o}C), and used the same hydrogen carrier flow, 3 slpm. In the first sample (a) silane was used as the precursor and the growth thickness was 60 nm. In the second sample (b) disilane was used as the precursor and the growth thickness was 100 nm. The growth rates are 2.1 and 7.8 nm/min for the silane and disilane samples. Despite having a higher growth rate the sample grown with disilane is smoother than the sample grown with silane. (Note the oxygen content in all samples in this roughness study was ~ 10^{18} cm^{-3} or less, so that roughness can not be explained by oxygen-related effects.)

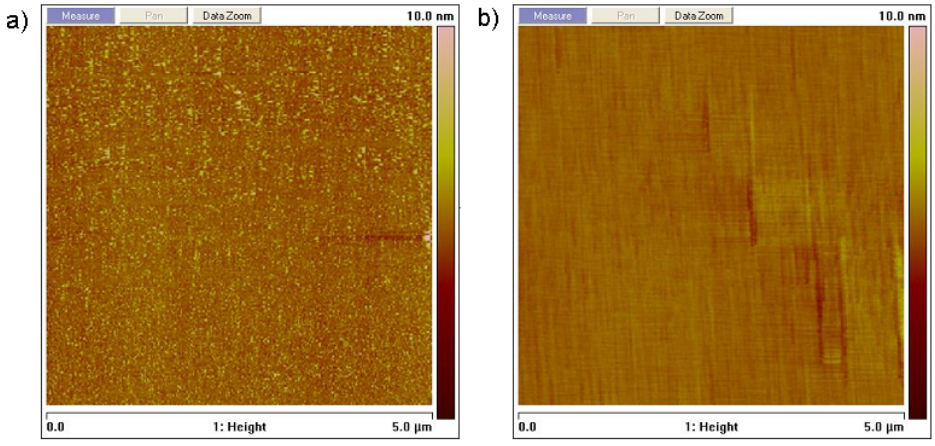

Figure 4.20. AFM scans of two samples grown at 600 ^{o}C, 6 torr and 3 slpm hydrogen carrier gas. The first sample a) is grown with 10 sccm of silane and has a total growth thickness of 60 nm. The second sample b) is grown with 5 sccm of disilane and has a total growth thickness of 100 nm. The growth rates are 2.1 and 7.8 nm/min for the silane and disilane samples respectively.

This is a very surprising result because standard models (explained in section 4.5.1) imply that faster growth rates leads to rougher surfaces. We plot the surface roughness measure by AFM for various samples grown using silane, disilane, and NPS in our RTCVD system at 600 ^{o}C and 6 torr hydrogen in Figure 4.21 below, with roughness (RMS) plotted as a function of growth rate.

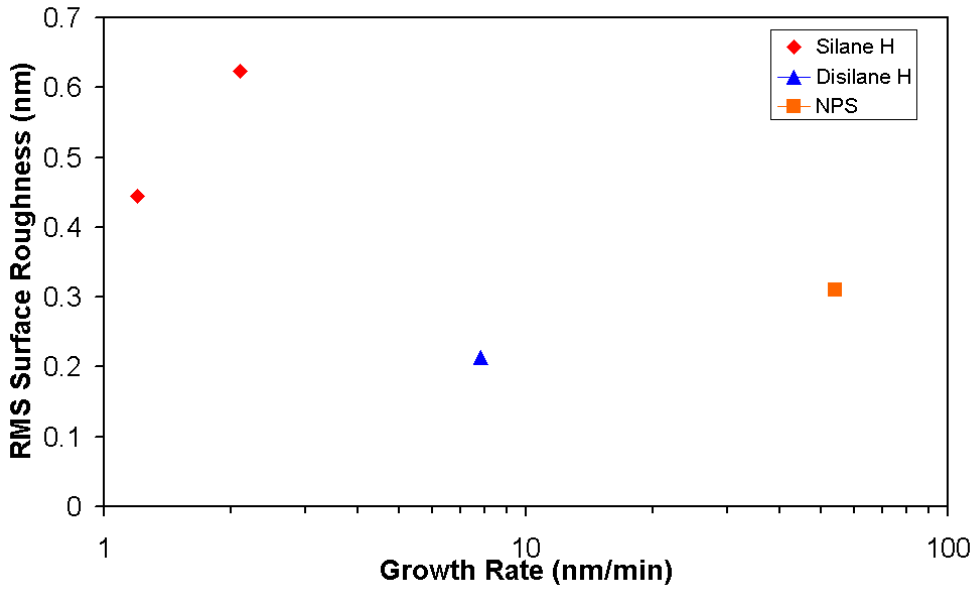

Figure 4.21. RMS surface roughness of epitaxial layers grown with silane, disilane and neopentasilane vs. growth rate for hydrogen ambient at 600 ^{o}C and 6 torr. The roughness is measured by atomic force microscopy (AFM). The partial pressure were 20 mtorr and 100 mtorr of silane, 10 mtorr of disilane, and 10 mtorr of NPS.

From the Figure 4.21 above, the epitaxial growth rate for disilane and NPS is higher than that of silane and yet the surface roughness is improving! We thus infer that growth with disilane and NPS increases the surface diffusion of the silicon adatoms compared to that during growth with silane.

4.5.4 Growth in Hydrogen vs. Nitrogen Ambient

We examine the surface roughness of films grown in a nitrogen ambient instead of hydrogen ambient. In Figure 4.22 below, we plot the surface roughness measured by AFM for various samples grown using silane, disilane, and NPS in our RTCVD system at 600 ^{o}C and 6 torr, in both hydrogen (solid) and nitrogen (open) ambients (carrier flow of 3 slpm).

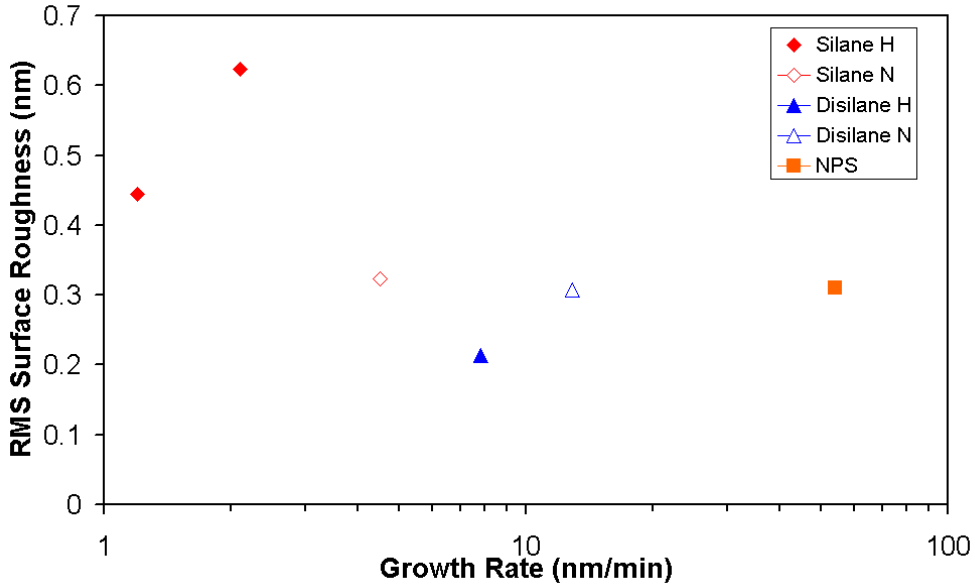

Figure 4.22. RMS surface roughness of epitaxial layers grown with silane, disilane and neopentasilane vs. growth rate for hydrogen (solid) and nitrogen (open) ambients at 600 ^{o}C and 6 torr. The roughness is measured by atomic force microscopy (AFM). The partial pressure were 20 mtorr and 100 mtorr of silane, 10 mtorr of disilane, and 10 mtorr of NPS.

With silane, we note that the change from hydrogen to nitrogen ambient not only increases the growth rate (0.6 to 1.8 nm/min Figure 4.12) for a silane flow of 10 sccm, but also improves the surface roughness measured by AFM. In the work done by another author [4.39], he observed a similar phenomenon where the switch from hydrogen ambient to nitrogen ambient not only enhanced the growth rate but also improved the surface roughness. Shown in Figure 4.23 below is his result.

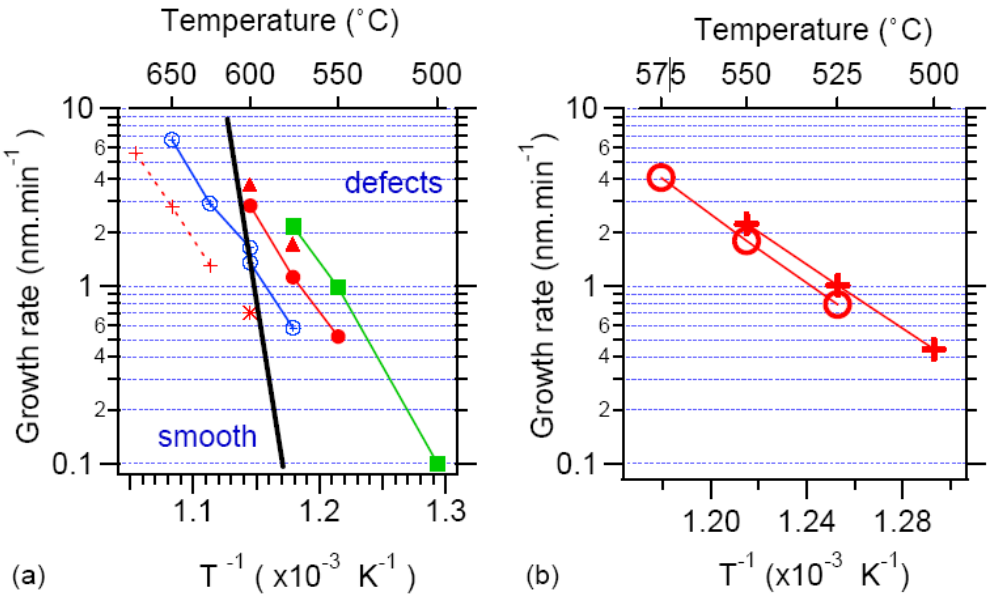

Figure 4.23. Growth rate vs. inverse temperature for low temperature Si epitaxy for silane using (a) H_2 as carrier gas and (b) N_2 as carrier gas. The growth conditions are: a) P = 40 torr H_2 = 22 slpm, SiH_4 = 20 sccm (red plus). H_2 = 33 slpm, SiH_4 = 100 sccm (red star), 200 sccm (blue circle), 400 sccm (red circle), 600 sccm (red triangle) and 800 sccm (green square). b) N_2 = 15 slpm, SiH_4 = 20 sccm, P = 80 torr (red cross) and P = 40 torr (red circle). [4.39]

In his work, the black line represents the transition from smooth (left of the line) to rough or defective epitaxial growth (right of the line). In Figure 4.23a, at a fixed temperature (i.e. 600 ^{o}C) as we increase the growth rate by increasing the silane flow, the surface of the resulting epitaxial layers is becoming increasingly rough. However, in Figure 4.23b the epitaxial layers grown with silane in nitrogen are all smooth, despite the lower temperatures and similar growth rates.

Both our work and a reference [4.39] indicate that a nitrogen ambient improves the surface roughness of the resulting films. We earlier (Section 4.3) described how a nitrogen (vs. hydrogen) ambient results in more surface open sites. We thus conclude that open sites greatly improve the surface roughness, even if the growth rate is increased.

4.5.5 Hydrogen and Surface Mobility

We will give a reason for the improvement of surface roughness due to an increase of open sites on the surface. It has been shown that the reduction of hydrogen coverage also increases the surface diffusion of adsorbed silane of silicon (100) surface. Shown in Figure 4.24 below is an experiment demonstrating in Molecular Beam Epitaxy (MBE) of how the presence of additional deuterium (H^2) can cause a rapid roughening of the silicon surface.

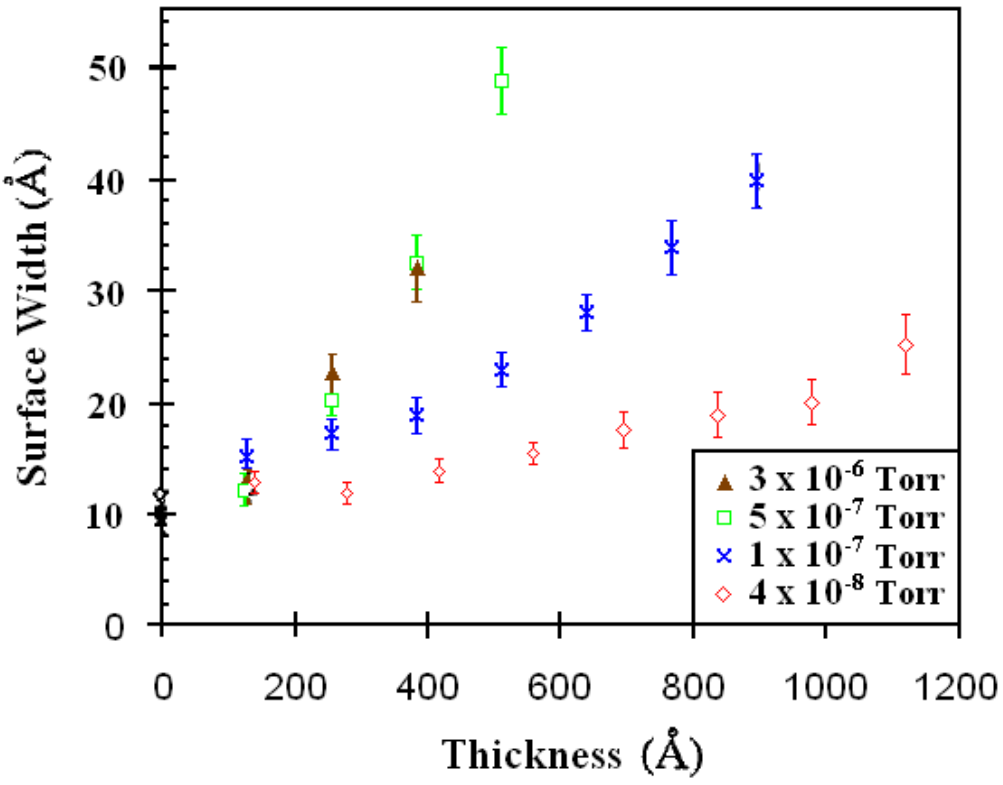

Figure 4.24. Surface roughness (Width) vs. layer thickness developed during silicon MBE in the presence of different deuterium partial pressures [4.40].

From Figure 4.24, in the MBE experiment it was observed that increasing the deuterium pressure, hence the surface coverage, the films grown increased in roughness for the same growth thickness. In this experiment as the deuterium partial pressure was increased the surface roughness increases with decreasing thickness. This implies that the surface diffusion of the adatoms is hindered by the surface deuterium. By the same logic, surface hydrogen also acts as a barrier to surface diffusion of adsorbed species in our CVD experiments.

When we switch over form hydrogen to nitrogen ambient, the surface diffusion of the silicon adatoms are increased due to an increase in the number of open sites (and thus decreased hydrogen coverage), explaining the improvement in both growth rate and surface roughness due to the switch from hydrogen to nitrogen. Experimentally, we observed both higher epitaxial growth rates and smoother surfaces resulting from the layers grown with disilane and NPS, we hypothesize the smooth surfaces result from more open sites on the surface. However, once the silicon adatom is incorporated onto the surface it does NOT matter whether it came from silane, disilane, or NPS; the kinetics of desorption of hydrogen are the same [4.41], and the open site coverage in equilibrium depends only on the temperature and pressure. This implies that during the growth process with high-order silanes (i.e. disilane, NPS), *open sites are being created so that there are a greater number of open sites during the growth process compared to that with silane.* (Note: we assume adsorption proceeds mostly on terraces, so that adatoms have to diffuse to step edges, and that the adsorption does not happen preferentially at step edges or kink sites. This assumption is verified in the next section.)

4.6 Doped Silicon Growth and its Implication on Hydrogen Coverage During Growth

4.6.1 Boron Adsorption Rates with Various Silanes

To confirm the presence of more open sites, the use of boron incorporation into silicon during CVD epitaxy was used. We make the assumption that B_2H_6 (diborane) absorption depends on the number of open sites, so we could use the resulting boron doping as a qualitative measure of the number of open sites during epitaxial growth. (We also assume that diborane does not desorb from the surface, so that the adsorption rate is reflected into the boron incorporated into the surface.) We grew boron-doped silicon from 550 ^{o}C to 700 ^{o}C using the same boron partial pressure (10^{-4} sccm in 3 slpm carrier at 6 torr) and the same growth rate (if possible) for silane, disilane, and NPS. From SIMS we obtain both the growth rate and the doping concentration. Using those two values and the diborane partial pressure, we can find the normalized adsorption of diborane defined as (boron atoms / cm^2 / second / diborane partial pressure in torr):

Eq. 4.28 $$\text{Normalized Adsorption Rate} = GR * N_B / 2\, PP_B,$$

where GR is the growth rate, N_B is the boron concentration in the solid, and PP_B is the partial pressure of boron (diborane is the boron source hence the 2). This normalized adsorption rate is proportional to the sticking coefficient, independent of partial pressure, assuming diborane does not affect the surface (assuming small changes in thermal velocity over our temperature range). We plot the results in Figure 4.25 and tabulated in Table 4.4 below.

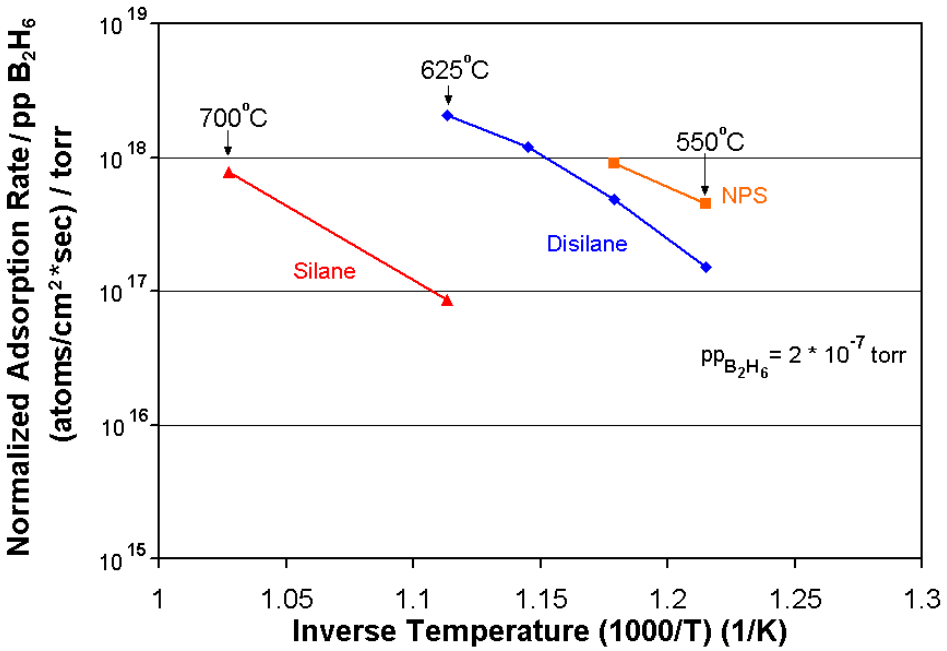

Figure 4.25. Normalized adsorption rate vs. epitaxy inverse temperature for the silicon sources of silane, disilane and NPS.

Table 4.4: Comparison of the boron adsorption rates of silane, disilane and neopentasilane. SIMS was used to determine the boron concentrations and growth rates. The chamber pressure was 6 torr and 3 slpm of hydrogen carrier was used for all samples.

Precursor	Temp	Source Gas Flow (sccm)	GR (nm/min)	Boron Concentration (atoms/cm^{-3})	Normalized Adsorption Rate atoms / (cm^{-2} s torr)
NPS	**550 °C**	**2**	**1.8**	**3 x 10^{19}**	**4.5 x 10^{17}**
NPS	**575 °C**	**2**	**5.4**	**2 x 10^{19}**	**9.0 x 10^{17}**
Disilane	**550 °C**	**7.5**	**1.8**	**1 x 10^{19}**	**1.5 x 10^{17}**
Disilane	**575 °C**	**7.5**	**5.8**	**1.5 x 10^{19}**	**4.9 x 10^{17}**
Disilane	**600 °C**	**5**	**11**	**1.3 x 10^{19}**	**1.2 x 10^{18}**
Disilane	**625 °C**	**5**	**22.5**	**1.1 x 10^{19}**	**2.0 x 10^{18}**
Silane	**625 °C**	**5**	**0.8**	**1.3 x 10^{19}**	**8.5 x 10^{16}**
Silane	**700 °C**	**5**	**8.5**	**1.1 x 10^{19}**	**7.8 x 10^{17}**

We observe that the normalized diborane adsorption rate is higher for NPS than disilane and silane, and higher for disilane than silane (Figure 4.24). The normalized adsorption rate also increases with temperature. All three rates increase with temperature, as the open site coverage is higher at higher temperatures. At 625 °C, the diborane adsorption rate was 25 times higher in disilane than in silane, and at 550 °C, the diborane

adsorption rate was 3 times higher. At 550 ^{o}C and at 575 ^{o}C, for similar epitaxial growth rates with disilane and NPS, there is more boron incorporated in the layers grown with NPS. The diborane adsorption data implies that a larger fraction of open sites are occurring during growth with high-order silanes (thereby allowing more boron to adsorb and incorporate). This could be due to open site generation by the growth process or a greater fraction of the high-order silane preferentially adsorbing on the step edges, leaving a higher surface concentration of open sites for the diborane to adsorb.

To test if the high-order silanes are preferentially adsorbing on step edges, experiments of increasing the NPS and disilane flow, while holding the boron flow constant at a fixed rate under fixed pressure and temperature sites were conducted. The results are summarized in Table 4.5 below:

Table 4.5: Comparison of the boron adsorption rates of disilane and neopentasilane vs. increasing growth rates. SIMS was used to determine the boron concentrations and growth rates. The chamber pressure was 6 torr and 3 slpm of hydrogen carrier was used for all samples.

Precursor	Temp	Source Gas Flow (sccm)	GR (nm/min)	Boron Concentration (atoms/cm^{-3})	Normalized Adsorption Rate atoms / (cm^{-2} s torr)
Disilane	**575 ^{o}C**	**2**	**1.6**	**1.2 x 10^{19}**	**1.9 x 10^{17}**
Disilane	**575 ^{o}C**	**5**	**3.1**	**8.3 x 10^{18}**	**2.1 x 10^{17}**
Disilane	**575 ^{o}C**	**7.5**	**4.5**	**7.2 x 10^{18}**	**2.7 x 10^{17}**
Disilane	**575 ^{o}C**	**10**	**5.4**	**6.4 x 10^{18}**	**2.9 x 10^{17}**
NPS	**575 ^{o}C**	**2**	**4.1**	**9.4 x 10^{18}**	**3.2 x 10^{17}**
NPS	**575 ^{o}C**	**3.9**	**5.8**	**7.5 x 10^{18}**	**3.6 x 10^{17}**
NPS	**575 ^{o}C**	**5.9**	**7.4**	**7.1 x 10^{18}**	**4.4 x 10^{17}**
NPS	**575 ^{o}C**	**11.8**	**11.5**	**5.1 x 10^{18}**	**4.9 x 10^{17}**

We note that as we increase the disilane and NPS flow, the normalized boron adsorption rate is increasing. The data implies that more open sites are generated as more precursor is injected. The data also invalidates the possibility that the high-order silanes are preferentially adsorbing on step edges. If the adsorption were on step edges, the amount of boron incorporated would be constant with increasing growth rate, since number of open sites would be constant. We note that adsorption rates calculated in Table 4.5 have

some discrepancy with the data in Table 4.4. We think this is due to the inaccuracy in the temperature measurement in the two samples (5036 for disilane and 5038 for NPS) grown for Table 4.5 compared to that for the samples of Table 4.4.

4.6.2 Phosphorus Adsorption Rates with Various Silanes

We conduct a similar test for open sites by using phosphine as the dopant source and the adsorption of phosphorus as a probe for the number of open sites during growth. We conducted phosphorus doping experiments in hydrogen at 6 torr for silane, disilane, and NPS, at temperatures of 625 ^{o}C and 575 ^{o}C. Phosphine gas was used to inject the phosphorus atoms into the system. The growth rates and phosphorus concentrations were determined by secondary ion mass spectrometry (SIMS). Using those two values and the phosphine partial pressure ($2*10^{-5}$ torr), we can find the normalized adsorption rate of phosphine at steady state defined as (atoms / cm^2 / second / phosphine partial pressure in torr).

Eq. 4.29 $$\text{Normalized Adsorption Rate} = GR * N_P / PP_P,$$

We observe that the normalized phosphine adsorption rate is higher for NPS than disilane and silane, and higher for disilane than silane (Figure 4.26). The results are summarized in Table 4.6 below. This trend is similar to that for diborane. The adsorption rate also increases with temperature. All three rates increase with temperature, as the open site coverage is higher at higher temperatures. At 625 ^{o}C, the phosphorus adsorption rate was 80 times higher in disilane than in silane, and 3 times higher for NPS than in disilane. The phosphorus adsorption data also implies that a larger fraction of open sites are occurring during growth with high-order silanes. This also implies that the growth

mechanism involves a generation of additional open sites. Phosphorus doping is difficult to achieve with conventional gases such as DCS and silane. Due to the generation of open sites, high-order silanes such as disilane and NPS are good candidates for achieving highly-doped phosphorus silicon epitaxial layers.

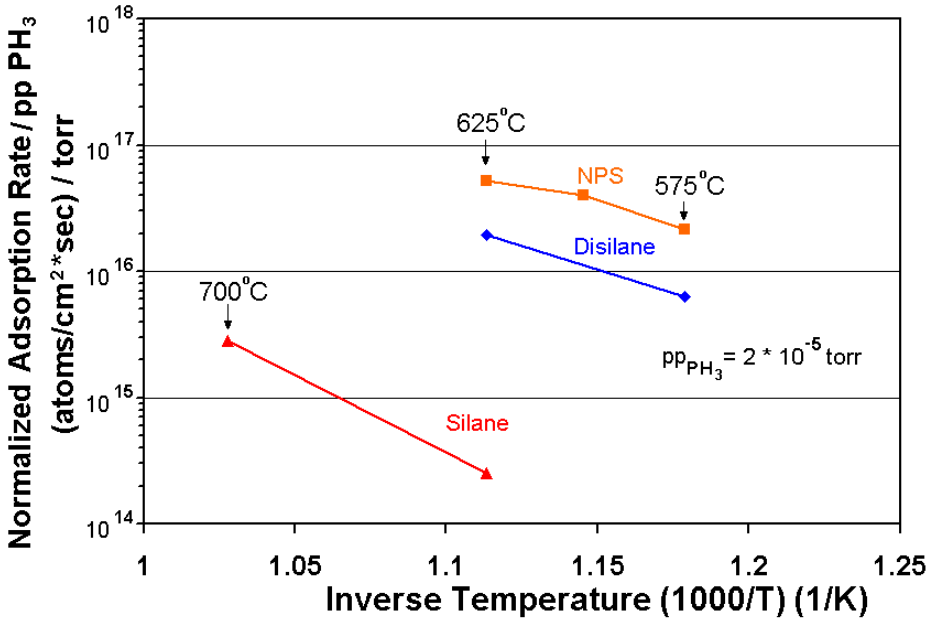

Figure 4.26. Normalized phosphine adsorption rate vs. epitaxy inverse temperature for the silicon sources of silane, disilane and NPS.

Table 4.6: Comparison of the phosphorus adsorption rates of silane, disilane and neopentasilane. SIMS was used to determine the phosphorus concentrations and growth rates. The chamber pressure was 6 torr and 3 slpm of hydrogen carrier was used for all samples.

Precursor	Temp	Source Gas Flow (sccm)	GR (nm/min)	Phosphorus Concentration (atoms/cm^{-3})	Normalized Adsorption Rate atoms / (cm^{-2} s torr)
NPS	**575 °C**	**2**	**5.2**	**4.9 x 10^{19}**	**2.1 x 10^{16}**
NPS	**600 °C**	**2**	**12**	**3.8x 10^{19}**	**3.8 x 10^{16}**
NPS	**625 °C**	**2**	**21**	**3 x 10^{19}**	**5.3 x 10^{16}**
Disilane	**575 °C**	**5**	**3.3**	**2.3 x 10^{19}**	**6.3 x 10^{15}**
Disilane	**625 °C**	**5**	**6.7**	**1.4 x 10^{19}**	**1.6 x 10^{16}**
Silane	**625 °C**	**10**	**0.3**	**9 x 10^{18}**	**2.5 x 10^{14}**
Silane	**700 °C**	**10**	**2.6**	**1.3 x 10^{19}**	**2.8 x 10^{15}**

4.7 Summary of High-Order Silane Growth Process Reactions

Earlier in the chapter, we provided a list of possible surface reactions for the growth of epitaxial silicon with disilane and NPS. In this section we will narrow down the list based on the experimental data in Sections 4.5 and 4.6, regarding surface roughness and dopant incorporation.

Table 4.7: Summary of surface reaction mechanisms for the adsorption of silane, disilane and NPS onto a silicon surface. Reactions in agreement with all experimental data are highlighted in bold. Note that the final reaction Equation for C and E, D and F, I and L, J and M, and K and N, are equivalent, although the mechanism for adsorption is different.

Process	Bond	Surface Reaction	Uptake of H*	# of Open Sites Required	Final Surface Species	# of Net Sites
Silane	**Si-H**	**H-SiH_3 + 2_ => SiH_3* + H***	**No**	**2**	**SiH_3**	**-2**
A (Disilane)	Si-Si	H_3Si-SiH_3 + 2_ => 2 SiH_3*	No	2	2SiH_3	+1
B (Disilane)	Si-H	H_3Si-SiH_3 + 2_ => Si_2H_5* + H*	SiH_4	2	SiH_2	-1
C (Disilane)	Si-Si	H_3Si-SiH_3 + _ + H* => SiH_3* + SiH_4(g) + _	No	1	SiH_3	0
D (Disilane)	**Si-H**	**H_3Si-SiH_3 + _ + H* => Si_2H_5* + H_2(g)+_**	**SiH_4**	**1**	**SiH_2**	**+1**
E (Disilane)	**Si-Si**	**H_3Si-SiH_3 + H* => SiH_3* + SiH_4(g)**	**No**	**0**	**SiH_3**	**0**
F (Disilane)	**Si-Si**	**H_3Si-SiH_3 + H* => Si_2H_5* + H_2(g)**	**3SiH_4**	**0**	**SiH_2**	**+1**
G (NPS)	**Si-Si**	**Si-4SiH_3 + 2_ => SiH_3* + Si-3SiH_3***	**3SiH_4**	**2**	**Si, SiH_3**	**+1**
H (NPS)	Si-H	Si-4SiH_3 + 2_ => H_2Si*-Si-2SiH_3 + H*	H-Si-2SiH_3	2	SiH_2	-1
I (NPS)	Si-Si	Si-4SiH_3 + _ + H* => SiH_3* + H-Si-3SiH_3(g) + _	No	1	SiH_3	0
J (NPS)	**Si-Si**	**Si-4SiH_3 + _ + H* => Si*-3SiH_3+ SiH_4(g) + _**	**3SiH_4**	**1**	**Si**	**+3**
K (NPS)	**Si-H**	**Si-4SiH_3 + _ + H* => H_2Si*-Si-2SiH_3 + _ + H_2(g)**	**H-Si-2SiH_3**	**1**	**SiH_2**	**+1**
L (NPS)	Si-Si	Si-4SiH_3 + H* => SiH_3* + H-Si-3SiH_3(g)	No	0	SiH_3	0
M (NPS)	**Si-Si**	**Si-4SiH_3 + H* => Si*-3SiH_3+ SiH_4(g)**	**3SiH_4**	**0**	**Si**	**+3**
N (NPS)	**Si-H**	**Si-4SiH_3 + H* => H_2Si*-Si-2SiH_3 +H_2(g)**	**H-Si-2SiH_3**	**0**	**SiH_2**	**+1**

Based on our hydrogen / nitrogen growth rate data (Figure 4.12), we concluded that either growth with high-order silanes does not require open surface sites, or the growth mechanism creates open sites (i.e net sites > 0). From this we can eliminate all of the reactions that depend on open sites and whose final reaction consumes surface sites (i.e. net site < 0). Reactions A, B, C, and H are eliminated based on the aforementioned criteria. The surface smoothness data (Figure 4.21), and the diborane and phosphine doping data (Figures 4.25 and 4.26 respectively) indicates that during the growth process with NPS there is a higher equilibrium concentration of open surface sites available than during the growth process with disilane, which has a higher equilibrium concentration open surface sites available than during the growth process with silane. Since the remaining possible growth reactions for disilane or NPS have a net site of either 0 or +1, this implies that the growth reactions with NPS must also have at least a +1 net site generation, eliminating reactions I and L as possible mechanisms.

In the cases where the reaction uses an open site and generates more open sites during the reaction process (reactions D, G, J and K); there still remains the question of why the growth rate does not increase faster than linearly instead of linearly with precursor flow rate as shown in Figure 2.10. This may be due to the fact that the by-product of the reaction can also be adsorbing back onto the surface and consuming the additional open sites (i.e. a silane by-product will have a higher reaction coefficient when there are more open sites). We also have to remember that the growth surface is mostly hydrogen terminated (0.9995) at our growth condition of 600 ^{o}C and 6 torr and the reaction must not require an open site to start the growth process. This seems to imply that the dominant growth reaction does not need open sites, although other open-site-dependent reactions may occur simultaneously. We can now reduce the list of possible surface reactions under our experimental conditions for disilane and neopentasilane to the following:

Table 4.8: Summary of possible surface reaction mechanisms for the adsorption of silane, disilane, and NPS onto a silicon surface. These growth mechanisms are in qualitative agreement with all of our experimental data.

Process	Bond	Surface Reaction	Uptake of H*	# of Open Sites Required	Final Surface Species	# of Net Sites
Silane	Si-H	$H\text{-}SiH_3 + 2\_ \Rightarrow SiH_3^* + H^*$	No	2	SiH_3	-2
E (Disilane)	Si-Si	$H_3Si\text{-}SiH_3 + H^* \Rightarrow SiH_3^* + SiH_4(g)$	No	0	SiH_3	0
F (Disilane)	Si-Si	$H_3Si\text{-}SiH_3 + H^* \Rightarrow Si_2H_5^* + H_2(g)$	$3SiH_4$	0	SiH_2	+1
M (NPS)	Si-Si	$Si\text{-}4SiH_3 + H^* \Rightarrow Si^*\text{-}3SiH_3 + SiH_4(g)$	$3SiH_4$	0	Si	+3
N (NPS)	Si-H	$Si\text{-}4SiH_3 + H^* \Rightarrow H_2Si^*\text{-}Si\text{-}2SiH_3 + H_2(g)$	$H\text{-}Si\text{-}2SiH_3$	0	SiH_2	+1

4.8 Hydrogen Desorption Limit

To determine if fact higher-order silanes can indeed adsorb without the need of conventional hydrogen desorption, we conduct the following thought experiment. We assume that for every hydrogen atom that desorbs off of the reconstructed 2 x 1 surface, a silicon adatom immediately lands on that newly created open surface site. The silicon adatom will also immediately decompose back to SiH and diffuse to the proper step site so that the original structure is recreated with a silicon layer grown. The silicon growth rate is now the same as the monohydride hydrogen desorption rate. This is the theoretical growth rate limit based on conventional hydrogen desorption. The rate of hydrogen desorption (D) is given in Equation 4.30 below:

Eq. 4.30
$$D = -\frac{d\theta_H}{dt} = -k_d \theta_H{}^n$$

where θ_H is the hydrogen coverage, n is the order of hydrogen desorption, and k is reaction rate given in Equation 4.31

Eq. 4.31 $$k = v * e^{(-E_a/k_B T)}$$

where v is the frequency factor, E_a is the activation energy and k_B is the boltzmann constant (8.617 x 10^{-5} eV / K). Since the growth is in a hydrogen ambient, θ_H is approximated as 1 (fully covered surface), so the order of hydrogen desorption is irrelevant. The theoretical maximum growth rate can now be calculated using Equation 4.32 below:

Eq. 4.32 $$GR = a_{Si} * v * e^{(-E_a/k_B T)}$$

where a_{Si} is the Si(100) lattice constant given as 1.35 angstroms. The hydrogen desorption rates were obtain from several references. (Note the value obtained in Equation 4.32 is equal to the maximum growth rate possible with silane at the hydrogen desorption limit shown earlier in Equation 4.11).

We calculate theoretical growth rates based on Equation 4.32 for the temperature range from 400 ^{o}C to 600 ^{o}C and compare with epitaxial growth rates of trisilane and NPS and Table 4.8 below.

Table 4.9 Theoretical growth rates based on assuming the monohydride desorption rate is equivalent to the growth rate from several references and actual epitaxial growth rates published for NPS and trisilane. k is the reaction rate of hydrogen desorption (atoms/sec), and GR is the growth rate (nm/min).

	Sinniah k [4.7]	**GR (nm/min)**	**D'Evelyn [4.42] Wise k [4.43]**	**GR (nm/ min)**	**Flowers [4.8] Hofer k [4.44]**	**GR (nm/ min)**	**NPS GR (nm/ min)**	**Si_3H_8 GR (nm/min) [4.45]**
Frequency Factor	**$7.9*10^{11}$**		**$5.6*10^{14}$**		**$5.5*10^{15}$**			
Activation Energy	**47.0**		**54.9**		**57.2**			
Technique	**LITD**		**TDS**		**SHG**			
400°C	**$4.4*10^{-4}$**	**$3.5*10^{-3}$**	**$8.4*10^{-4}$**	**$6.8*10^{-3}$**	**$1.5*10^{-3}$**	**0.12**		
450°C	**$4.9*10^{-3}$**	**0.04**	**$1.4*10^{-2}$**	**0.12**	**$2.9*10^{-2}$**	**0.23**		**0.8**
500°C	**$4.1*10^{-2}$**	**0.33**	**0.17**	**1.38**	**0.37**	**3.04**		**5**
525°C	**0.11**	**0.87**	**0.52**	**4.22**	**1.20**	**9.74**	**3.4**	**10**
550°C	**0.26**	**2.13**	**1.49**	**12.1**	**3.6**	**29.1**	**10**	**20 (80 [4.46])**
575°C	**0.61**	**4.97**	**4.01**	**32.5**	**10.1**	**81.6**	**21**	
600°C	**1.36**	**11.0**	**10.18**	**82.5**	**26.6**	**216**	**54 (130)**	**40**

In the table above, the reaction rate k, (atoms / s) was found from several references using a variety of techniques such as LITD (Laser-Induced Thermal Desorption), TDS (Thermal Desorption Spectroscopy), and SHG (Second Harmonic Generation). The theoretical growth rates (nm/min) are calculated and tabulated for each reaction rate, and compared with the NPS and trisilane growth rates from this thesis and references [ASM][B]. The growth rates with trisilane and NPS are higher than the theoretical maximum growth rate based on hydrogen desorption for all three references at temperatures from 450 °C to 550 °C. Only the theoretical growth rate calculated from references [4.8][4.44] at 575 °C and 600 °C are higher than the growth rates obtained with trisilane and NPS.

In another paper, growth experiments with trisilane were conducted in nitrogen and hydrogen ambients environments. The author found that the growth rate enhancement in a nitrogen ambient with trisilane was minimal, while the growth rate

enhancement was a factor of 5 in nitrogen ambient for silane [4.47]. Furthermore, in another paper an experiment was conducted on Si(111) substrates for disilane adsorption. It was found that at 490 ^{o}C, deuterium was removed from the surface by disilane dosing [4.48]. The authors speculated that the disilane gas could remove hydrogen from the surface, and proposed the possibility of disilane insertion onto the silicon surface without the need for conventional hydrogen desorption in a mechanism similar to those proposed in this chapter [4.48].

It is evident in our data and the work of others that conventional hydrogen desorption cannot account for the high growth rates obtained with high-order silanes. Without hydrogen desorption, there can be no epitaxial growth. Therefore, there must be another form of hydrogen desorption taking place. This hydrogen desorption is in the form of silane, or disilane molecules (and possibly other high-order silanes, when larger chains are used), either due to a hydrogenolysis type surface reaction, or via a concerted surface reaction. While we are unable to identify the exact dominant growth mechanism, we can conclude based on our data that additional open sites are generated during the growth process with higher-order silanes. Much further work is needed to identify the precise reaction. This unconventional hydrogen desorption that occurs in the presence of high-order silanes is the main technological point of this chapter.

4.9 Summary

In this chapter we provide the fundamental background theory of chemical vapor deposition. The two different growth regimes and boundary layers were covered as well as the Si (001) 2x1 reconstructed surface. A calculation of the number of open sites versus hydrogen pressure and temperature was conducted. The conventional hydrogen desorption growth model based on silane adsorption to open-sites on a silicon surface

was discussed. Experimental data demonstrated that this model was inappropriate for high-order silanes, as it appeared that high-order silanes can either adsorb onto the silicon surface without the need for open surface sites or generate additional open sites during the growth process. A set of possible growth mechanisms for disilane and NPS which involve the conventional 2 open sites, or concerted reaction process with only one open site, or even zero open sites for the adsorption of the high-order silane. The films grown with disilane and NPS were also smoother than those films grown with silane, despite higher growth rates. This implies that either there are more open sites, or growth with disilane and NPS occurs preferentially at step edges. The possibility that the high-order silane can generate its own open sites during growth was tested by the use of diborane and phosphorus doping to get a quantitative measure of the number of open sites during growth. It was found that the normalized adsorption rates of both boron and phosphorus are higher during the growth with NPS than in disilane, and higher in disilane than in silane. This implies that there more open sites during the growth reactions with high-order silanes and that the growth with disilane and NPS does not preferentially occur at step edges. These open sites are generated via desorption of surface hydrogen by the formation of a silane molecule analogous to the hydrogenolysis of alkanes. While we are unable to identify the exact dominant growth mechanism, we can conclude based on our data that additional open sites are generated during the growth process with higher-order silanes.

Chapter 5

Epitaxial Growth of $Si_{1-y}C_y$ Alloys

5.1 Introduction

Traditionally, the incorporation of substitutional carbon into silicon and silicon-germanium alloys during growth is of great interest for engineering the strain in silicon layers. Carbon incorporation in SiGe can be used to compensate the compressive strain in SiGe layers grown commensurately w.r.t. silicon. As little as 1% carbon can compensate for the compressive strain induced by 10% Ge in silicon. Achieving high substitutional carbon fraction (> 1% carbon) in $Si_{1-y}C_y$ alloys is important to achieve significant strain for electron mobility improvement by compressively straining the silicon channel. The growth of epitaxial strained silicon-carbon alloys on Si (100) substrates is used in the source-drain regions of MOSFETs to induce tensile stress in channel regions to enhance electron carrier mobility [5.1][5.2]. Carbon in silicon has also been shown to reduce the boron diffusion in silicon [5.3][5.4][5.5]. Only a small fraction of carbon (10^{19} cm^{-3}) [5.3] needs to be incorporated to suppress the diffusion of boron. This was effect was used for the growth of $Si_{1-x-y}Ge_xC_y$ bases for hetero-bipolar junction transistors (HBTs).

5.2 Growth of Si:C Alloy Layers

There are several challenging issues in the growth of $Si_{1-y}C_y$ alloys. First, unlike growth with $Si_{1-x}Ge_x$ where it is easy to achieve high Ge fractions, it is difficult to achieve high substitutional carbon percentages in silicon. This is due to a significantly larger lattice mismatch between silicon and diamond (35%) than the lattice mismatch